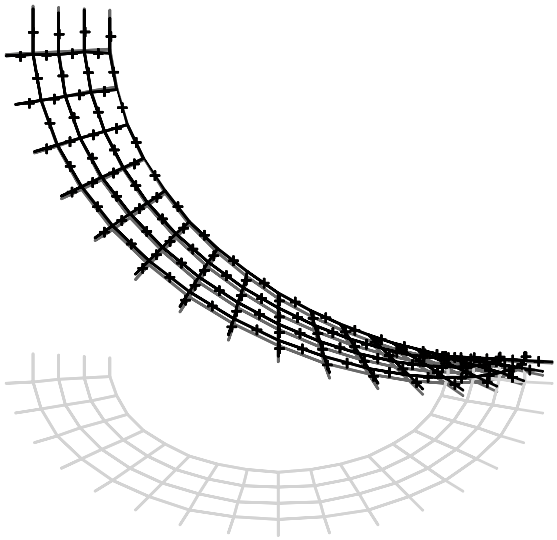

MaNACoH – User Manual

Masonry **N**etwork **A**nalysis for **Co**nstruction **H**istory

July 16, 2018

Abstract: Manacoh is an open-source software that studies the stability of historic masonry vaults. It uses an extended version of the thrust network analysis. This method replace the well-known inverted catenary by an inverted net, called thrust network. Our implementation of the technique focus on the field of construction history and on the effect of stereotomy on stability. Pre-set examples taken from XVIIIe to XXe century scientific literature are included.

MaNACoH was written by Mathias Fantin for the second French conference on history construction that took place in Lyon in January 2014, with the help of Thierry Ciblac (MAP-Maacc Laboratory in Paris — CNRS-MCC UMR 3495), and then during a PhD thesis at GSA Laboratory of ENSA Paris-Malaquais (2015-2017), with the help of Maurizio Brocato and Thierry Ciblac.

Important

Par manque de temps, un manuel complet n'a pas été écrit pour la version actuelle de Manacoh. **Le manuel actuel correspond donc au manuel de la version de 2014 de Manacoh, avec des renvois à la thèse de Mathias Fantin (2017 [17]) où ont été développées les extensions de la méthode des réseaux de forces utilisées dans la version actuelle de Manacoh**.

En particulier, les extensions suivantes qui font partie de la version actuelle du logiciel et qui ont été présentées dans Fantin (2017 [17]), ne font pas l'objet d'explication dans ce manuel :

— les branches partielles additionnelles (branches verticales) ;
— la construction point par point des domaines des chargements admissibles ;
— fonction puissance p utilisée à la place de la fonction min pour faciliter la recherche des optimums.

*

* *

La première version de MaNACoH a été développé par Mathias Fantin pour la seconde conférence francophone d'histoire de la construction qui a eu lieu à Lyon en janvier 2014, avec l'aide de Thierry Ciblac, alors enseignant-chercheur au laboratoire MAP-Maacc Laboratory à Paris (CNRS-MCC UMR 3495).

La seconde version du logiciel (2015-2017), visant plus spécifiquement l'influence de la stéréotomie sur la stabilité des voûtes, a été développée par Mathias Fantin dans le cadre d'un doctorat d'architecture dans le laboratoire GSA de l'ENSA Paris-Malaquais, sous la direction du professeur Maurizio Brocato et l'encadrement du professeur Thierry Ciblac.

Voir : M. Fantin. *Étude des rapports entre stéréotomie et résistance des voûtes clavées.* Thèse de doctorat, Université Paris-Est, Paris, 2017. URL `https://tel.archives-ouvertes.fr/tel-01834617`.

Contents

1 Introduction **5**
1.1 Purpose . . . 6
1.2 Prerequisite . . . 7
1.2.1 Knowledge . . . 7
1.2.2 Programs . . . 7
1.3 Open-source license . . . 8
1.4 Quick overview with a basic example . . . 8
1.4.1 Main steps . . . 8
1.4.2 Step-through . . . 8
1.5 Conclusion . . . 13

2 Using Manacoh **15**
2.1 Creation of the model . . . 16
2.1.1 Introduction . . . 16
2.1.2 Parametric geometries . . . 16
2.1.3 Import custom model . . . 22
2.2 Degrees of freedom . . . 26
2.2.1 Indeterminate structures . . . 26
2.2.2 Boundary node degrees of freedom . . . 26
2.2.3 Branch degrees of freedom . . . 27
2.2.4 Degrees of freedom of parametric geometries . . . 27
2.2.5 Import custom degrees of freedom . . . 29
2.3 Typology and equilibrium . . . 30
2.3.1 Computing typology . . . 30
2.3.2 Computing equilibrium . . . 31
2.4 Optimization . . . 33
2.4.1 Principles . . . 33
2.4.2 Pre-set optimization procedures . . . 33
2.4.3 Solver manual settings . . . 33
2.4.4 Hints for finding an admissible solution . . . 34
2.5 Graphical output . . . 35
2.5.1 Excel charts . . . 35
2.5.2 Accuracy . . . 35
2.5.3 Exporting graphical results . . . 36
2.6 Excel and VBA errors . . . 36
2.6.1 Introduction . . . 36
2.6.2 Common errors when first using Manacoh . . . 36
2.6.3 Common problems when using Manacoh . . . 37
2.6.4 Common errors when modifying the macros . . . 38

3 Theory **39**

4 Worked examples **41**
4.1 Introduction . . . 42
4.2 Domes with frictionless joints — Bossut 1774 - 1776 . . . 42
4.2.1 Introduction . . . 42
4.2.2 Practise and theory . . . 43
4.2.3 Minimal thrust . . . 44
4.2.4 Comparison with network analysis . . . 47
4.3 Domes without hoop forces . . . 51
4.3.1 Durand-Claye 1867 - 1880 . . . 51
4.3.2 Eddy 1877 . . . 59
4.3.3 Minimum and maximum thrust — Lau 2006 . . . 63
4.4 Domes with hoop forces - towards membrane analysis . . . 66
4.4.1 Introduction . . . 66
4.4.2 Wolfe 1921 . . . 66
4.4.3 Membrane theory - Reese 2008 . . . 73
4.4.4 Minimum thickness of domes . . . 76
4.5 Oval domes . . . 78
4.5.1 Oval domes in construction history . . . 78
4.5.2 Affine transformations — Rankine 1858 . . . 78
4.5.3 Elliptical dome with constant thickness . . . 82
4.6 Cylindrical arch - classical results . . . 87
4.6.1 Minimum thickness of an arch . . . 87
4.6.2 Minimum and maximum thrust of an arch - Oikonomopoulou 2009 . 91
4.6.3 Minimum thrust of an arch with consideration of friction - Smars 2000 94
4.6.4 Arches with fill . . . 94
4.7 Helicoidal stairs . . . 96
4.8 Pavilion vaults . . . 101
4.9 Conclusion . . . 103

5 Conclusion **105**

6 License **113**

Chapter 1

Introduction

In short...

This first chapter introduces Manacoh (MAsonry Network Analysis for COnstruction History). It is an open-source software that studies the stability of historic masonry vaults that have a strong 3D geometry: domes, helicoidal vaults. It uses the thrust network analysis. This method replace the well-known inverted catenary by an inverted net, called thrust network. Our implementation of the technique focus on the field of construction history. A basic example is provided in this first chapter to illustrate the use of Manacoh.

1.1 Purpose

Manacoh is an open-source software intended primarily for scholars and students who study ancient methods for assessing the stability of masonry vaults, in the field of construction history. It is well suited to study structures that have a strong 3D geometry (for example ellipsoid vaults, as opposed to simple arches that can be studied easily in 2D). Classical 2D geometries can be studied as well. It uses the thrust network analysis. **This method replaces the well-known inverted catenary by an inverted net, called thrust network.** Passing from 2D to 3D widens the possible equilibrium solutions that can be searched. The drawback is the increased difficulty to solve the equilibrium equations in three dimensions. Manacoh is an all-in-one tool to study 3D structures: it builds the geometry for parametric pre-set examples, solves the equilibrium equations, and offers the possibility to explore various equilibrium solutions, through optimization strategies.

The *force network method* was first published by O'Dwyer in 1999 [30], and then extended by Block in 2009 [2] under the name of *thrust network analysis* [1]. Tools using thrust network analysis exist (Van Swinderen et Coenders 2009 [41], Rippmann et al. 2012 [37]), and several advances and extensions have already been proposed in recent years, concerning the optimization procedures (Vouga et al 2012 [42], Block et Lachauer 2014 [3]), and/or the related variational formulations (Fraternali 2010 [19], De Goes et al. 2013 [11]). Our implementation of the technique focus on the field of construction history. It aims at providing a tool capable of reproducing various equilibrium solutions of published studies of historic interest, using for each of them their own stability criterion. Also, the study of more complex 3D geometries using these historic criteria is possible. The signification of the thrust network was re-evaluated with respect to the line of thrust and the line of pressure. To do so the geometric characteristics of the joints were taken into account, whereas previous studies usually disregard this aspect of the modelisation and consider only vertical joints. Thus Manacoh is designed primarily to study existing structures, the drawback being that it offers only restricted possibilities for form finding of innovative 3D forms.

The main application of Manacoh so far has been to investigate existing studies of various authors: Bossut 1776 [5], Rankine 1858 [35], Eddy 1877 [16], Durand-Claye 1880 [15], Wolfe 1921 [43], Heyman 1967 [22] etc. Equivalent formulations in term of optimization under constraints have been formulated, and checked against results published in scientific literature. Although there is an obvious risk of anachronism by studying all these authors with a numeric tool, this technique proved fast and effective to compute results that help understand and compare these historic methods. It allows also to rediscover forgotten techniques that would be very difficult to apprehend without a numerical tool (Durand-Claye is a good example in that respect).

See also the study of the influence of stereotomy on vaults stability in Fantin [17]

Video tutorials have been created to show the basic functions of the program. Visit the website `http://bestrema.fr/manacoh/`. A basic example of Manacoh's use is also given in the first chapter.

This manual has been divided in four chapters. The first chapter provide the context of this work, the installation procedure of the program, and a quick overview of the program

1. The thrust network analysis by Block directly stems from the force network method, with a decisive advance: the use of reciprocal figures. Our implementation only partially use the potentiality of the thrust network analysis of Block, since we produce the reciprocal figures without using their full potential. Our implementation is a middle-way between the force network method and the thrust network analysis. For simplification, we will use Block's denomination of the technique.

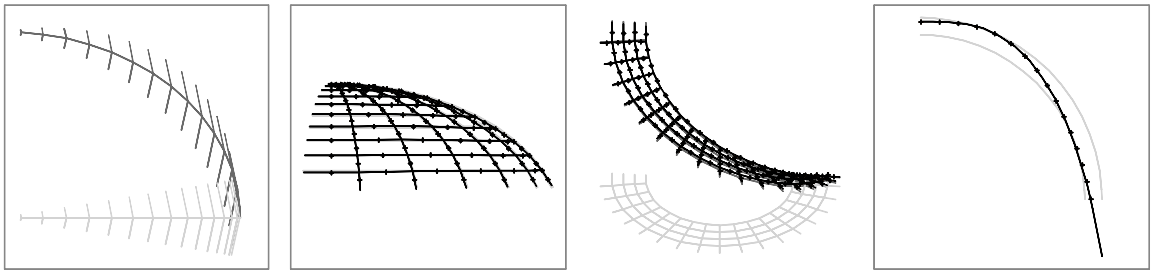

Fig 1.1 – Example of figures created by Manacoh

with a basic example. The second chapter describes the program use, its functions, options, and results. The third chapter addresses the theory of the thrust network analysis, its signification with respect to the line of thrust and line of pressure, and the definition of coefficients of safety. The fourth chapter examines various examples from construction history, in order to demonstrate the possibilities of the program. These examples were studied as a preparation for an oral communication by Mathias Fantin and Thierry Ciblac at the second French conference on history construction that took place in Lyon in January 2014.

1.2 Prerequisite

1.2.1 Knowledge

The user should know the basic concepts of static graphics and/or of limit analysis applied to historic masonry structures (see Heyman 1995 [23]). The user should know how to use the basic functionalities of Microsoft Excel. No VBA [2] knowledge is required to use the program.

1.2.2 Programs

Manacoh is a Microsoft Excel spreadsheet enhanced with VBA macros. It does not work with spreadsheet programs other than Microsoft Excel (for example OpenOffice.org Calc). We chose to develop this spreadsheet with Microsoft Excel primarily because of its widespread use.

Manacoh needs Microsoft Excel 2007 or superior [3] to be used. It uses VBA macros and ActiveX controls: the security parameters must enable their use (see page 36 to turn them on). Also, the user must activate Excel Add-in Solver so that the research of admissible equilibrium solutions is enabled (see page 37).

Microsoft Excel and Excel Solver are products developed by Microsoft. Manacoh has no affiliation with, nor is recommend by, Microsoft. All trademark terms are the property of their respective owners.

2. Visual Basic for Applications is the programming language that is used by Manacoh to create geometry, find the typology, and construct the matrices related to equilibrium.

3. Microsoft Excel 2003 cannot be used to use the Manacoh spreadsheet because it cannot inverse matrices larger than 52x52 – see `http://office.microsoft.com/en-001/excel-help/minverse-HP005209179.aspx`

1.3 Open-source license

Manacoh is a open-source software available under the terms of the Expat License. In exchange for citation obligations (in all software using the source-code of Manacoh, and in all written communication or website using its results), the author authorizes the reuse of its software without any other constraints. Manacoh is provided "as is", without warranty of any kind. The license is available in appendix page 113.

This software is intended primarily for **researchers** and **students** that study the stability of historic masonries in the academic field.

1.4 Quick overview with a basic example

1.4.1 Main steps

This section is designed to help someone that has never used Manacoh to get familiar with the basic functionalities of the program. Some video tutorials are also available on the website (`http://bestrema.fr/manacoh/`). Let us consider a basic parametric example with default parameters, in order to obtain step by step a first admissible equilibrium solution. We will use the following steps:

— Definition of the model (nodes, branches, and their connectivity). Most common geometries can be created automatically by Manacoh with a few parameters given by the user (radius, angles, number of blocks, etc.)

— Computation of the typology: done automatically by Manacoh. The branches projection on the horizontal plane define a form diagram. The reciprocal figure of the form diagram is a force diagram. The computation of the typology is the determination of these diagrams.

— Computation of the equilibrium: done automatically by Manacoh. At the end of this step the thrust network is known in function of a choice of parameters: the degrees of freedom (DOFs).

— Optimization in order to find meaningful solutions: in other words, choice of optimal values for every DOFs. The optimization is executed with Excel Solver Add-in.

Each of these steps is described in detail in the next chapter 2. For now, the *graphical user interface* (GUI) will guide the user through those steps. The principal zones of this interface are described on the figure 1.2. The scrollbars rotate the network and diagrams in 3D. The buttons launch the macros related to each step described below. The blue arrows on the interface indicate which button should be pressed by the user for the next step to begin. The user can modify the size of the interface columns and rows, and the charts size. The interface will automatically be regenerated to fit these new measures when the next model is created.

1.4.2 Step-through

Create model First, click on button `Create model`. A window opens asking the user to choose among various geometry: cylindrical arch, spherical dome, helicoidal vault etc. Choose number 6 `Examples from published studies`, and then number 1 corresponding to this basic example: a helicoidal vault. Manacoh generates automatically the characteristics of the nodes and branches corresponding to this example. The structure is not drawn

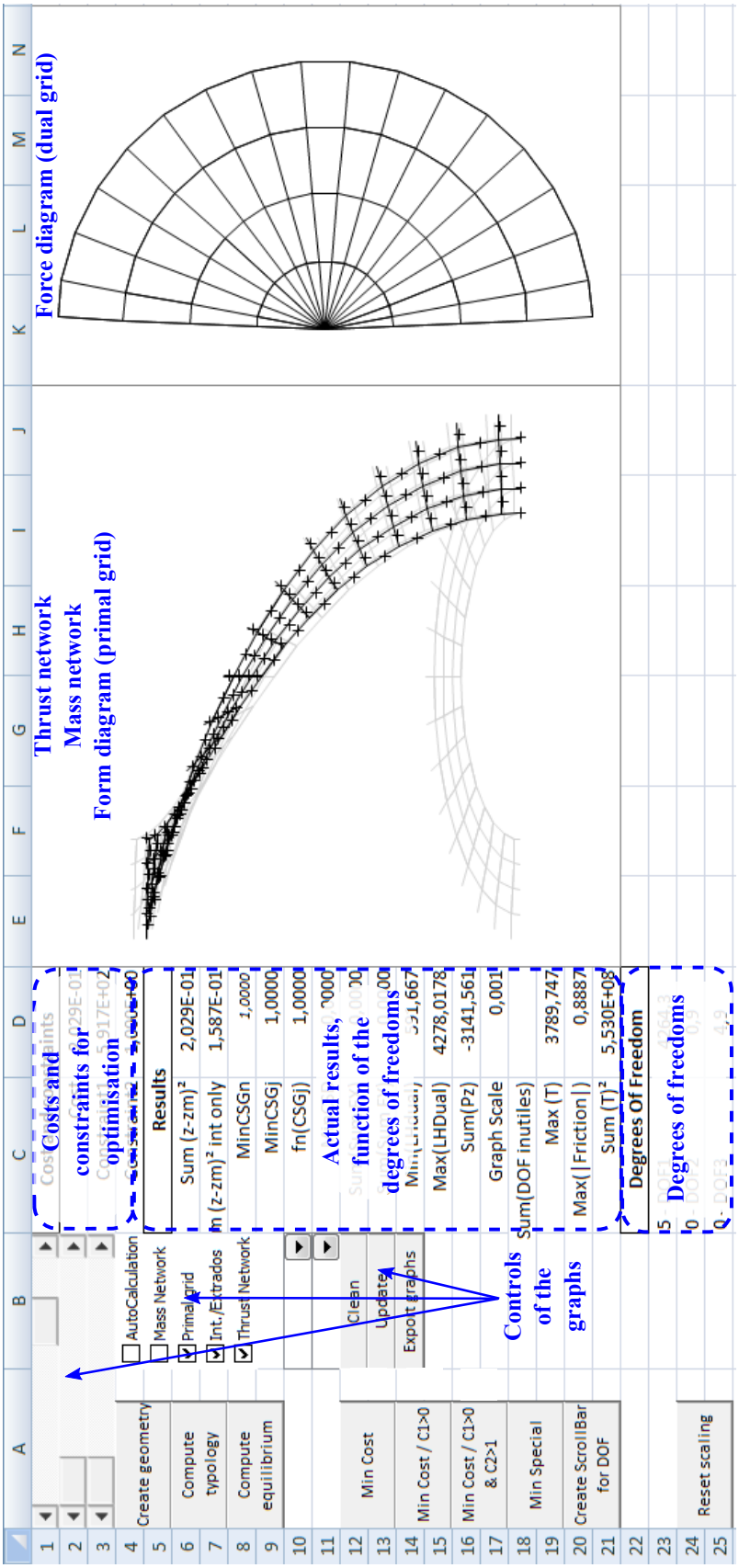

Fig 1.2 – Graphical User Interface

yet on the interface (since the typology is not computed yet), but the characteristics of the nodes and branches are written in the file: they can be consulted respectively on worksheets `N` and `B`.

During the execution of a macro, the sub-steps of the algorithm can be read on the status bar of excel (grey bar on the bottom left of the screen).

Compute typology Then, click on button `Compute typology`. Manacoh then computes various topological data, and creates the graphical representation of the model: see figure 1.3 on the left. On this figure is drawn the *mass network*, which is constituted by the nodes drawn at centre of gravity, and their connecting branches. The vertical projection of this network is the *form diagram* or *primal grid*. It is also drawn on figure 1.3 on the left.

Compute equilibrium Finally, click on button `Compute equilibrium`. First, Manacoh computes equilibrium in the horizontal plane. Then it computes the interior nodes vertical position Z needed to assure equilibrium along the vertical direction. The nodes at their equilibrium position and their related branches constitute the *thrust network*, that is similar to a generalized line of pressure [4] in 3D. The *force diagram* or *dual grid* is the union of all equilibrium polygons of horizontal forces applied to interior nodes. It is the reciprocal figure of the form diagram.

Just after equilibrium computation, the thrust network and force diagram obtained are displayed on figure 1.4. They fulfil the equilibrium equations, but they do not comply with the resistance criterion of masonry [5]. Here the thrust network lies outside the masonry. The current solution is an unstable equilibrium solution. The user must look for a stable equilibrium solution among the various "in equilibrium" but "potentially unstable" solutions. That is the subject of the final step.

Looking for an stable equilibrium solution The equilibrium solution that Manacoh found during the previous step depends on a set of parameters whose values can be chosen by the user freely. We call these parameters degrees of freedom (DOF) of the system. These degrees of freedom are the boundary nodes vertical position, and the value of horizontal forces in a subset of branches. The choice of optimal values for these degrees of freedom that corresponds to a stable equilibrium solution is a matter of optimization. The optimization choices are the heart of a good solution, and we will come back on that topic later in this document. For now, just click on button `Min Cost`. This button trigger Excel Solver, and search a set of degrees of freedom values such as the positions of the nodes is as close as possible of the centre of gravity of each block. The thrust network of the resulting stable equilibrium solution is drawn on figure 1.5. We can see that in that case the thrust network is superimposed with the mass network. This situation is particularly favourable, we will see other example later on in which the thrust network cannot be superimposed with the mass network.

To conclude this first introduction on optimization, the user can compare the thrust network on figure 1.4, before optimization, and figure 1.5 after optimization.

4. This comparison is of course insufficient. We study in detail the relation between *line of trust*, *line of pressure* and *thrust network* in section **??** "Thrust network: a renaissance of the line of pressure".

5. We will come back on those points with much more details and diverse solutions later in this manual.

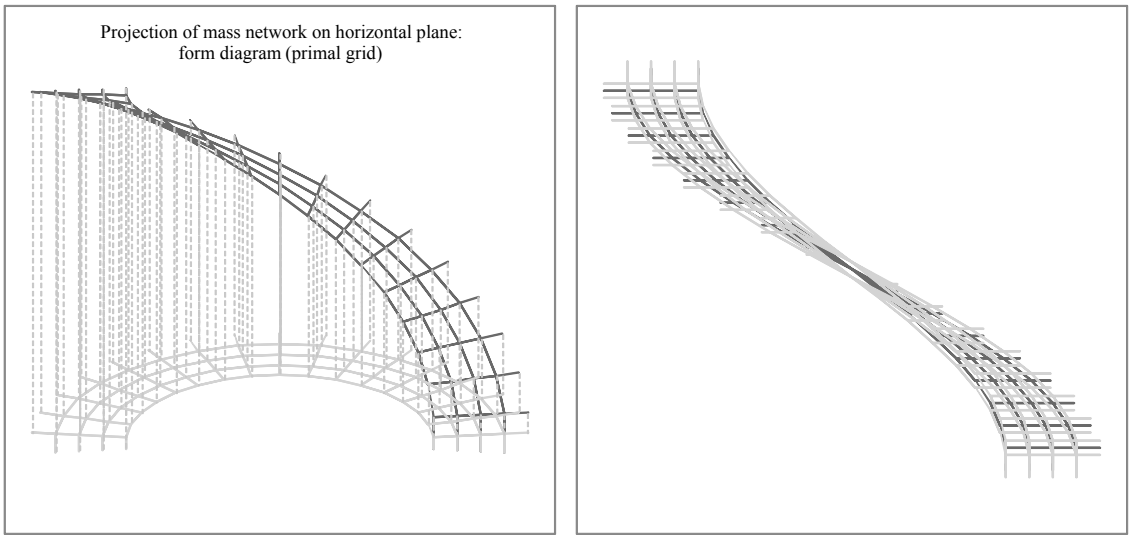

Fig 1.3 – Mass network and form diagram (left)
Mass network, its intrados and its extrados (right)

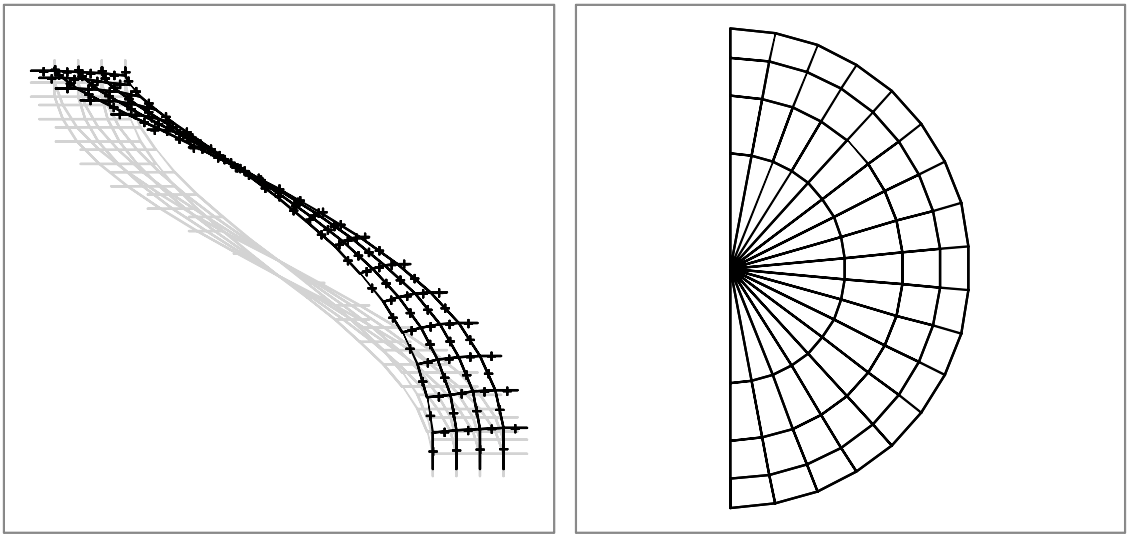

Fig 1.4 – Thrust network before optimisation (left)
Force diagram corresponding to the thrust network (right)

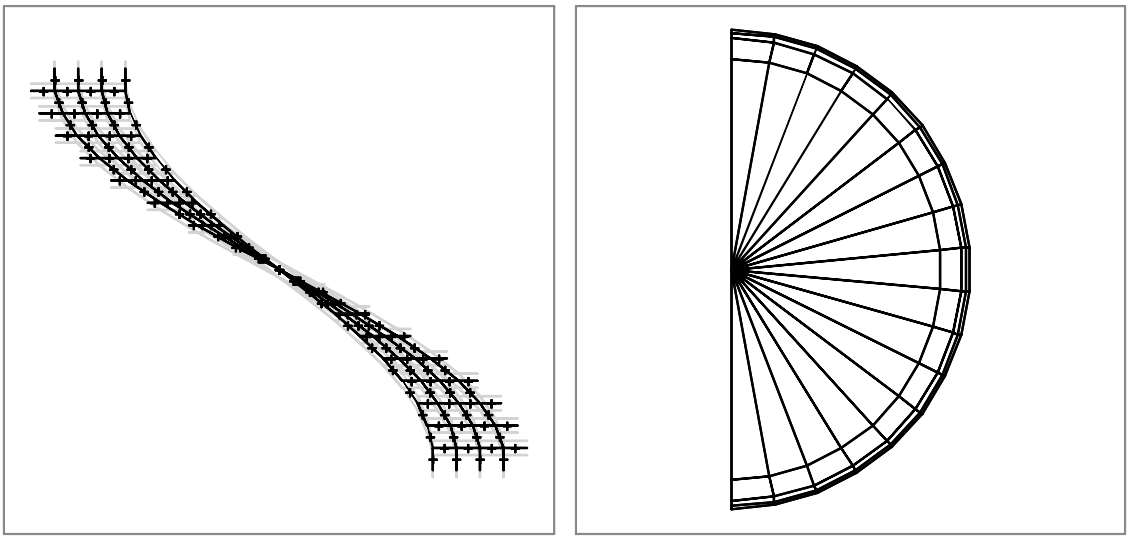

Fig 1.5 – Thrust network after optimisation (left)
Force diagram corresponding to the thrust network (right)

1.5 Conclusion

The basic example we addressed has only one purpose: help the user when he first uses Manacoh. It is based on the geometry of an helicoidal stair that we will study in the worked examples. In order to compute solution that truly represent existing studies from construction history, the choices made for generating the geometry and the choice of optimization functions is of paramount importance, and were disregarded in this first simplistic example. The two following chapters give the user the information he needs in order to be able to reproduce equilibrium solutions from existing publications (Bossut 1774-1776, Rankine 1864, Durand-Claye 1867-1880, Eddy 1878, Wolfe 1921, Heyman 1967...). The last chapter exposes worked example using Manacoh.

Chapter 2

Using Manacoh

In short...

The second chapter provides all information needed to use Manacoh in practise. The models creation, their degrees of freedom, and the equilibrium are presented. Basic information about optimization, graphical output, and common errors are detailed in this chapter.

2.1 Creation of the model

2.1.1 Introduction

A model is constituted of geometrical information: centres of gravity of the blocks, blocks joints (see section **??**), head and tail nodes of each branch. A model also contains other information such as: block weights, constraints on boundary nodes vertical position, and constraints for the horizontal components of forces in the branches. The last two are degrees of freedom of the system. They can be chosen by the user in order to avoid arbitrary choices that would make the interpretation of results more difficult [1].

There are two ways of creating a 3D block structure model in Manacoh. Users can either:

— use the parametric geometries already implemented in Manacoh and requiring very few input. They include spherical and elliptical domes, tunnel vaults and cylindrical arches, helicoidal vaults, pavilion vaults, and classical examples from scientific literature.

— import their own model on the related Excel worksheets. This solution is for advanced users, used to Excel, degrees of freedom, and the general use of Manacoh.

2.1.2 Parametric geometries

Basics

Manacoh guides users through the creation of the model. Once button `Create model` has been pressed, dialogue boxes show up to define the appropriate parameters (see figure 2.1). Users enter some parametric values (intrados radius, extrados radius, angle of embrace and so on). Everything else related to the geometry is calculated automatically by Manacoh. Specific options are available for generating specific geometries, for the sake of generality. They are detailed below. Generally, the default values are correct for most users.

Let us define some notations and basic concepts that will be used in the following sections:

— x, y, z the cartesian coordinates (see figure 2.2 on the left)

— r, φ, θ the spherical coordinates (see figure 2.2 on the centre)

— r, φ, y the cylindrical coordinates, with yy the principal axis of related tunnel vault or cylindrical arch (see figure 2.2 on the right)

— the geometry is defined by given intervals in a well chosen coordinate system. The boundary values of these intervals are indexed by 0 (start) and 1 (end). For example in spherical coordinates $\varphi_0 = 0°$, $\varphi_0 = 60°$, $\theta_0 = 0°$ and $\theta_1 = 10°$ define a lune (or slice) of a dome with an aperture angle of 60°, and with a lune plan angle equal to 10°.

— The border or boundary of the geometry will be designated by their related coordinate. For example boundary φ_0 is the boundary where $\varphi = \varphi_0$.

— A *boundary node* is a monovalent node (*c.-à-d.* a node connected to only one other node). Most of the time, the boundary nodes are located on the borders of the geometry.

— A *boundary branch* is a branch connected to a boundary node.

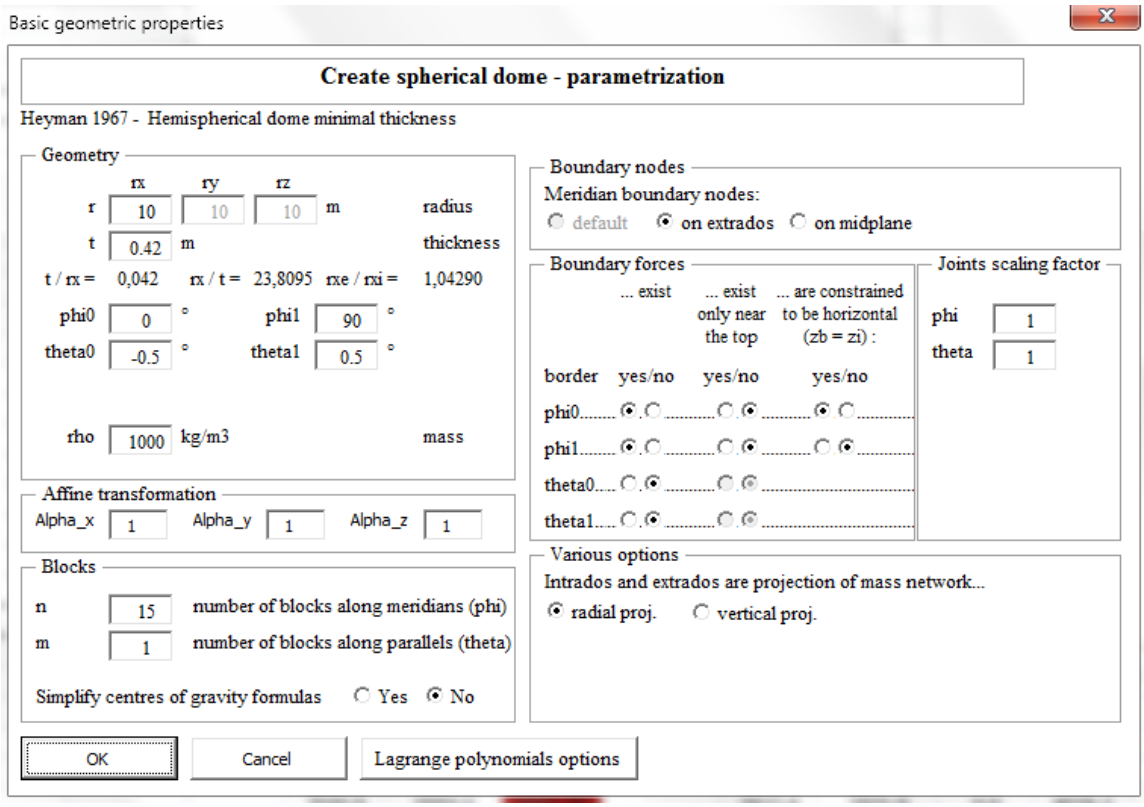

Fig 2.1 – Dialogue box used to define the model characteristics

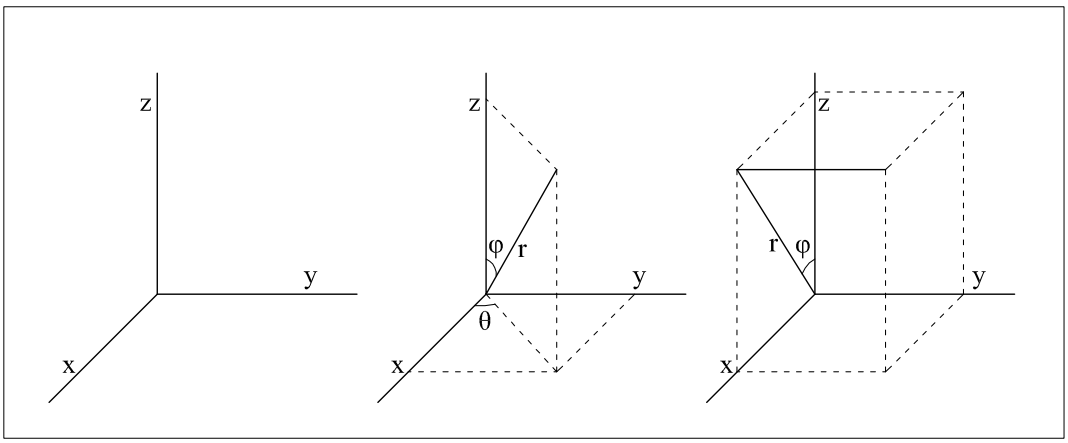

Fig 2.2 – Coordinates systems
from left to right: Cartesian, spherical, cylindrical coordinates

The use of parametric geometries drastically reduces the possibility of errors. Nonetheless some alerts might be displayed during the geometry creation. This is usually the case when it is not possible to compute joints for the given parameters: some joints simply do not exist (see section 2.6.3 for help).

Users can modify manually the geometry after it has been created on the related worksheets. Unwanted branches can be deleted, additional weights can be set on specific blocks, etc. In particular, point loads can be added to a specific block.

Options

Number of blocks On the one hand, n is the number of blocks along direction $\varphi\varphi$. On the other hand, m is the number of blocks along direction $\theta\theta$ in spherical coordinates, or yy in cylindrical coordinates. As a result, in the case of domes there will be $n+1$ branches generated along the meridians, and $m+1$ branches generated along the parallels.

Oikonomopoulou illustrated the following trend [2] with an example: the results do not fluctuate much as soon as there are more than 11 blocks for a half arch ring (2009 [31, p.97]). In our experience, 10 to 15 blocks is generally enough along $\varphi\varphi$ for a half vault (dome or cylindrical arch) in order to get results precise enough to be compared with analytical solutions in published literature (see computation of minimum thickness of domes and cylindrical arches in chapter 4).

Affine transformation An affine transformation can be applied on each parametric geometry. In that case, three affine transformation coefficients must be entered: coefficients along xx, yy, and zz.

The default value used by Manacoh is 1, unless an other value is entered by the user. The default value used in chapter 4 (worked examples) is also 1, unless stated otherwise explicitly. Self-evidently, the value 1 corresponds to no affine transformation.

The affine transformations are defined and their use considered in section 4.5.2 page 78 on Rankine.

Simplify centre of gravity formulas The centre of gravity of the blocks are computed according to the analytic [3] formulas given in appendix. However, the user can choose to approximate the centre of gravity with $r_G = 0.5 \cdot (r_i + r_e)$ and $\varphi_G = 0.5 \cdot (\varphi_0 + \varphi_1)$ (both in spherical and cylindrical coordinates). This option is useful to compare the results with membrane theory, as we will see later (see section 4.4.3).

The default value used by Manacoh and in chapter 4 (worked examples) is `false`, unless stated explicitly otherwise. The keyword `SimplifyCentreGravityFormulas` will be used to specify the value of this option in the examples.

1. We refer here to the choice of the degrees of freedom themselves, not to the choice of the values of the chosen degrees of freedom.
2. Oikonomopoulou considered a half semi-cylindrical arch and calculated the minimal and maximal thrust for structures between 3 and 30 blocks (2009 [31, p.97]).
3. Except for elliptical domes, see appendix page **??**.

Boundary branches The user can choose to create or not boundary branches in the dialogue box. Moreover, he can choose to only create one branch for the whole border [4]. The effect of this option is clearly visible in all graphical outputs.

This option is useful in the case of domes. Hoop branches can be created if their effect is considered (see figure 2.4 on the left). They also can be discarded lunes are to be studied independantly from one another (see figure 2.4 on the right). This second case is useful to compare Manacoh results with Durand-Claye's or Heyman's method (see section 4.3 in worked examples). Finally, the user can create only one hoop branch near the top of the lune in order to create an *oculus* (see figure 2.4 on the centre).

Manacoh cannot study several independent network at the same time. If the model is composed of independent arches (such as unconnected slices of a dome), they must be connected to one another by at least one branch [5]. The force in these branches can be set to zero later if necessary.

Boundary nodes The boundary nodes that belongs to a meridian branch are called *meridian boundary nodes*. Three possibilities are offered to the user regarding the position of these boundary nodes. These possibilities are best explained with drawings: see figure 2.3, where the three possibilities are defined along their keyword.

Most of the time the position of meridian boundary nodes does not have any effect on the final result. However, they must be carefully chosen in some specific cases (*p. ex.* membrane analysis page 73, computing simplified maximal thrust page 91).

Joints scaling factor Joints can be scaled around their midpoint. The defaut value is 1, *c.-à-d.* the computed joints are the real joints (figure 2.5 left). If the scaling factor is 2, the joints will be twice as large as the real joints, and if it is 0 the joints are reduced to the midpoint position. For example if the user wishes to use hoop forces, but does not want to take into account the geometrical coefficient of safety of their related joints, choosing a high value for the joint scaling factor along axis $\theta\theta$ will artificially deliver a model with high coefficient of safety for hoop branches (figure 2.5 right).

Intrados and extrados drawing The intrados and extrados are poly-lines. The vertices of these poly-lines are either the radial projection of the nodes (figure 2.6 on the left), or the vertical projection of the nodes (figure 2.6 on the right). The user can choose on the dialogue box which projection will be used.

Masonry compressive strength The criteria used by Durand-Claye (1880 [15]) and Delbecq (1983 [12]) requires the use of a masonry compressive strength value. It can be entered in the dialogue box. If the unit of distance is meters, and the unit of specific weight is the kilograms per cubic meter, then the unit of the strength should be kilograms per squared meters.

Example: for $10\text{kg/cm}^2 = 1.0\text{MPa} = 1.0\text{N/mm}^2$, enter 100000.

4. For example if this option is selected for border φ_0, the only boundary branch that is not deleted is the one closest to θ_0.

5. The network is explored with recursive functions. If the model is composed of several unconnected networks, Manacoh will "see" only one of those networks

6. When no hoop branch is created, a meridian boundary node and branch is created at the crown.

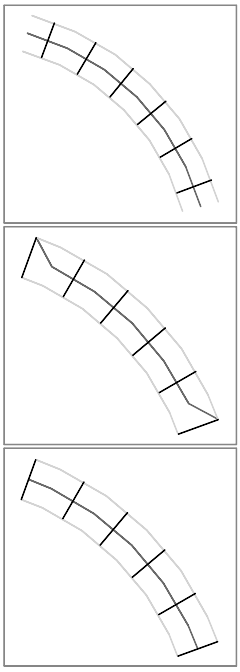

Default : the boundary nodes of meridian branches are located on the centre of gravity of the first voussoir that is not included in the model.

`MeridianBoundaryNodesOnExtrados`: the meridian boundary nodes are located on the extrados of the boundary joint.

`MeridianBoundaryNodesOnMidPlane`: the meridian boundary nodes are located on the intersection of the mid plane and the boundary joint.

Fig 2.3 – Position of meridian boundary nodes

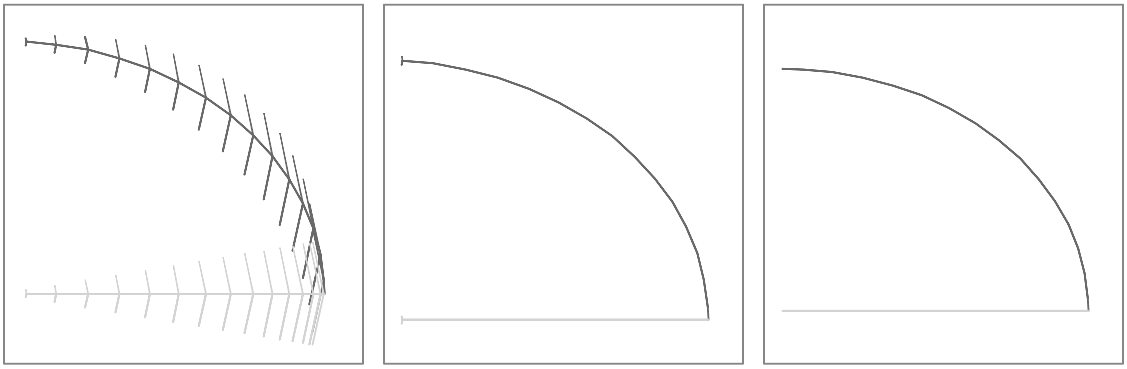

Fig 2.4 – Control of creation of boundary branches
From left to right, create all, create one, create none [6]

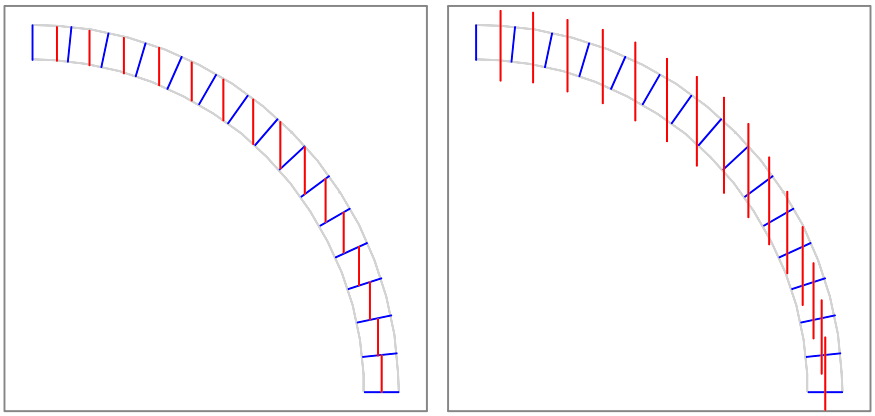

Fig 2.5 – Joints scaling factor
factor 1 (left); factor 2 for hoop branches joint (right)

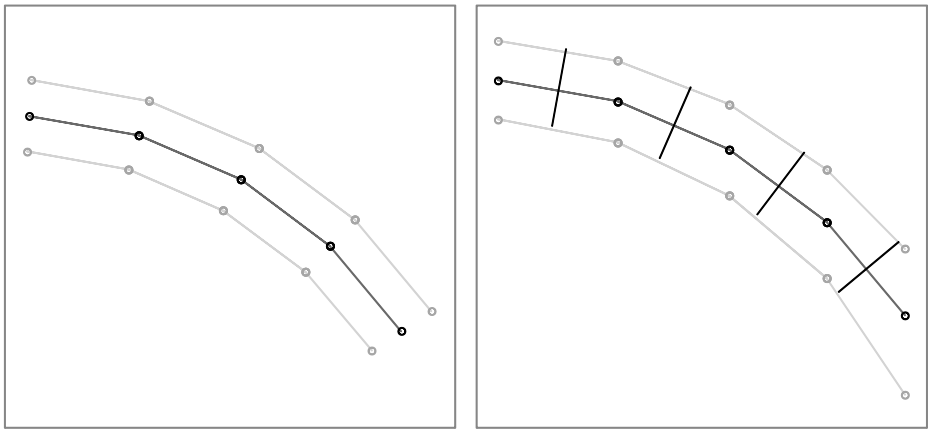

Fig 2.6 – Intrados and extrados drawn at radial projection of nodes (left)
Intrados and extrados drawn at vertical projection of nodes (right)

Lagrange polynomials options The use of Lagrange polynomials will be exposed later. Their options (degree and variable) can be defined in their own option window, that is accessible from the main parametric geometries window. For more information about Lagrange polynomials, see sections 2.2.5, 2.4.4 and **??**.

Changing default values In case of repetitive generation of a geometry, it might be useful to change the default values that appears in the dialogue box. The defaut values are written in the `VBA` module `c_CreateModel`. To access these values, open the VBA window (`ALT+F11`), select the module `c_CreateModel`, and modify the values in one of the following procedures:

— `a2_CreateGeoCyl`: for cylindrical arches and vaults
— `a2_CreateGeoSphe`: for spherical domes
— `a2_CreateGeoOval`: for oval domes
— `a2_CreateGeoHel`: for helicoidal vaults
— `a2_CreateGeoPav`: for pavilion vaults

2.1.3 Import custom model

For advanced users - most users can skip section 2.1.3 of the manual.

Principles

The information describing the model, and that will use later to compute the typology and the equilibrium, is stored on two worksheets: nodes worksheet `N` and branches worksheet `B`. The user can manually modify a parametric model after it has been generated, or import its own model in the program. We expose in this section how and where the model is stored on the worksheets. Please note that no empty lines are allowed on the worksheets where data is stored.

Nodes

The data related to nodes is stored on worksheet `N`. This worksheet is organized column-wise. The first columns define the geometry. The following columns are computed using the geometry (for example to transform the cartesian coordinates in spherical coordinates). The last columns are used to store the results that will be computed later. Table 2.1 describes each of these columns, and indicates if the column must be filled by the user (or by the parametric models), or if it will be filled automatically by the program during the following steps (*compute typology* and *compute equilibrium*).

Some of the columns might be left blank if the user does not use their related data:

— The radial projection of the nodes on intrados and extrados are only used for the graphical output of the intrados and extrados (no bearing on the results of the analysis). They can be left blank.

— The vertical projection of the nodes on intrados and extrados can be left blank, but the geometrical coefficient of safety on nodes will not be calculated in that case.

— If the weight column is not filled, the thickness column is used to determine a coarse estimate of the weight (considering a density of 1000) of the blocks. The user should fill either the weight or the thickness column. The recommended choice is to fill the weight column, since Manacoh computes only a coarse estimate of the weight, whose precision highly depends on the type of geometry considered [7].

Branches

The data related to branches is stored on worksheet `B`. This worksheet is organized column-wise. The first columns give the connectivity of the branch (head and tail nodes) and data about the joints. The following columns are computed using the geometry (for example the areas formed by the loops of branches). The last columns are used to store the results that will be computed later. Table 2.2 describes each of these columns, and indicates if the column must be filled by the user (or by the parametric models), or if it will be filled automatically by the program during the following steps (*compute typology* and *compute equilibrium*).

7. The weight applied to a node is calculated as the mean value of the surfaces of surrounding areas, multiplied by the thickness. If one of the surrounding area is a boundary area that is not subset by boundary branches (it is the case for lunes without hoop branches for example), this estimate will not be correct. The weight estimate was not thoroughly investigated

Column	**Description**	**Data types**	**Can be entered or overwritten manually by the user**
Num	Index of the node	integer	true
$x = x_G$	Position of the node in mass network	double	true
$y = y_G$		double	true
z_G		double	true
z_i	Vertical projection on the intrados of the node in mass network (only for graphical output - see page 19 and figure 2.6)	double	true
z_e	Vertical projection on the extrados of the node in mass network (only for graphical output - see page 19 and figure 2.6)	double	true
radial proj. x_i	Radial projection on the intrados of the node in mass network (only for graphical output - see page 19 and figure 2.6)	double	true
radial proj. y_i		double	true
radial proj. z_i		double	true
radial proj. x_e	Radial projection on the extrados of the node in mass network (only for graphical output - see page 19 and figure 2.6)	double	true
radial proj. y_e		double	true
radial proj. z_e		double	true
Thickness	Thickness of the structure	double	true
Weight W	Weight of the voussoir or block	double	true
$Z_b = Z_i$	Constraint on a boundary node vertical position. See details in manual section 2.2.2	integer	true
chosen dof	See details on degrees of freedom in manual section 2.2.5	string	true
chosen dof category	See details on degrees of freedom in manual section 2.2.5	integer	true
Boundary node	Indicates if the node is a boundary node	boolean	false
Temp	Not used	-	-
r_G	Position of the node in spherical coordinates, in mass network	double	false
φ_G		double	false
θ_G		double	false
Z_b	Vector used for implementation of boundary conditions only (0 if constraint, =Z if DOF or normal boundary node)	double	false
Z	Position of the node in thrust network	double	false
CSGn	CSG_n Geometrical coefficient of safety - expressed on node (see details in manual section **??**)	double	false

Table 2.1 – Columns in nodes worksheet `N`

Column	**Description**	**Data types**	**Can be entered or overwritten manually by the user**
Num	Index of the branch	integer	true
Head node index	Index of the head node	integer	true
Tail node index	Index of the tail node	integer	true
Joint on intrados x_i	The joint is a segment between intrados and extrados. This point defines the point of the joint on intrados. See more details on the definition of the joints in section **??**.	double	true
Joint on intrados y_i		double	true
Joint on intrados z_i		double	true
Joint on extrados x_e	The joint is a segment between intrados and extrados. This point defines the point of the joint on extrados. See more details on the definition of the joints in section **??**.	double	true
Joint on extrados y_e		double	true
Joint on extrados z_e		double	true
Surface of Joint	Surface of the initial joint between voussoirs. Used to calculate coefficient of safety when the admissible compression is not infinite.	double	true
chosen dof	See details on degrees of freedom in manual section 2.2.5	string	true
chosen dof category	See details on degrees of freedom in manual section 2.2.5	integer	true
u	$x_{\text{head}} - x_{\text{tail}}$	double	false
v	$y_{\text{head}} - y_{\text{tail}}$	double	false
w	$z_{\text{head}} - z_{\text{tail}}$	double	false
L	$\sqrt{u^2 + v^2 + w^2}$	double	false
LH	$\sqrt{u^2 + v^2}$	double	false
Head area	In the dual grid (force diagram), the areas are the vertices of the branches. This area is the head area.	integer	false
Tail area	In the dual grid (force diagram), the areas are the vertices of the branches. This area is the tail area.	integer	false
order in head area	In the primal grid, the branches form loops that defines the areas. This is the position of this branch in the loop of the corresponding area.	integer	false
order in tail area		integer	false
Alpha	Angle of the branch with the horizontal	double	false
wDual	Composant of the force in the branch along zz	double	false
LHDual	Horizontal force in the branch	double	false
SignF	not used	double	false
F	Force in the branch	double	false
N	Normal force on the joint corresponding to this branch	double	false
T	Tangential force on the joint corresponding to this branch	double	false
M	Moment on the joint corresponding to this branch, w.r.t. the mid-point of the joint	double	false
Friction	Friction coefficient T/N	double	false
Cost	LHDual/LH - not used	double	false
Lambda	Parametric coordinate of the centre of pressure on the joint	double	false
CSGj	Geometrical coefficient of safety expressed on joint CSG_j (see details in manual section **??**)	double	false
CSD	Delbecq's coefficient of safety CSD (see details in manual section **??**)	double	false
CSDC	Durand-Claye's coefficient of safety CSDC (see details in manual section 4.3.1)	double	false
XF	Coordinates of the centre of pressure on the joint (related to the considered branch)	double	false
YF		double	false
ZF		double	false
uDual	Composant of the force in the branch along xx	double	false
vDual	Composant of the force in the branch along yy	double	false

Table 2.2 – Columns in branches worksheet B

If the points that define the joints are missing, the program will not be able to compute the results related to these joints (geometrical coefficient of safety on joint, normal and tangential force on joint etc.). However, the thrust network will still be computed.

Numbering

The numbering of the nodes and the branches must follow these rules:

— The index of the nodes and of the forces must be given in mounting order, with no gap, beginning with 1 (ie. 1 2 3 4 5 etc.). Since the first row is filled with the titles on the column, object i will always be found on line $i + 1$.

— All interior nodes must have an index lower than any boundary nodes. If it is not the case the nodes will be automatically renumbered. The program will issue a warning message in order to alert the user that this renumbering took place.

— Indexes of the head and tail nodes must respect the following convention : the index of the head node must be lower than the index of the tail node. If it is not the case the related branch will be automatically inverted. The program will issue a warning message in order to alert the user that this modification took place.

Degrees of freedom

The degrees of freedom can be chosen arbitrarily by the program when it is computing the equilibrium equations. Nonetheless, one should use sensible degrees of freedom with physical meaning so that the search for an admissible solution is made easier, both for the program and the user. The user can choose which degrees of freedom will be used. This choice must be made and stored when the model is created. For example, the parametric examples create and store information on columns `chosen dof` and `chosen dof category`, both on the nodes worksheet and the branches worksheet. Since the choice of the degrees of freedom is a delicate matter, this issue is addressed in an independent section (see section 2.2 below).

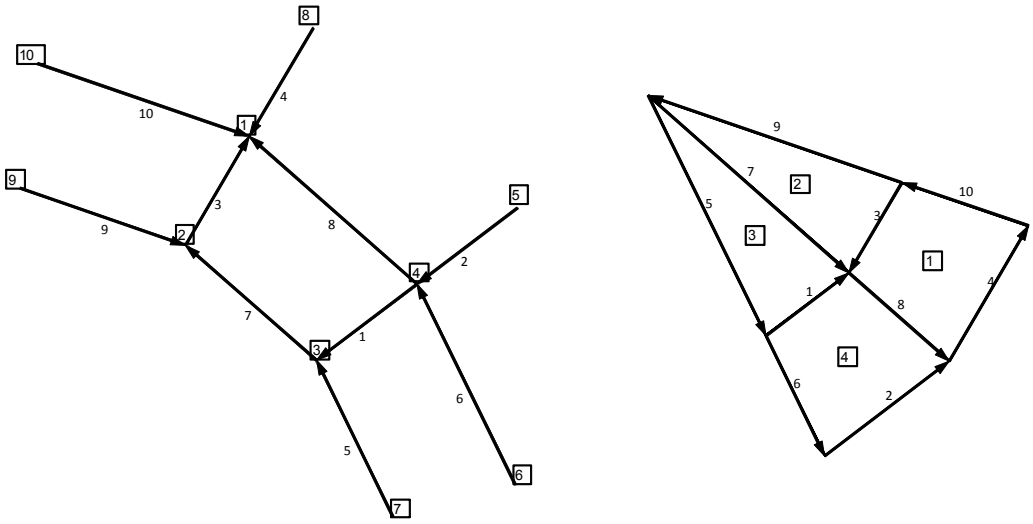

Fig 2.7 – Numbering example printed on primal and dual grid

2.2 Degrees of freedom

2.2.1 Indeterminate structures

Let us consider a basic example. An arch is an indeterminate structure, which means that three parameters can be independently chosen, so that each set of value for these parameters expresses a different equilibrium of the arch. For example these three parameters can be the horizontal force, the vertical force, and the point of application of the force, all taken at the crown. These parameters are called degrees of freedom.

In thrust network analysis [8], there is also such degrees of freedom. There is two kind of degrees of freedom:

— the boundary nodes vertical position. We will call them node-DOF in this manual.

— the horizontal force in some of the branches. We will call them branch-DOF in this manual.

Each set of values for the degrees of freedom defines an equilibrium solution. This equilibrium solution might not be stable, so an optimization procedure is applied in order to find a set of value for the degrees of freedom that defines a stable equilibrium solution (if such a solution exists).

2.2.2 Boundary node degrees of freedom

The boundary nodes vertical position is a value that must be chosen by the user. For that reason, we call them degree of freedom. There is several strategies for that choice, according to the situation. We consider below these strategies one by one.

8. Block's use of degrees of freedom and reciprocal figures in the original thrust network method is more complex than the simple approach that we give here (2009 [2]). See chapter on theory below.

Optimized value The most common situation is to include the node-DOF in the optimization process, and thus look for a value that is admissible regarding the constraints (for example the boundary node must be in the masonry), and the optimization function (for example the thrust network as close as possible to the mass network). In that case, the user should declare that the boundary node is a degree of freedom (we will see later how to do so).

Constraint boundary force to be horizontal A boundary node is linked to a unique interior node by a branch. If both nodes have the same height z in thrust network, then the boundary force will be horizontal. This might be a wanted behaviour for the keystone of an arch, of for the hoop branches of a dome. To get this behaviour, enter the index of the linked interior node `ni` in the column `zb=zi` for the considered boundary node on worksheet `N`.

Fixed value If the boundary node is not declared to be a degree of freedom, then its value will be fixed by the program to the value given in column zg. The position of the boundary node in thrust network and mass network will be the equal. Moreover, even if the boundary node is declared to be a degree of freedom, the user can still exclude it from the optimization process. In this situation the vertical position of the considered boundary node is still a degree of freedom, but its value is fixed. We will see later how to exclude some specific degrees of freedom from the optimization process, using degree of freedom categories.

Example Figure 2.8 shows graphically the node degrees of freedom for an oval dome. In that example, the hoop branches are constrained to be horizontal, and the boundary nodes at the base of the dome will be used in optimization.

2.2.3 Branch degrees of freedom

The degree of indeterminacy of the network is the number of needed branch-DOF to define completely the forces in all branches. It can be determined analytically (see Block 2009 [2, p.72-74]). Manacoh's approach is simpler: the program will automatically add new degrees of freedom to the ones chosen by the user, if they are required (see section **??**). However, it cannot remove degrees of freedom if too many degrees of freedom are provided by the user (ill-conditioned input data).

Figure 2.8 shows graphically the branch degrees of freedom that were chosen for an oval dome. In that example, all branch degrees of freedom are located on the hoop branches on one side of the model.

2.2.4 Degrees of freedom of parametric geometries

When using parametric geometries, there is no particular action required on the user's part regarding which degree of freedom should be chosen. Everything concerning the degrees of freedom, for both nodes and branches, is written during the creation of the model by the macro `Create model`. We will show later that some options are available concerning Lagrange polynomials (for advanced use of the degrees of freedom).

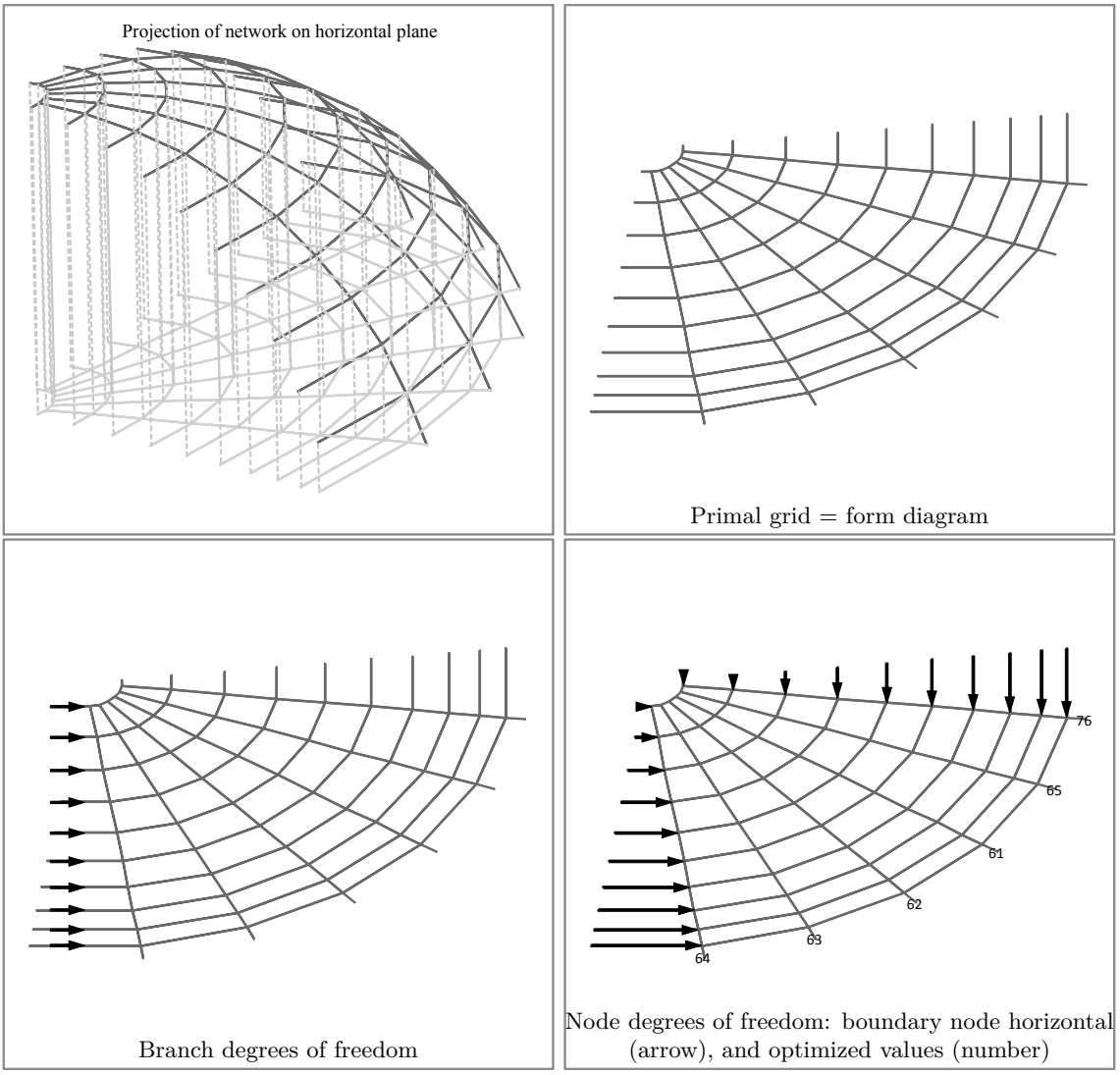

Fig 2.8 – Degrees of freedom — example for an oval dome

2.2.5 Import custom degrees of freedom

For advanced users - most users can skip section 2.2.5 of the manual.

Basic example

First, let us consider a simple example. The geometric characteristics of the blocks have been written by the user on the worksheets `N` and `B` according to the principles given above. The user must now declare the DOF that he wishes to use **before** executing the next step `Compute typology`

Node degrees of freedom Let us consider that there is a total of three boundary nodes. The user enters in the column `chosen dof` of the nodes worksheet `N`:

— `101/0/x` for the first boundary node
— `102/0/x` for the second boundary node
— `103/0/x` for the third boundary node

The program will read this information when computing equilibrium, and create three independent node-DOF : `101`, `102` and `103`. We will come back later on the meaning of `0` and `x` in these expressions. Here, the three boundary nodes will have the height corresponding to the value of their respecting node-DOF. However, if the user enters:

— `101/0/x` for the first boundary node
— `101/0/x` for the second boundary node
— `101/0/x` for the third boundary node

then the program will create only one node-DOF when computing equilibrium: `101`. The three boundary nodes will have the same height: the value of the node-DOF `101`.

branch-DOF The user cannot choose an arbitrary set of branches for his branch-DOF. For example in the case of the simple arch, he can choose one and one only branch-DOF, that will define the horizontal thrust of the arch. Choosing two branch-DOF in this case is nonsensical, since there is the horizontal thrust is constant in an arch. In term of algebra, the rank of the equilibrium matrix must not diminish when the vectors related to the chosen branch-DOF are removed. If the number of chosen branch-DOF is not sufficient, the program will automatically choose additional branch-DOF. A particular case is when the user does not enter any branch-DOF, then all branch-DOF are chosen by the program.

Declaring chosen degrees of freedom

The optimization process that we will see later can be time-consuming, or even do not yield satisfying results if the numbers of parameters, that is degrees of freedom, is too high. Manacoh offers a polynomial approximation in such cases, using Lagrange polynomials. The basics are quite simple: the implemented DOFS in the program are not values, but polynomials. Each polynomial-DOF has a name (`101`, `102` and `103` in the basic example above), a degree (`0` in the example above), and a polynomial variable (`x` in the example above). Each node-DOF or branch-DOF is affected to a polynomial-DOF, and its value is the value of the related polynomial-DOF at the position of the node or branch.

In order to declare a degree of freedom (either node-DOF of branch-DOF), the user should enter in the column `chosendof` a string describing the polynomial that he wishes to

use, under the format `name/degree/variable`, with no spaces. `name` should be an integer, `degree` the degree of the polynomial, and `variable` one of these values: `x`, `y`, `z`, `phi`, `theta`, `rcyl`, `num`. If a same polynomial is used for several degrees of freedom, the same definition should used each time.

This technique might seem tricky at first, but it can reduce greatly the number of parameters for the optimization process, from "number of node-DOF + number of branch-DOF" to the sum of coefficients of the polynomials. The latter are the new parameters, that is the new degrees of freedom. Furthermore, instead of writing the polynomials such as $a_0 + a_1x + a_2x^2 + ... + a_nx^n$, we use Lagrange polynomials, so that the polynomials of degree n are written directly in function of $n + 1$ values of node-DOFs or branch-DOFs. Thus the degrees of freedom will not be obscure coefficients, but real values of corresponding heights or horizontal forces of the degrees of freedom.

The technique of Lagrange polynomials is further developed in section **??** of the chapter on theory.

In order to launch the optimization process on subsets of degrees of freedom, a category is declared for each degree of freedom. This category is to be written in the column `chosen dof category` next to the related `chosen dof`. For the parametric geometries we chose the following (and arbitrary) categories:

— 0 node-DOF (vertical position Z of a boundary nod)
— 1 branch-DOF chosen by the algorithm when computing equilibrium
— 2 branch-DOF, generally thrust of an arch or a lune at the crown
— 5 branch-DOF corresponding to hoop force

2.3 Typology and equilibrium

Now that the user has entered the geometry and chosen which degrees of freedom he wishes to use, the two following steps do not require any input on his part: `Compute typology` and `Compute equilibrium`. The user should not modify manually the geometry after the typology or equilibrium has been computed, because the results will not be correct [9]. We will come back on those subjects in the chapter on the theory behind Manacoh. Here is a quick outline of what does the program when the user execute `Compute typology` and then `Compute equilibrium`

2.3.1 Computing typology

Up to now, the only existing data on the typology is the connectivity of the nodes, given for each branch by the index of head node and tail node. The macro `Compute typology` realizes the following steps:

— Calculation of additional geometric values for nodes and branches, such as the spherical coordinates of the nodes, the components of the branches u (along xx), v (along yy) and so on.
— Recursive function to find all the loops formed by branches in primal grid. These loops are called areas in our implementation.

9. Some typology and equilibrium formulas are written using values (and not range adresses) in order to save computing time. It is in theory possible to write the formulas using range adresses in Excel, and thus allowing form finding processes. This is not implemented in the current version of Manacoh.

— Recursive function to construct the formula of all x^* and y^* (position of the areas in dual grid).
— Creation of the graphs, using recursive functions and Excel charts. The graphs are updated dynamically.
— Computation of a coarse estimate of the weight of the voussoirs if no weight was submitted by the user when creating the geometry.

2.3.2 Computing equilibrium

Once the typology is computed, the equilibrium can be solved. Note that up to now the degrees of freedom were not created: only some information necessary for guiding their creation by the algorithm is stored on the nodes and branches worksheets.

The macro `Compute equilibrium` realizes the following steps :
— Construction of the branch-node matrix
— Equilibrium equations in horizontal plane written in one non-square matrix $\boldsymbol{K}$
— Creation of polynomials-DOFs according to the user input, and possibly creation of additional polynomials-DOFs if needed, in order to transform $\boldsymbol{K}$ in a square invertible matrix
— Inversion of $\boldsymbol{K}$, so that the horizontal forces are now known in function of the branch-DOFs
— Computation of the vertical position of all nodes, using the node-DOFs. At the end of this step, the forces in the branches and the position of all the nodes are known (in function of the DOFs) : the thrust network is determined
— Computation of some additional formulas (coefficient of safety, normal and tangential forces on the joint etc.)
— Output on the graphical user interface of the results that might serve as basis for the optimization process: see table 2.3

The user should not manually alter the equilibrium after it has been created on the related worksheets. It is however possible to modify the results that are produced, for example by changing the formula of the coefficient of safety etc. It is best in that case to modify directly the formula in the macro `SetResultFormulas` on the class module `cFor` inside visual basic editor. Otherwise the modification of the formulas will be replaced by the default formulas each time the equilibrium is computed.

Column	**Formula**	**Description**
Sum (z-zm)^2	$\sum_{\text{nodes}} (z - z_G)^2$	Sum of the squared distance between thrust network and mass network
Sum (z-zm)^2 int only	$\sum_{\text{int. Nodes}} (z - z_G)^2$	Sum of the squared distance between thrust network and mass network, only for interior nodes
MinCSGn	$\text{CSG}_{\mathcal{N}} = \min_{n \in \mathcal{N}} \text{CSG}_n$	Geometrical coefficient of safety of the structure, expressed at the nodes (see section **??** page **??**)
MinCSGj	$\text{CSG}_{\mathcal{J}} = \min_{j \in \mathcal{J}} \text{CSG}_j$	Geometrical coefficient of safety of the structure, expressed at the joints (see section **??** page **??**)
fn(CSGj)	$\text{fn}(\text{CSG}_j)$	Specific function of the geometrical coefficient of safety at the joints, designed to ease optimization (see section **??** page **??**)
MinCSD	$\min_{j \in \mathcal{J}} \text{CSD}_j$	Delbecq's coefficient of safety (see section **??**)
MinCSDC	$\min_{j \in \mathcal{J}} \text{CSDC}_j$	Durand-Claye's coefficient of safety (see section 4.3.1)
Sum(Sum FX)	$\sum_{int.nodes} \left\lvert \sum_{\text{branches}} F_x \right\rvert$	Sum of the residu of equilibrium along x at each interior node. Should be zero.
Sum(Sum FY)	$\sum_{\text{int. nodes}} \left\lvert \sum_{\text{branches}} F_y \right\rvert$	Sum of the residu of equilibrium along x at each interior node. Should be zero.
Min(LHdual)	$\min_{j \in \mathcal{J}} l_H^*$	Minimum of the horizontal forces.
Max(LHDual)	$\max_{j \in \mathcal{J}} l_H^*$	Maximum of the horizontal forces.
Sum(W)	$\sum_{\text{int. Nodes}} W$	Sum of the weights of the blocks
Graph Scale	—	Used to scale arrows drawn on the graphs. Can be modified by the user at any time.
Max (T)	$\max_{j \in \mathcal{J}} T$	Maximum of the tangential forces on joints
Max(|Friction|)	$\max_{j \in \mathcal{J}} \lvert T/N \rvert$	Maximum of the friction coefficient on joints
Sum (T)^2	$\sum_{j \in \mathcal{J}} T^2$	Sum of squared tangential forces on joints

Table 2.3 – Results given on GUI

2.4 Optimization

Mise à jour : l'optimisation est maintenant simplifiée en utilisant les fonctions puissances décrites dans Fantin [17, p.228-233]

2.4.1 Principles

Any set of degree of freedom values will give a solution in equilibrium. But this solution does not necessarily respect the criterion of resistance that the user wishes to use. There are many criteria that can be used, so we will just give one example, and refer the reader to chapter 4 about worked examples, for a insight of other criteria.

Let f, c_1 and c_2 be three functions that depends on the degrees of freedom values $\boldsymbol{\zeta}_{\text{dof}}$. The optimisation problem is written as:

$$\min_{\boldsymbol{\zeta}_{\text{dof}},\ c_1>0,\ c_2>0} f \tag{2.1}$$

f is called the *cost function*, and c_1 and c_2 are called *constraints*. A possible choice for f is $\sum_{k=1}^{n}(z_k - z_{G,k})^2$. It measures the sum of the square of the distance between the mass network nodes and the thrust network nodes. l_H^* is the horizontal force in a branch. A possible choice for c_1 is $\min l_H^*$ to assure that there is no traction forces in the system.

2.4.2 Pre-set optimization procedures

The most common functions that the user might want to use as cost function or constraint are readily available on the graphical user interface, in the column called result (see table 2.3 above, that describes these results). In order to use a particular function as the cost function, just click on the cell `cost`, type "=", and then click on the cell that you wish to use. Do the same for each constraint function, if necessary. Then click on one of the three buttons `Min Cost`, `Min Cost / C1>0` or `Min Cost / C1>0 and C2>1` whose names are self explanatory. The program will guide you through the following optimization steps:

1. Randomize : choose a randomize-factor r. Each DOFs will be multiplicate by $1 + r \times \text{RAND}$, with RAND a number between -1 and +1.
2. Choose category: choose the category of DOFs that will be used for optimization.

Once the Solver ends, the graphical results that were written on the network (*p. ex.* coefficient of safety, forces values) are automatically updated.

2.4.3 Solver manual settings

If the pre-set optimization procedure is not sufficient for the user, for example if additional constraints are needed, it is possible to directly use the Solver. Select tab `Data` in Excel ribbon, and then click on `Solver` (usually the rightmost button in the tab). The following rules must be followed:

— all cells referenced in the Solver must be located on the same worksheet (here worksheet `GUI`). The user might want to copy result values from `N` worksheet, `B` worksheet, or `DOF` worksheet to `GUI` worksheet.

Once the Solver ends, the thrust network is naturally updated in his new form, however the graphical results that were written on the network (written numbers such as coefficient of safety, forces values etc.) **will not be automatically updated**. The user should use button `Update` to update these written values.

2.4.4 Hints for finding an admissible solution

It can be quite difficult to find a optimum solution, or even a stable solution, if some care is not taken in the way optimisation is conducted. Here are some hints to help the user in this respect.

One step at a time

It might be difficult to find a solution if no sensible starting point is given. By default, the starting point for the degrees of freedom is:

— for node-DOF: their vertical position in mass network

— for branch-DOF: a fraction of the total weight of the blocks

With these very coarse values, the thrust network is often far away from the mass network, and thus probably not admissible for the user constraints. Before using its own cost function and constraints, the user should try to optimize first with $f = \sum_{k=1}^{n} (z_k - z_{G,k})^2$. It will be more easy to find an optimum solution respecting the user's constraints from this better starting point.

Divide and conquer

When the number of degree of freedom is high, it might help to optimize on a subset of degrees of freedom. Manacoh divides the degrees of freedom into coherent category when creating the parametric geometries (category 0 for boundary nodes, category 2 for forces at the crown, category 5 for hoop forces etc.).

The degree of freedom categories are first chosen in the parametric example or by the user when the geometry is entered (see above). However, the user can override these category if needed during the optimization, by changing the related category on the degree of freedom worksheet `DOF`. Note that the other columns on worksheet `DOF` should not be modified.

Lagrange polynomials

We already described the basic use of Lagrange polynomials above (see section 2.2.5). The polynomials were introduced in Manacoh to help with problems with high number of degrees of freedom. They reduce the computation time of the optimization process. The higher the degree of the polynomials is, the more accurate the results are, but the more time-consuming the optimization process is. On the contrary, the lower the degree of the polynomials is, the less accurate the results are, but the quicker the optimization process is. The efficiency and accuracy of Lagrange polynomials is tested on an example in section 4.4.3.

The basic properties of the Lagrange polynomial implementation are the followings:

- If n degrees of freedom are affected to a polynomial, then the maximum degree of the polynomial is $n-1$. Thus if only one DOF is affected to a polynomial, its degree is 0: the polynomial is a constant. The optimization process will have this constant vary.
- Affecting various DOFs to a same polynomial of degree 0 is an easy way to ensure that all those degrees of values will have equal values.
- Using a different polynomial for each node-DOF and branch-DOF is the same as not using any polynomial.
- The polynomials must either all node-DOF or all branch-DOF
- If the user chooses manually its polynomials, it should always respect two basics principles:
  - gather inside a same polynomial the same kind of branch (hoop forces in one, meridian force in another etc.)
  - choose for the variable of the polynomial a variable that vary regularly along the degrees of freedom. For example do not choose `num` if the indexes of the nodes or the branches are not consecutive. For hoop forces `phi` might be a good choice, for meridian thrusts at the bottom of a dome `theta` might be a good choice.

In the case of parametric geometries, the degree and variable of Lagrange polynomials can be defined in their own option window, that is accessible from the main parametric geometries window.

Manual control of degrees of freedom

The user can create scroll-bars for specific degrees of freedom, in order to visually follow on the thrust network the effect of the related degree of freedom change. At any time after the equilibrium has been computed, the user can click on button `Create scrollbar for DOF`, enter the index of the degree of freedom. Manacoh will create the scrollbar next to the value of the related degree of freedom in the interface. The scrollbars will be deleted if an automatic optimization procedure is launched.

2.5 Graphical output

2.5.1 Excel charts

Figures produced by Manacoh are Excel charts, with shapes such as text-boxes, lines, arrows etc. superimposed on those charts. While the charts themselves should be accurate enough, there is sometimes small offsets between the real position of a shape and its printed position on the chart.

In order to have a optimum working space, the user should minimize Excel ribbon [10], or work in full screen. To switch to full screen view, click on the View tab in the ribbon, and then select Full Screen.

2.5.2 Accuracy

Outside of the vicinity of the nodes, the intrados and extrados poly-lines are approximate with respect to the real intrados and extrados. For that reason there is often an offset

10. See `http://office.microsoft.com/en-au/excel-help/minimize-the-ribbon-HA010166329.aspx`

between the representation of the joints and the intrados and extrados (see for example figure 2.6 on the right, page 21). This is just a matter of representation, and not a problem of accuracy or definition of the intrados and extrados for the calculus. For this reason, it might seems that some centres of pressure on the graphical output are slightly outside the joints, when in reality they are located on the joint. The definitive answer to know if a centre of pressure is inside or outside the joint is not the graphical output, but the numerical results. The geometrical coefficient of safety of the related joint conveys that information with precision.

2.5.3 Exporting graphical results

The figures can be exported via button `Export graphs` on the graphical user interface. The images are exported in gif format and in vector image format emf in a sub-folder `Export` of the working folder. They might also be exported in pdf format, if Inkscape [11] is installed on the user's computer.

The user should not try to print directly the figures, because the figures will be stretched (a circle will become an oval).

2.6 Excel and VBA errors

2.6.1 Introduction

The user of Manacoh should have a minimum working knowledge of Excel. No knowledge of VBA is required, but some common errors may occur when first using Manacoh if some files of VBA and Excel are not found by the program (Add-in solver and VBA references). We give below some solutions that can be used in most cases.

2.6.2 Common errors when first using Manacoh

Security alert Macros and ActiveX controls are necessary for Manacoh to run. They might be disabled when the user open the spreadsheet.

If a message bar with a security warning that indicates *Some active content has been disabled* appears when Manacoh spreadsheet is opened, the user can activate the macro by clicking on *Options...* and then on *Enable this content*

If buttons of Manacoh do not trigger any event, and no message bar appears, then the following procedure might help:

— Click on the Office button (round button, top left of the screen)
— Click on *Excel options*
— Click on *Trust Center*
— Click on *Trust Center Settings...*
— Select *Show the Message Bar in all applications when content has been blocked.* From now on Microsoft Excel will prompt the user when macros might be used.
— Confirm and go back to your spreadsheet

11. Inkscape is an open-source vector graphics editor. It can be downloaded at `www.inkscape.org`. Inkscape is executed via Manacoh in command line to convert the existing emf file in a pdf file.

— Close the spreadsheet, open it again, and follow the instructions given previously for the message bar

For more informations on macros and security, see `http://office.microsoft.com/en-au/excel-help/change-macro-security-settings-in-excel-HP010096919.aspx`

Solver is not installed Excel Solver add-in must be available for Manacoh to work. See the install procedure here: `http://office.microsoft.com/en-us/excel-help/load-the-solver-add-in-HP010021570.aspx`. For more informations on installing add-ins in Excel, see `http://peltiertech.com/WordPress/installing-an-add-in-in-excel-2007`

Reference is missing You need the following references to be activated in VBA for Manacoh to function:

— Visual Basic For Applications
— Microsoft Excel 12.0 Object Library or superior
— Microsoft Forms 2.0 Object Library or superior
— Microsoft Office 12.0 Object Library or superior

In order to check the reference, open the VBA window (`ALT+F11`), go to Tools menu, and select References. For more informations on Missing References in VBA, see `http://www.cpearson.com/excel/missingreferences.aspx`.

2.6.3 Common problems when using Manacoh

Errors messages when computing parametric geometry The creation of parametric geometries might trigger errors. Most of the time, they are due to ill-conditioned boundary conditions for φ_0, φ_1, θ_0, θ_1 etc. The following tips might help the user to find first a working geometry (error-free parametric geometry), from which he can progressively work towards his wanted geometry:

— increase thickness;
— increase the number of blocks;
— select meridian boundary nodes on extrados;
— keep default values for Lagrange polynomials.

The creation of pavilion vault is particularly subject to errors of the type “we haven’t found intersection point of face” (see section 4.8 page 101). The spherical vaults and helicoidal vaults are also subject to that kind of error when there is not enough blocks along axis $\theta\theta$. This is not per say an error: sometimes the intersection of a joint with the vertical plane passing through the branch of the joint is void (see section **??** page **??**). The joint scale factor might be useful to study this kind of geometry (see related option for parametric geometries page 19).

Excel is very slow Sometimes the execution of the algorithms is very slow for steps that should not take long (for exemple : creation of geometry). This happens when a same spreadsheet is used repeatedly to generate geometries. In that case, saving your file, closing and reopening the spreadsheet might solve the problem.

Solver Assume Positive If you use manually the solver, you might encounter errors if you use the option "Assume Positive" to ensure no-tension, since the boundary nodes vertical position might need to be negative.

2.6.4 Common errors when modifying the macros

Advanced users might want to add additional functionalities to Manacoh or modify default values from within the macros. Here are some common errors that might be triggered during the modifications.

Can't Enter Break Mode We use Active-X scrollbars in the interface. These have an advantage: they allow to dynamically see the changes on the graphs when the user scrolls. With non-active-X scrollbars, the change appear only when the user stop scrolling.

The Active-X scrollbars have a drawback: they prevent VBA from entering in break mode, thus making it difficult to debug. (see `http://support.microsoft.com/kb/155051/en-us`XL97: "Can't Enter Break Mode" Stepping Through a Macro). If you need to debug the code, you may need to comment the line `Call CreateOLEScrollbars` on module `b_CreateInterface`.

Runtime error 1004. select method of y class failed It seems that if the program is used too many time, the index of controls can reach their upper bound, causing the following errors :

— Runtime error 1004. select method of button class failed

— Runtime error 1004. select method of checkbox class failed

The easiest solution is to use a new excel file with Manacoh, and copy your data to this new file. Another solution is to create a new worksheet, copy all the data from the GUI worksheet to the new worksheet, including the macros that are specific to that worksheet, delete the GUI worksheet and rename the new worksheet as GUI.

Chapter 3

Theory

see Fantin [17]

Chapter 4

Worked examples

In short...

This chapter considers various examples taken from the scientific literature between 1774 and 2009. The principal hypotheses of each author will be exposed, and then we will try to reproduce their results. Most of these examples are pre-set examples in Manacoh, so that the reader can reproduce each study, and see how the results change if the hypotheses are modified
This chapter has a double goal. First to validate the results of Manacoh with respect to published results. Second to learn more from historic methods through their numerical replication.

4.1 Introduction

We expose in this chapter various worked examples to demonstrate the possibilities of Manacoh and validate its results. We will consider examples for which published results exist (memoires, thesis, articles etc.). It is also an opportunity to show, when possible, the translation in optimization terms, with the cost and constraints functions f, c_1 and c_2, of various historical studies.

This chapter is organized by type of structure and type of hypothesis. We will first study domes, considering successively frictionless joints, absence of hoop forces, presence of hoop forces. Then we will address the topic of semi-cylindrical arches. Finally, we will expose a short example on helicoidal stair.

Although there is an obvious risk of anachronism by studying all these authors with a numeric tool, we hope that this small studies will give the reader some additional insights in historic methods.

4.2 Domes with frictionless joints — Bossut 1774 - 1776

4.2.1 Introduction

Bossut publishes at the end of the XVIIIe century two memoires about the equilibrium of vaults (1774 [4] and 1776 [5]). In his first memoire Bossut exposes his theory for tunnel vaults. Concerning domes, his first memoire is limited to the equilibrium of their abutments. He states: "Mon objet, qui est de déterminer les dimensions que doivent avoir les pieds-droits des voûtes en dôme, pour l'équilibre, n'a rien de commun avec le travail de M. Bouguer [1]". In his second memoire, Bossut extends to domes his theory on tunnel vaults. The detail of Bossut's memoires are beyond the scope of this manual. Those memoires are described in Benvenuto 1991 [1, p.375-385]. Let us just remind the reader of Bossut's main hypotheses in the case of domes:

- geometry :
  - dome with axial symmetry
  - the width of the lune considered is infinitesimal (influence of width of the lune is not considered [2])
- forces :
  - no hoop force
  - no friction (forces are normal to joints — in Benvenuto: *smooth frictionless voussoirs* 1991 [1, p.377])

These hypotheses lead Bossut to a differential equation describing the relation between the geometry of the dome on the one hand (or to be more precise, the geometry of the surface of pressure), and the law of force on the other hand. This equation is written with modern

1. Bossut's memoires are written 40 years after Bouguer's 1734 memoire on domes (1734 [6]). Bouguer considers frictionless joints, and includes in his reasoning the action of hoop forces (see Paradiso et al. 2003 [32, p.1571]). However his numerical example corresponds to the dome in which the hoop forces were zero ("dimensions de la dernière de toutes les lignes courbes qui est propre à former des domes"). For more information on Bouguer's memoire, see Benvenuto 1991 [1, p.344], Radelet-de-Grave 1999 [34] and Paradiso et al. 2003 [32].

2. Note that in Como's example (that we will see in a short while) the fact that the studied slice has a magnitude of 1 rad ([9, p.197]) does not mean that the slice is not infinitesimal. 1 rad is just used in order to not mention this angle in the derivations of equations.

notation by Benvenuto (equation 12.11 [1, p.385]). Bossut makes the following remark about his equation for barrel vaults – which fully apply to his equation for domes:

> *This equation is the basis of all the problems we can propose on this subject. Now there are two principal questions to examine. One is to find the figure of the vault when we know the law of the forces that press the voussoirs; the other, on the contrary, is to find the law of the forces which must press on the voussoirs when the figure of the vault is known.*
>
> *Bossut translated by Benvenuto 1991 [1, p.381]*

In the first case, Bossut derives the equation of a pressure surface, using the following additional hypotheses about the law of forces:

— dead load only (vertical loads)
— load is applied on the pressure surface, not on the medium surface (implicit)
— load by square meter is constant (dome of uniform thickness and uniform specific weight)

Benvenuto shows that these hypotheses lead to the following equation for the pressure surface (see axes convention on figure 4.1):

$$y = \int_0^x \sinh\left(-\frac{u^2}{2A} + B_1\right) \mathrm{d}u + B_2 \tag{4.1}$$

with A, B_1, B_2 three unknowns, that can be related to their physical meaning:

— $\sinh B_1$ is the pressure surface slope at the crown
— B_2 is the pressure surface vertical position at the crown
— A is directly related by equation 4.2 to the horizontal thrust of the lune h, through the radius at the base r_m and the unit load per mean surface $t\rho$. h is expressed per unit length of the base circumference.

$$h = t\rho A / r_m \tag{4.2}$$

4.2.2 Practise and theory

Benvenuto states about Bossut, Mascheroni and Salimbeni: "These authors pay only superficial attention to the possible applications of their results. Instead they favor a spectacular analytical elaboration which rejoins the subject of arches and domes to the theme of flexible curves through a rather narrow analogy between their corresponding differential equations." Indeed **in Bossut's theory, the dome mid-surface and the pressure surface are superimposed** [3]**.**

Within Bossut's framework, if the geometry of the dome is given, the law of force (*p. ex.* the weight of the voussoirs) needed for stable equilibrium without friction is a result. If the weight of the voussoirs is known, the necessary geometry for equilibrium is a result. However it is not possible to draw any conclusion related to stability if the geometry **and** the law of force are given, except this one in the case of hemispherical domes: the equilibrium equation of Bossut is not satisfied. Bossut is aware of this difficulty, and writes about differences between theory and practise:

3. Bossut's equilibrium equations just state that the reciprocal forces that act from one voussoir to another are normal to joints and opposite. Benvenuto writes "In fact, this is not a sufficient condition ; we have to decide through which point in the bed between the voussoirs the forces F_{1l}, F_{2r} pass. But this further condition may be disregarded, since Bossut implicitly reduces the arch to a curved line tangential to the compression forces at each of its points." 1991 [1, pp.376,378]

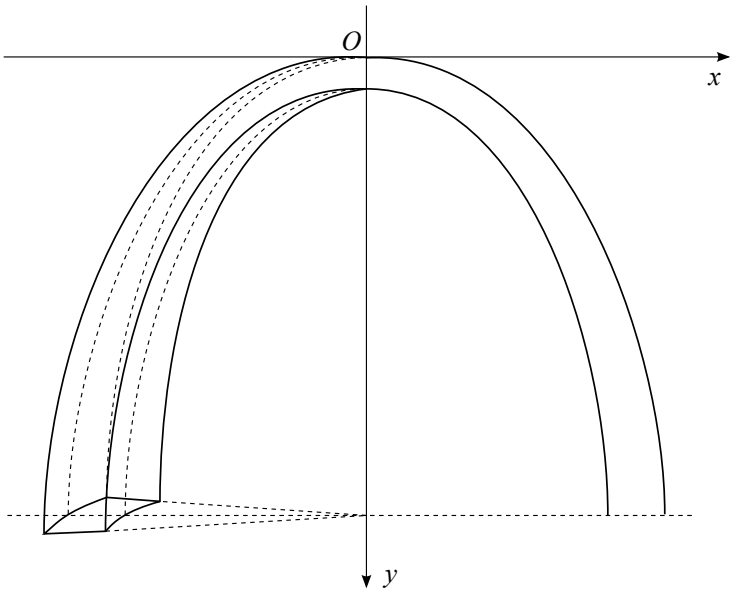

Fig 4.1 – Convention of axes used by Benvenuto 1991 [1]
Schematic figure adapted from fig. 2 in Bossut 1776 [5]

VI. Il est indubitable qu'une voûte, de quelque nature qu'elle soit, auroit toute la solidité dont elle est susceptible, si conformément aux principes établis dans le Mémoire précédent & dans celui-ci, les forces qui poussent les voussoirs, & la figure de l'intrados, étoient tellement combinées, que toutes les autres parties fussent en équilibre, de proche en proche, sur l'étendue de chaque ceintre partiel; car alors elle n'auroit pas plus de tendance à se rompre en un point qu'en un autre; & les pieds-droits n'auroient à soutenir que la seule poussée résultante des voussoirs extrêmes qui s'appuyent sur eux; mais cet état d'équilibre mathématique & rigoureux, est comme impossible à obtenir dans la pratique. ***Quel que soit l'objet d'une voûte, les circonstances locales de son emplacement ne permettent presque jamais de soumettre la figure & les poids dont elle est chargée, aux proportions que nous avons indiquées****; d'ailleurs les erreurs inévitables qui se glissent dans la coupe des voussoirs, les liaisons du mortier qui varient souvent d'un voussoir à l'autre, les changements de figure que la voûte subit pendant la construction [...] sont autant de nouvelles causes qui troublent & altèrent les mesures déterminées par la théorie. Mais s'il est impossible de parvenir sur ce sujet à des résultats précis,* ***la théorie peut du moins éclairer la pratique jusqu'à un certain point , elle peut diriger l'attention du Constructeur vers les parties qui ont le plus besoin d'être renforcées, relativement à l'état physique & actuel des choses****.*

Bossut 1776 [5, p.591]

4.2.3 Minimal thrust

Como gives an example of application of formula 4.1 (2013 [9, p.195-201]). He searches the minimum horizontal thrust of a hemispherical dome. There is one important difference here with Bossut's original theory: the pressure of surface and the mean surface of the studied dome are distinct. They are distinct, but sufficiently close so that any pressure of surface that is subjected to the unit load [4] of the mean surface is considered representative of an equilibrium solution (stable or not) for the dome. Como implicitly consider that the offset between the real location of the weights (near the mean surface) and their location in the calculus (on the surface of pressure distinct from the mean surface) can be neglected.

4. "We define the unit load g per mean surface of the dome; approximately the same load will act on the unknown surface [of pressure]"Como 2013 [9, p.195]

Of these surface of pressure, only those that lie within the intrados and extrados of the hemispherical lune are considered representative of a stable equilibrium.

We will keep in the following the notations of Benvenuto for clarity. Como considers the following additional conditions to determine the unknowns that define the surface of pressure that represent the minimum thrust (see figure 4.2):

— symmetry condition at the crown: $\frac{dy}{dx}(x=0) = \sinh B_1 = 0$ thus $B_1 = 0$

— according to Como "the pressure curve must pass through the extrados point at the dome key (necessary in order for it to represent the minimum thrust state)": $y(0) = B_2 = 0$

— the pressure surface touches the intrados near the haunches at a unknown point $(\overline{x},\overline{y})$ of unknown co-latitude $\overline{\varphi}$.

The first two conditions give directly $B_1 = 0$ and $B_2 = 0$. Determining A with the third condition requires additional derivations, and notably the following trigonometric equality:

$$\sinh\left(\ln\frac{1+\sin\psi}{\cos\psi}\right) = \tan\psi \quad \forall\psi \in \mathbb{R} \tag{4.3}$$

We don't know an analytic formula for A, but its value can be evaluated numerically through a simple iterative procedure (see table 4.3). Then, the minimum thrust h_{min} is calculated thanks to equation 4.2. Como gives for A the following estimate (implicitly for $t \ll r_m$):

$$A = r_m^2(0.257 - 0.337 \cdot t/r_m) \quad \text{if } t \ll r_m \tag{4.4}$$

The pressure surface corresponding to Como's choice of boundary conditions is given on figure 4.4 on the left. This choice of boundary conditions is incorrect, since the pressure surface exits the extrados near the crown. **Contrary to cylindrical arches, no hinge forms at the crown in the case of hemispherical dome's minimum thrust.** This false hypothesis is taken by Como and others (see for example Lau 2006 [28, p.58]) in order to **estimate** the minimum thrust. It is a sensible approximation in order to simplify the analytical calculus and find a first estimate value for the minimum thrust. It is remarkable that even with these particularly favourable boundary conditions with respect to simplification of calculations, the derivations are not trivial in this case. True boundary conditions would lead to even more complex derivations. Indeed, Como states that "real domes are generally much more complex than the simplified case analysed here, so graphical approaches are frequently adopted" 2013 [9, p.201].

Como gives an numerical example for a hemispherical dome with the following parameters: $t = 2\text{m}$, $r_m = 20\text{m}$, $\rho = 1.8\text{t/m}^2$. With Como's estimate, the minimum horizontal thrust of the lune per unit length of the base circumference is[7] $h_{min} = t\rho A/r_m = t\rho r_m(0.257 - 0.337t/r_m) = 16.07\text{t/m}$. Since here the condition $t \ll r_m$ is not fulfilled the calculus procedure described on table 4.3 gives a different result ($\overline{\varphi} = 74{,}19°$, $A = 84.63\text{m}^2$, and finally $h_{min} = t\rho A/r_m = 15.23\text{t/m}$). If we considered an alternative thickness $t = 0.2\text{m}$, the two methods would give a closer result (1.83t/m and 1.82t/m for Como's formula and our procedure respectively).

5. We will show in the following that the pressure curve described on this figure is not possible: the pressure curve would exit the masonry near the crown at the extrados.

6. This image was not produced with Manacoh. It was computed with equation 4.1 and the procedure described on table 4.3.

7. Como indicates 15.79t/m in his text. Maybe the difference comes from the value taken for the weight of mean surface: we take $t\rho$, but Como does not indicate which value he took for the weight per mean surface. He only gives the density.

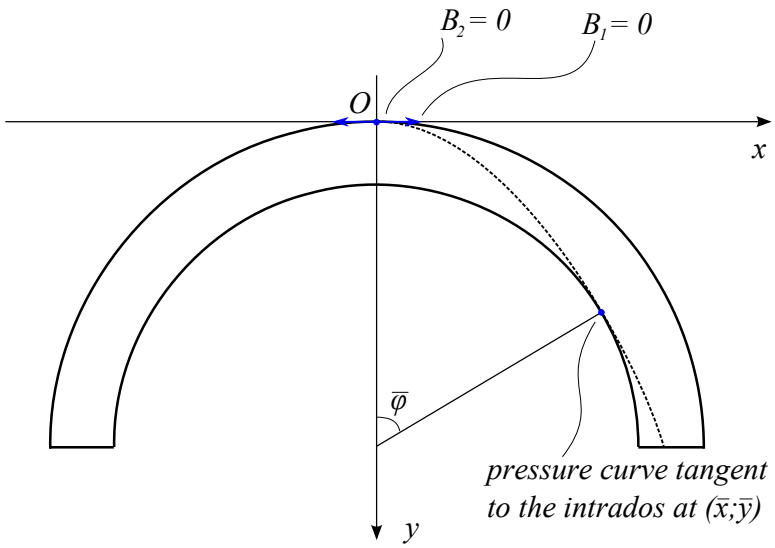

Fig 4.2 – Como's hypotheses related to minimum thrust of a lune [5]
This is only a schematic figure

1. Choose a rough estimate for $\overline{\varphi}$. For exemple $\overline{\varphi} = 70°$
2. Calculate $\overline{x} = r_i \sin \overline{\varphi}$, which means $\overline{x}$ is on the intrados
3. Calculate $A = \frac{\overline{x}^2}{2} \left(\ln \frac{1+\sin \overline{\varphi}}{\cos \overline{\varphi}} \right)^{-1}$ which means the curve is tangeant (with a gap) with the intrados
4. Calculate $\overline{y} = \int_0^{\overline{x}} \sinh \left(-\frac{u^2}{2A} \right) \mathrm{d}u$ (we compute this value with a Riemann integral in `VBA`)
5. Check if $\overline{y}$ is above or below the intrados, and choose a new estimate for $\overline{\varphi}$ accordingly. Go back to step 2. If the estimate is sufficiently close to the intrados, end of the procedure.

Fig 4.3 – Calculation steps for finding A

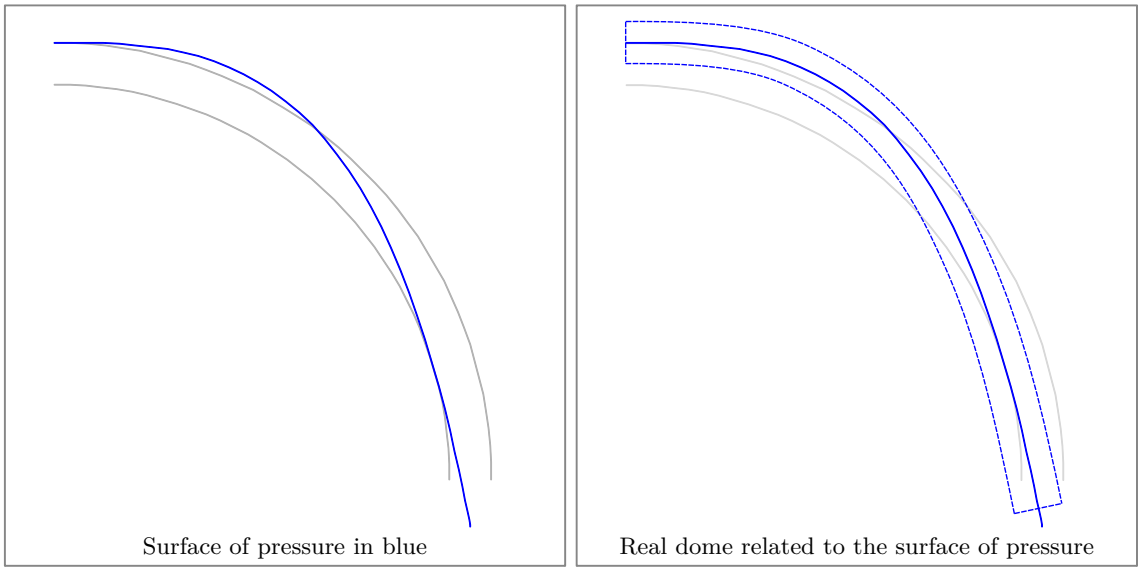

Fig 4.4 – Surface of pressure related to the minimum thrust with Como's method [6]

4.2.4 Comparison with network analysis

Research of Como's minimal thrust

In order to find a minimal thrust similar to the one found using Como's method, we use the following optimisation problem with Manacoh:

— $f = h$, horizontal thrust of the lune
— $c_1 > 0$ with $c_1 = z - z_i + \epsilon$
— $c_2 > 1$ with $c_2 = CSG$, excluding interior nodes near the crown

The results are given on figure 4.5. We found a minimum thrust 12% lower than with Como's method. This difference is linked to the difference between the two modelisations:

— Weights position: in thrust network analysis the weights are located on the voussoir centres of gravity. In Como's approach they are located on the surface of pressure.
— Weights values: even if the total mass of the studied lune seems to be the same in our example, the repartition of this total mass in the lune is different. There is more mass near the crown in Como's approach than in thrust network analysis. This might be the main reason for the superior thrust with Como's approach.

Our computed solution contains friction, while the previous result 15.23t/m while Como's solution is frictionless. However this difference is not relevant here, because it is related to the orientation of the joints. It is more meaningful to compare the surface of pressure (in blue) and the line of thrust on figure 4.5 (bottom left drawing). Despite the differences of the methods, their global shape is analogous.

As noted above, we must stress out here that this method for calculating the minimum thrust is only an estimate. **We are trying to fit a blue curve into an hemispherical dome (figure 4.4 on the left), whilst this blue curve is in fact related to a non hemispherical dome (figure 4.4 on the right).** The minimum thrust was an excuse to study Bossut's and Como's methods. We will see in the section on arches a more effective and accurate method to determine the minimum thrust with a thrust network software.

Geometry:
lune of a spherical dome
15 voussoirs
mean radius $r_m = 20$
thickness $t = r_m/10$
$\varphi \in [0°; 90°]$
$\theta \in [-0.05°; 0.05°] \Leftrightarrow \delta\theta = 0.1°$
$\rho = 1800$

Optimization:
$f = h$, horizontal thrust of the lune
$c_1 > 0$ with $c_1 = z - z_i + \epsilon$
$c_2 > 1$ with $c_2 = CSG$, excluding interior nodes near apex

Results with Manacoh:
$h_{min} = 13.54\text{t/m}$
$W_{tot} = 72.06\text{t/m}$
$h_{min}/W_{tot} = 0.1879$

Result with Como's approach:
$h_{min} = t\rho A/r_m = 15.23\text{t/m}$
$h_{min}/W_{tot} = 1/y' = 0.2116$
$W_{tot} = h_{min}y' = 71.98$

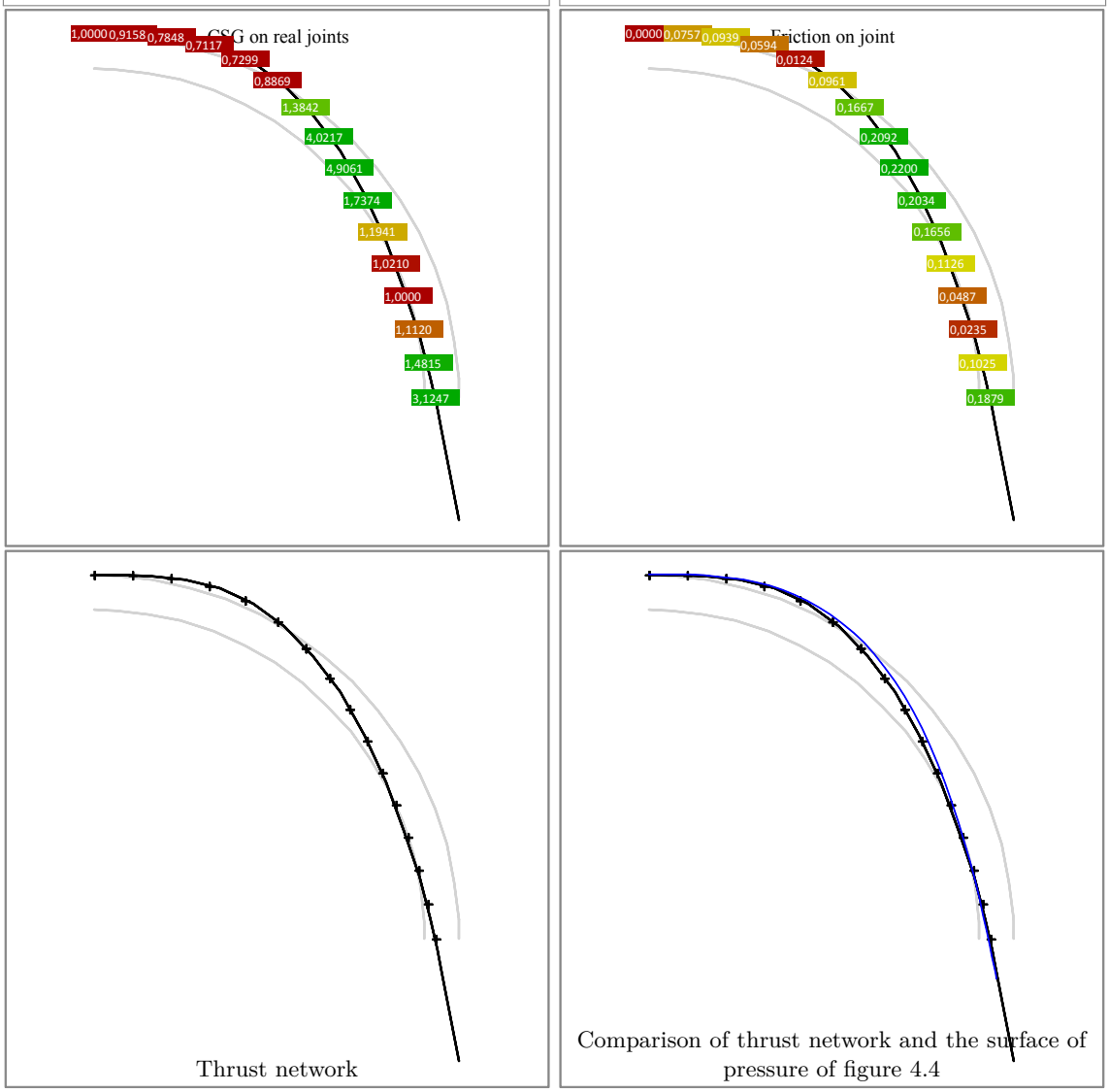

Fig 4.5 – Minimal thrust of a lune
Comparison of Como's method and network analysis

Extrapolating Bossut's hypotheses with network analysis

To conclude on Bossut's memoire, let us consider a theoretical question. What conclusion is reached with a network analysis, using Bossut's hypotheses, concerning a hemispherical dome whom both the geometry **and** the law of force is known. The studied structure will be a thin lune ($\theta_1 - \theta_0 = 0.1°$), without hoop forces, and with an angle of aperture strictly lower than 90° (since there cannot be a solution without friction if $\varphi_1 = 90°$). The orientation of the joints is fixed: joints are normal to the mid-surface.

The results are the followings. They are illustrated on figure 4.6.

1. Since we use a symmetry condition at the crown, there is only two degrees of freedom here: the thrust of the dome and the position of the boundary node at the bottom. The sum of the squared friction forces (forces tangent to the joint) only depends on the thrust of the dome, and not on the boundary node vertical position [8]
2. No equilibrium solution can be found without friction forces at the joints for the geometries considered ($\varphi_0 = 90°, r/t = 5$ and 10).
3. The equilibrium solution that represents the lowest sum of squared friction forces lies within the masonry (first optimization on the thrust with $f = \sum T_i^2$, and then second optimization on the boundary node vertical position with $f = \min \mathrm{CSG}_j$)

This example shows that form finding would be needed to study with the thrust analysis method frictionless domes. Moreover, it is not possible to find a frictionless solution for hemispherical domes subjected only to dead load, with joints normals to the mid-surface.

8. This result is experimentally observed with Manacoh. It can be proven theoretically by considering the polygon of forces: if the polygon is fixed, the friction forces are fixed. The polygon does not depend on the position of the lowest boundary node. Thus the friction forces do not depend on the position of the lowest boundary node.

Geometry:
lune of a spherical dome
15 voussoirs
mean radius $r_m = 20$
thickness $t = r_m/10$ and $t = r_m/5$
$\varphi \in [0°; 80°]$
$\theta \in [-0.05°; 0.05°] \Leftrightarrow \delta\theta = 0.1°$
$\rho = 1800$

Optimization:
1st: $f = \sum T_i^2$
2nd: thrust is fixed, and we use $f = \min \mathrm{CSG}_j$

Results:
No frictionless equilibrium solution can be found for the 2 considered geometries
First optimization on friction forces determines the thrust for which the sum of squared friction forces is minimum.
Second optimization centres the solution within the masonry, while the sum of squared friction forces is kept constant (to its minimum).

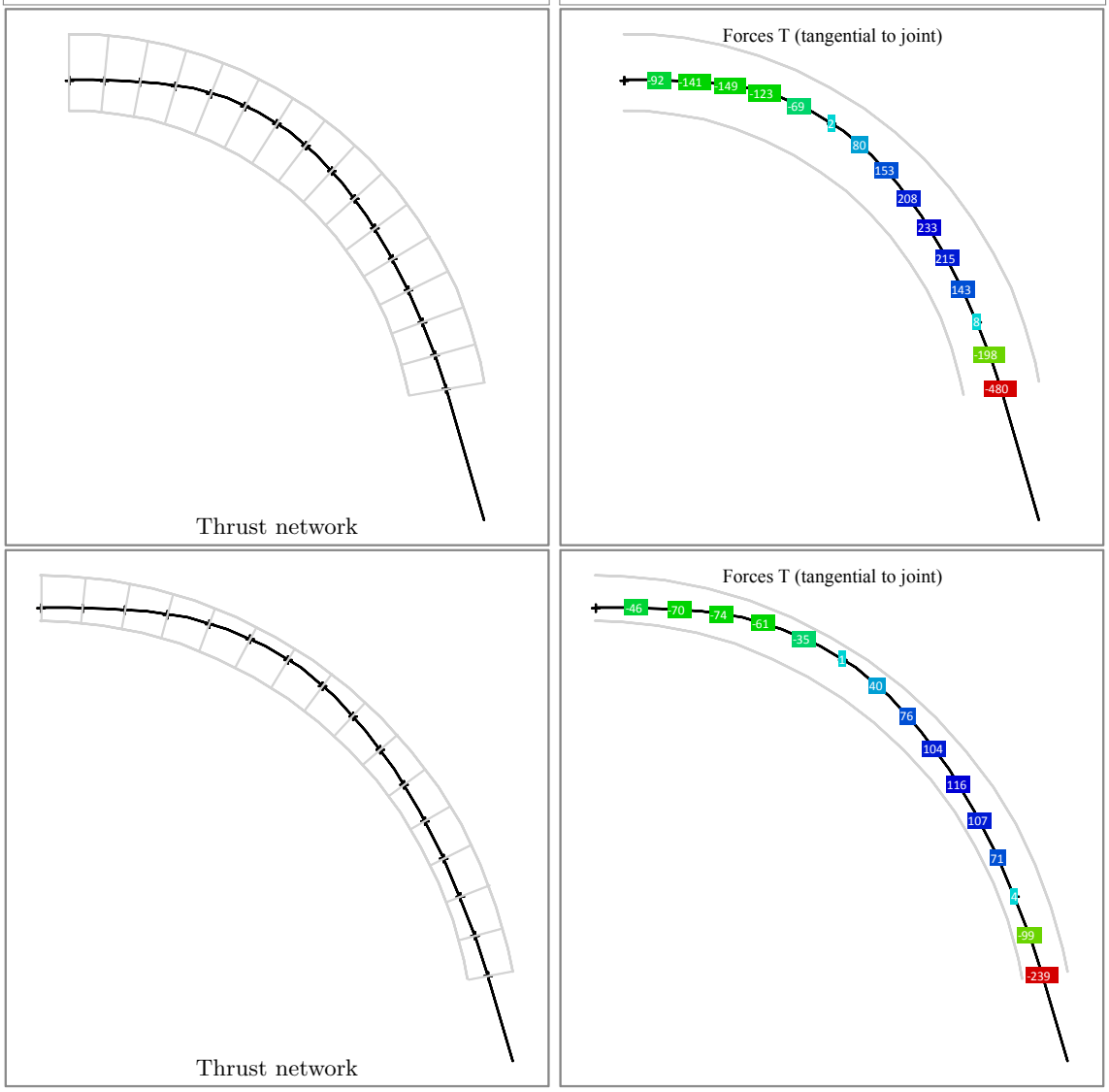

Fig 4.6 – Hemispherical lunes, with research of frictionless equilibrium solution

4.3 Domes without hoop forces

4.3.1 Durand-Claye 1867 - 1880

All possible thrust lines

Durand-Claye publishes in 1867 an analytic-graphical method to study the stability of barrel vaults [14]. His 1880 memoire extends his method specifically for domes [15]. Instead of drawing single thrust lines, Durand-Claye draws areas of stability that represents all possible thrust lines, regarding three criteria (rotational equilibrium, translational equilibrium, limited resistance in compression). The three following citations from Foce et Aita 2003 [18] will give the reader an insight on Durand-Claye's methodology [9]:

— "This methodology preserves the non-deterministic character of the limit analysis and, at the same time, embodies the main aspect of the elastic analysis by imposing a restriction on the stress level."

— **"Instead of searching for a single thrust line regarding it as the *actual* one, all the admissible thrust lines have to be determined."**

— "As it is easy to understand, we find here a particular form of what we modernly call the safe theorem of limit analysis. This theorem is implicit also in the stability conditions of Persy, Navier and Michon. The only difference is that now the range of admissible solutions is restricted in order to consider the actual strength of materials. In this sense Durand-Claye's method is a rational mediation between limit and elastic approach."

Durand Claye's method gives a coefficient of safety related to the admissible compressive strength. He used himself the term of coefficient of safety and stated: "C'est une sorte de coefficient de stabilité, donnant la mesure de la hardiesse des ouvrages.". Again, let us turn to Foce et Aita regarding the definition of this coefficient: "Let $r_i s_i p_j q_j$ be the area of stability for the admissible compressive strength σ^*. By decreasing this strength, the area $r_i s_i p_j q_j$ will correspondingly decrease and shrink to a point for a certain ultimate value σ_u. The ratio σ^*/σ_u provides the safety coefficient of the real arch according to Durand-Claye's method." (2003 [18]).

Despite its theoretical qualities, Durand-Claye's method did not spread among practitioners. Résal writes in 1887: "la méthode de M. Durand-Claye [...] ne semble pas avoir pénétré dans la pratique. Nous en trouvons la raison [...] dans la complication et le nombre des constructions graphiques qu'entrainent la méthode" [38, p.99]. Delbecq adds in 1983 that "Cette méthode est arrivée trop tôt, car en l'absence de moyens de calculs puissants, elle nécessite des calculs très laborieux que les méthodes graphiques n'ont pas réussi à simplifier" [12, p.76]. Durand-Claye himself was well-aware of the difficulty of his method, and concluded his 1867 memoire by the following remark.

> *Nous ne nous dissimulons pas qu'en pratique les soins d'exécution et les détails de main-d'œuvre peuvent avoir aux yeux des constructeurs infiniment plus de valeur que les remarques un peu théoriques que nous avons présentées. Mais nous croyons qu'il n'est jamais inutile d'étudier avec quelque soin des problèmes se rattachant plus ou moins directement aux faits d'expérience.*
>
> *Durand-Claye 1867 [14]*

9. See also Smars's PhD thesis on the use of stress criteria and on Durand-Claye's method (2002 [39, p.48]).

Durand-Claye's coefficient of safety

The use of these areas of stability requires a good knowledge of theory of curves. Manacoh allows the user to retrieve Durand-Claye results (to some extent) without this knowledge. The rotational equilibrium and translational equilibrium are transcribed respectively with the geometrical coefficient of safety and the friction coefficient. As for the compressive strength of the masonry, a transcription of Durand-Claye's criterion is given by Foce et Aita in modern notation [18, p.903]. With h the length of a joint, S its area, and σ_0 the "admissible" compressive strength, this criterion can be transformed in a local coefficient of safety at any joint:

$$\mathrm{CSDC}_j = \frac{\sigma_0 S}{Nh} \begin{cases} \dfrac{h^2}{h + 6|M/N|} & \text{if centre of pressure in middle third} \\ \dfrac{3}{4}\left(h - 2\,|M/N|\right) & \text{if centre of pressure outside middle third} \end{cases} \tag{4.5}$$

As for the other coefficient of safety that we exposed in the chapter regarding theory, this local coefficient of safety at the joints, is transformed in a global coefficient by taking the minimum value for the whole structure. It is a function of the degree of freedom of the system ζ_{dof}, and denoted here $\mathrm{CSDC}_{\mathcal{J}}$.

$$\mathrm{CSDC}_{\mathcal{J}} = \min_{j \in \mathcal{J}} \mathrm{CSDC}_j \tag{4.6}$$

Durand-Claye's coefficient of safety is computed by optimization: it is the maximum value reached by the global coefficient of safety when the degrees of freedom vary ζ_{dof}. It is not a function, but a value denoted $\overline{\mathrm{CSDC}_{\mathcal{J}}}$:

$$\overline{\mathrm{CSDC}_{\mathcal{J}}} = \max_{\zeta_{\mathrm{dof}}} \mathrm{CSDC}_{\mathcal{J}} = \max_{\zeta_{\mathrm{dof}}} \min_{j \in \mathcal{J}} \mathrm{CSDC}_j \tag{4.7}$$

In theory the use of this coefficient of safety should allow the calculation of the same coefficient of safety that Durand-Claye gives in his publications. However, we were not able to fully validate this result. Examples are given below.

Comparison with Delbecq's coefficient of safety

If the centre of pressure lies outside the middle third, the coefficient of safety of Durand-Claye and the Delbecq's coefficient of safety are related in a simple manner, as long as the same maximal compressive strength is used:

$$\mathrm{CSDC}_j = 3/4 \cdot \mathrm{CSDC}_j \tag{4.8}$$

However Durand-Claye uses the admissible compressive strength, whereas Delbecq uses the characteristic compressive strength. Furthermore these values are related to different security theory of masonry strength. Durand-Claye's admissible strength is the tenth of the mean strength. An admissible solution for Durand-Claye is thus a solution in which his coefficient of safety is 1 or above 1. However Delbecq use the characteristic strength, and states that the stresses should be at least inferior to 3 times the characteristic stress (in some specific cases 2.5 times). An admissible solution for Delbecq is thus a solution in which his coefficient of safety is 3 or above 3.

Durand-Claye's and Delbecq's coefficients of safety can thus be compared theoretically, but a great care must be taken regarding the signification of the maximum stress used for their definition.

Simple example of an arch

Manacoh cannot calculate several thrust lines at the same time, but it can explore the domain of thrust lines corresponding to the criteria used by Durand-Claye. We need to use the following constraints:

— translational equilibrium : take $c_1 = \max |T/N| - \mu > 0$ — *c.-à-d.* sliding of blocks is considered

— rotational equilibrium : take $c_2 = \mathrm{CSG}_{\mathcal{J}} = \min \mathrm{CSG}_j > 1$ — *c.-à-d.* thrust line inside masonry

We checked that we can find the same results as Foce and Aita for the two criteria on the example given in their paper of 2003 [18]. This example can be loaded in the pre-set examples of Manacoh. See the results on figure 4.7.

It would be interesting to compare the results obtained with the thrust network method regarding the coefficient of safety of Durand-Claye for masonry strength. He gave numerical examples of his method in his paper of 1867 [14]. However the examples considered are arches with fill, that cannot be generated with the actual implementation of the parametric geometries. We will only consider this coefficient of safety in the case of domes below.

Geometry:
cylindrical arc
15 voussoirs
mean radius $r_m = 10$
$K = r_e/r_i = 1.1136 \Leftrightarrow t/r = 0.1075$ thickness
$t = 2r_m(1.1136 - 1)/(1.1136 + 1)$
$\varphi \in [0°; 90°]$
$y \in [0; 1] \Leftrightarrow \delta y = 1$
$\rho = 1000$
`MeridianBoundaryNodesOnExtrados = True`

Optimization:
$f = -\min \mathrm{CSG}_j$
No constraints

Results with Manacoh:
The geometrical coefficient of safety is 1.0003, so that the criterion of rotational equilibrium is reached (collapse mode figure 7 in Foce et Aita) The maximum friction coefficient is reached at the base (0.3953), so that the arch is stable only if $\mu > 0.3953$ (collapse mode figure 8 in Foce et Aita)

The network analysis produced the same results as Foce et Aita (2003 [18]).

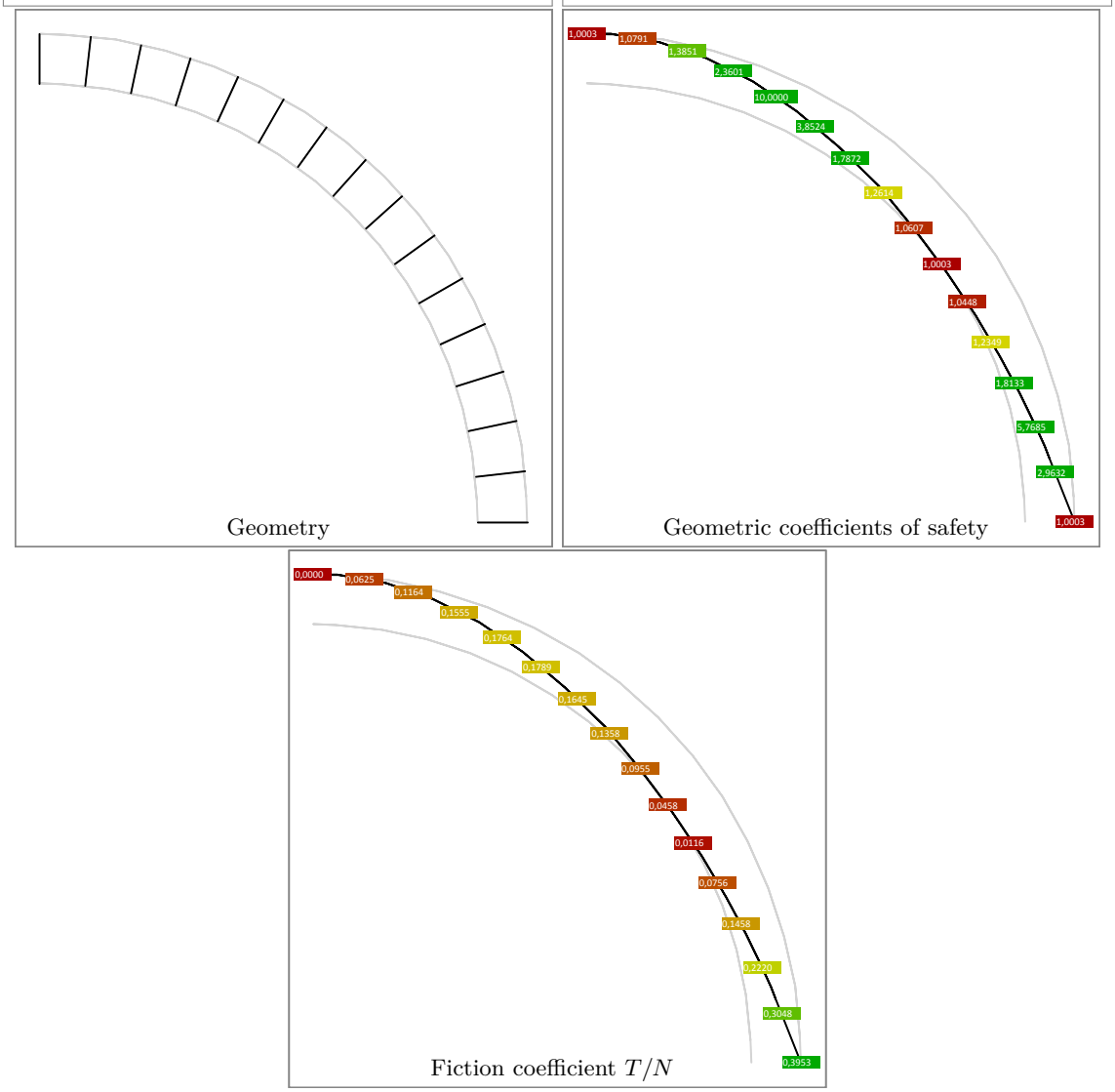

Fig 4.7 – Minimum thickness of an arch
Comparison of Foce et Aita (2003 [18]) and network analysis

Bramante's dome project for Saint-Peter

Durand-Claye analysis of domes is similar to the one of a cylindrical arch of variable depth. The hoop forces are not considered, except for the keystone or in the case of *oculi*. He applied his method to Bramante's dome project for Saint-Peter (see figure 4.8).

Durand-Claye considers a lune of the dome of angle $\delta\theta$ in plan. This lune is then cut in 7 large blocks denoted I to VII. These blocks are sub-divided in smaller blocks by Durand-Claye to allow calculation of the weights and centres of gravity. He shows that all quantities are proportional to $\delta\theta$. Centres of gravity of the blocks are approximated to be centres of gravity of the surface on the drawing, and the volumes are the surfaces multiplied by the distance of the centre of gravity to the central axis.

Durand-Claye assessed the stability of the part formed by the voussoirs II to VI (in blue on figure 4.8), and loaded by the voussoir I (oculus and lanterne), with his analytic-graphic method. For a compressive strength of 10kg/cm^2, the area of stability exists. For a compressive strength of 5kg/cm^2, the area of stability does not exist [10]. Thus there is a compressive strength situated between 5kg/cm^2 and 10kg/cm^2, that correspond to an area of stability reduced to a single point. Durand-Claye estimates that it should correspond to a strength of 7 or 8kg/cm^2, but it does not draw this area of stability reduced to a point. Thus Bramante's dome is stable with a coefficient of security between $\frac{10}{8}$ and $\frac{10}{7}$ (between 1.25 and 1.43) regarding the compressive strength according to Durand-Claye (1880 [15, p.435-437]).

We tried to reproduce this result. We considered a lune with $\delta\theta = 1\,\text{rad}$ to simplify calculations (it is in fact an infinitesimal angle [11]). Using Durand-Claye's drawing, we derived the weights, centres of gravity, and surface of joints S given on table 4.1.

Block	x_G (m)	y_G (m)	$W/10^3$ kg
I metal	0.85	44.09	16
I masonry	5.65	25.96	620
II	10.57	17.2	241
III	14.48	14.64	376
IV	17.77	11.36	509
V	20.66	6.79	915
VI	22.75	2.2	890
VII	24.65	-1.09	835
total	—	—	4402

Joint	R (m)	h (m)	$S = Rh$ (m^2)
I - II	8.43	2.28	19.24
II - III	12.6	2.6	32.81
III - IV	16.26	2.95	47.89
IV - V	19.18	3.29	63.06
V - VI	21.98	4.04	88.71
VI - VII	22.84	4.2	95.86

Table 4.1 – Bramante's dome for St-Peter in Rome by Durand-Claye
Characteristics measured on figure 25 of figure 4.8

The total weight that we computed for the whole dome (blocks I to VII) is $2\pi/1\,\text{rad} \cdot 4402 \cdot 10^3 = 27657 \cdot 10^3$kg, which is close to the value given by Durand-Claye

10. For a compressive strength of 5 kg/cm^2 the area is not reduced to one point but really does not exist at all (see the drawing on the bottom left of figure 25 of Durand-Claye). Durand-Claye's exact words are "la voûte de Bramante pourrait donc tenir en équilibre avec des matériaux résistant à 10 kilog. de pression par centimètre carré, avec une tendance à produire des efforts maxima vers les reins à l'intrados; elle ne pouvait être stable avec des matériaux résistant à 5 kilog. Il suffisait donc de la constituer avec des matériaux, pierre et mortier, donnant une résistance moyenne de 7 à 8 kilog. pour la réaliser dans de bonnes conditions de stabilité." The estimation of the coefficient of safety 10/5=2.0 in Foce and Aita's article seems to be inexact (2003 [18, p.904]).

11. "courbes de pression construites après suppression du facteur commun $d\theta$ et remplacement des poids réels par les poids obtenus en multipliant les sections par leur distance à l'axe." p430 and 433 — see also remark on "infinitesimal" angles of 1 rad in Bossut's example

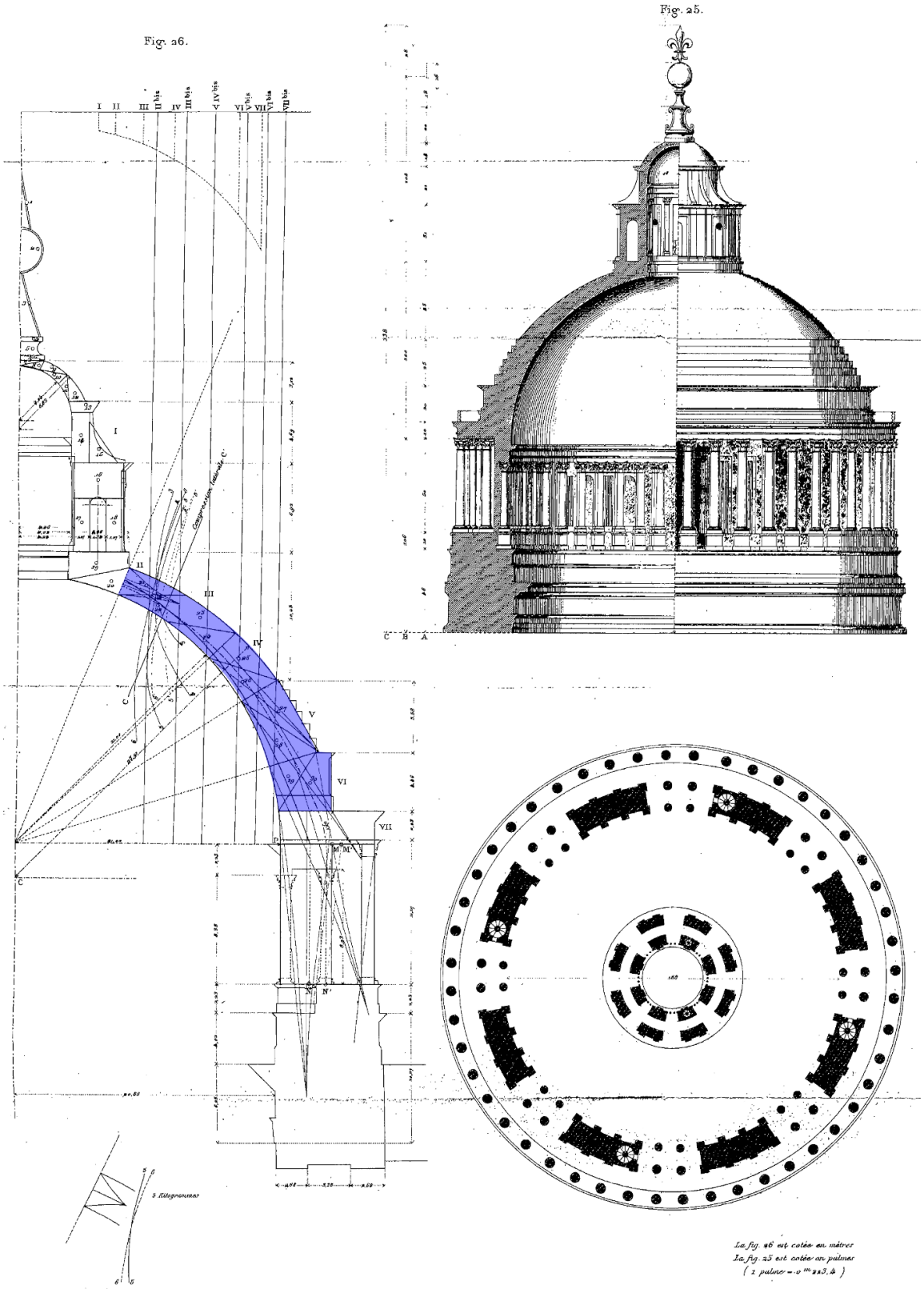

Fig 4.8 – Study of Bramante's dome for St-Peter in Rome — from Durand-Claye 1880 [15]

($27511 \cdot 10^3$kg — relative error of 0.5%). However there seems to be an offset between the centres of gravity that we computed and Durand-Claye's centres of gravity [12].

Our work-procedure is given below.

1. compute manually the weights and centre of gravity (partial results given on table 4.1).
2. measure on Durand-Claye's drawing the position of the joints, that are necessary to compute the coefficients of stability.
3. input manually these values in Manacoh
4. optimize with $f = -\mathrm{CSDC}_{\mathcal{J}}$, with an additional constraint so that the weight of the oculus and lantern is taken into account. This constraint is $w^* = W_I$, with w^* the vertical boundary force at the top of the lune.

The results are given on figure 4.9. We found a coefficient of safety $\overline{\mathrm{CSDC}_{\mathcal{J}}}$=1.16, which is inferior to the actual coefficient of safety given by Durand-Claye (between 1.25 and 1.43). The results are thus not completely satisfactory (error margin 10-20% with respect to Durand-Claye's result). In order to improve this result, a deeper understanding of Durand-Claye's centres of gravity would be needed.

12. There is a small approximation on Durand-Claye's determination of the centres of gravity of triangles that are indicated by small circles on his drawing, that can be detected easily using a CAD software. More importantly, it seems that the horizontal position of centres of gravity of the large blocks are indicated by the verticals I, IIbis, IIIbis, IVbis etc. above his figure 25 of the dome – see figure 4.8. At the top of the drawing there is a regular offset of around 0.30m between our computed values, and the positions of Durand-Claye's vertical. However, this verticals are not exactly vertical, which might be a graphical trick of unknown purpose, or a distortion due to the scanning of the original book. We were not able to reach a conclusion regarding the precision of our computed centre of gravities with respect to Durand-Claye's.

Geometry:
Parametrical geometries cannot be used. This geometry cannot be loaded among Manacoh's pre-set geometries.

Geometry was measured on Durand-Claye's drawing and entered manually in Manacoh — see table 4.1

Optimization:
$f = -\mathrm{CSDC}_{\mathcal{J}}$
additional constraint: $w^* = W_I$, with w^* the vertical boundary force at the top of the lune, and W_I the weight of block I (lantern)

Results:
We found a coefficient of safety $\overline{\mathrm{CSDC}_{\mathcal{J}}}$=1.16, which is inferior to the actual coefficient of safety given by Durand-Claye (between 1.25 and 1.43). The joint IV-V should be with the lowest coefficient of safety according to Durand-Claye [15, p.435] but it is not the case in our solution.

The line of thrust related to $\overline{\mathrm{CSDC}_{\mathcal{J}}}$=1.16 is rather centred (in the middle third everywhere except at the base). It should not be compared to the two lines of thrust drawn by Durand-Claye, because they are used for the verification of the drum and are not related to the coefficient of safety for the dome [15, p.438]).

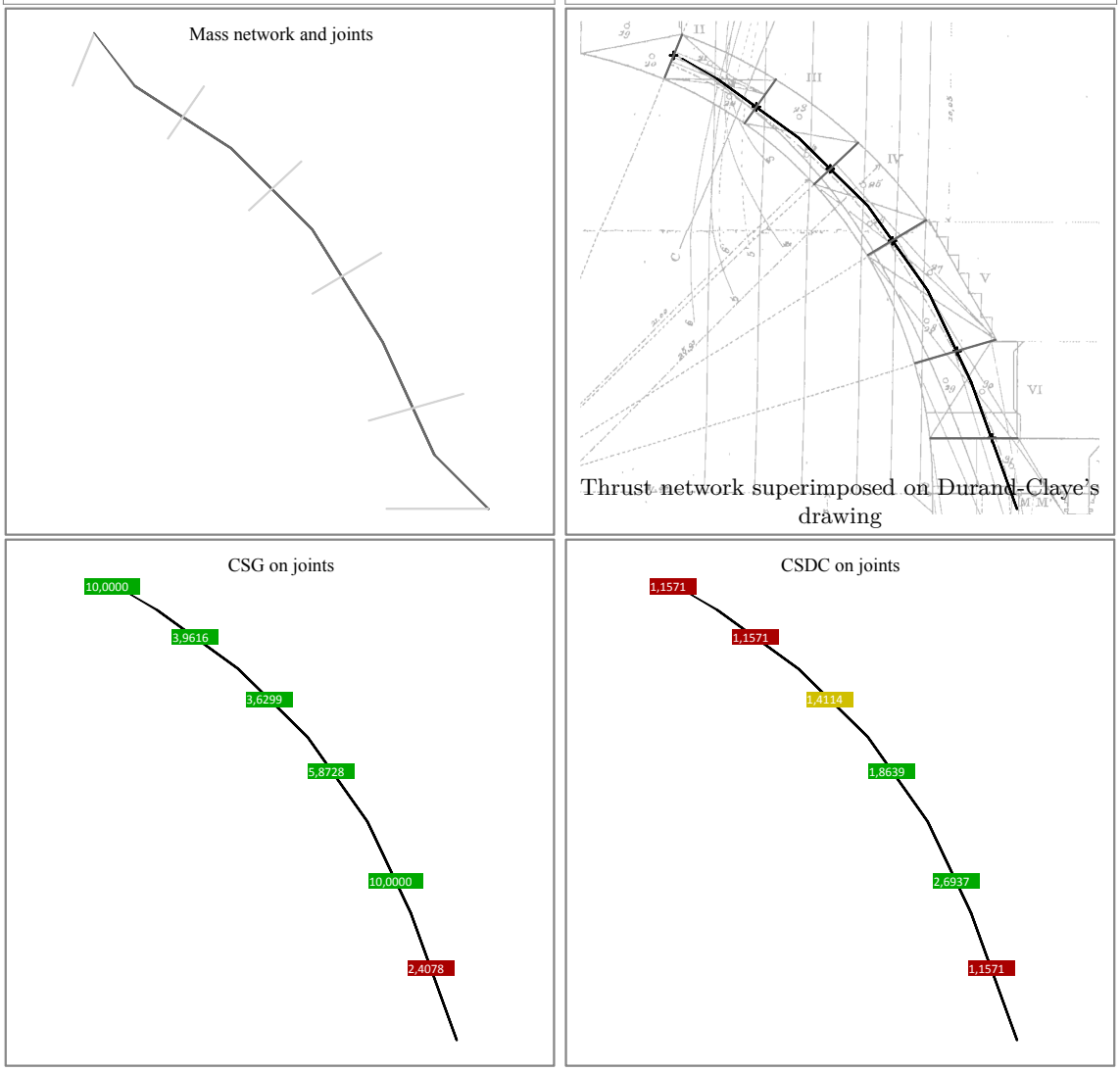

Fig 4.9 – Study of Bramante's dome for St-Peter in Rome by Durand-Claye (1880 [15]) Comparison with network analysis

4.3.2 Eddy 1877

The graphical method of Eddy is often cited in the literature related to masonry domes (*p. ex.* Parasido et al. 2003 [32], Lau 2006 [28], Huerta 2008 [26], Zessin 2012 [44]). In his 1877 book, Eddy first studies spherical *domes of metal* [16]. The studied domes are so thin that the "thrust along a meridian section is necessarily in a direction tangent to that section at each point of it". The graphical method he uses for thin domes of metal considers hoop forces, in compression and tension, in order to constraint the line of thrust to lie on the median surface of the studied lune (see figure 4.10 bottom left).

However, the graphical method that Eddy exposes for masonry domes does not take into account hoop forces. His example consider a lune cut in voussoirs with an elegant technique [13] that gives voussoirs of equal weight and an direct estimate of their centre of gravity. He draws a first line of pressure (that he calls *curve of equilibrium* [16, p.57]) corresponding to the following conditions:

1. the line of resistance lies on the extrados of the middle third at the base
2. the polar distance (*c.-à-d.* horizontal thrust in the lune) used corresponds to the highest horizontal thrust in a dome analysed with the method he described for metal domes (with hoop forces)

From this arbitrary [14] start point, he devised a technique to draw an updated thrust line that lies within the middle third. The outline of his polygon of forces is given on figure 4.10 (bottom right). This figure can be misleading, since the cubic curve on the right of the figure is used only for metal domes, and has no effect on the final result of the construction for masonry domes. It can be seen that no hoop forces are used for the curve of equilibrium, since the lines ww_n and vv_n of the equilibrium polygons are vertical.

Eddy states that "the proposed construction applies equally to domes of any different form generated by the revolution of the arc of some curve about a vertical axis: such forms are elliptic, parabolic or hyperbolic domes, as well as pointed or Gothic domes, etc." [16, p.53-54].

The first *curve of equilibrium cc* and the revised *curve of equilibrium ee* in Eddy's construction are lines of pressure, not lines of thrust. However, he states clearly that the points to be considered are "the point of application of the resultant pressure", so that he checks in reality the line of thrust. Eddy constrains the pressure centres to lie in the inner third of the masonry [15]. However his technique can be directly adapted to get rid of the middle third rule.

As a result, Eddy's graphical construction for masonry domes is a graphical way to find a possible line of pressure with centres of pressure lying in the inner third of the masonry, without hoop forces. Let us consider this property stated by Eddy: "A dome of which the thickness is one fifteenth of the internal diameter, is almost exactly stable." (Eddy 1877 [16,

13. " If we consider a lune between meridian planes making a small angle with each other, the center of gravity of the parts of the lune between the conical joints lie at g_1, g_2, etc. on the horizontal midway between the previous horizontals. These points are not exactly upon the central line aa, but if the number of horizontals is large, the difference is inappreciable. We assume them upon aa. That they fall upon the horizontals through d_1, d_2, etc., midway between those through u_1, u_2, etc. is a consequence of the equality in area between spherical zones of the same height." Eddy 1877 [16, p.56]

14. *Arbitrary* start point in the sense that the final solution does not depend on this start point.

15. "It has been shown by Rankine, Woodbury and others, that for perfect stability, — *c.-à-d.*, in case no joint of the arch begins to open, and every joint bears over its entire surface, — that the point of application of the resultant pressure must everywhere fall within the middle third of the arch ring." (Eddy 1877 [16, p.47])

p.57-58]). We computed with Manacoh the results corresponding to such a lune (see results on figure 4.11). We found indeed a geometrical coefficient of safety of 2.90, somewhat lower than 3 as stated by Eddy (*almost exactly stable* with the middle third rule).

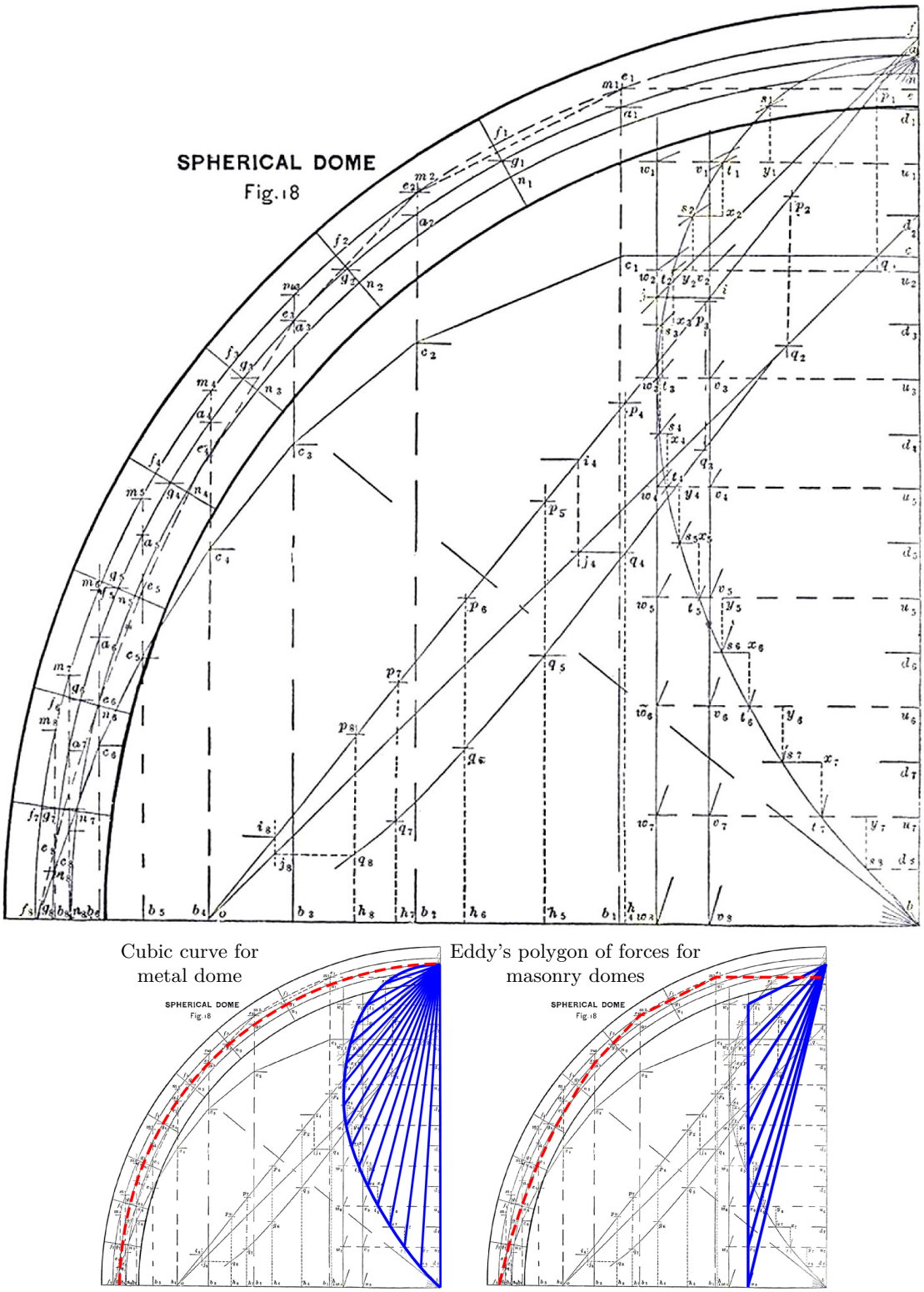

Fig 4.10 – Graphical constructions of Eddy 1877 [16]

Geometry:
lune of a spherical dome 15 voussoirs
mean radius $r_m = 10$
thickness $t = r_m/8$
$\varphi \in [0°; 90°]$
$\theta \in [-0.5°; 0.5°] \Leftrightarrow \delta\theta = 1°$
$\rho = 1000$
`MeridianBoundaryNodesOnExtrados = True`

Optimization:
$f = -\min \mathrm{CSG}_{\mathcal{J}}$

Results:
$\overline{\mathrm{CSG}_{\mathcal{J}}} = 2.9050$ (Eddy: $\overline{\mathrm{CSG}_{\mathcal{J}}} = 3$)
$t/R/\overline{\mathrm{CSG}_{\mathcal{J}}} = 0.04303$ (see section about Heyman results on minimum thickness of spherical domes without hoop forces)

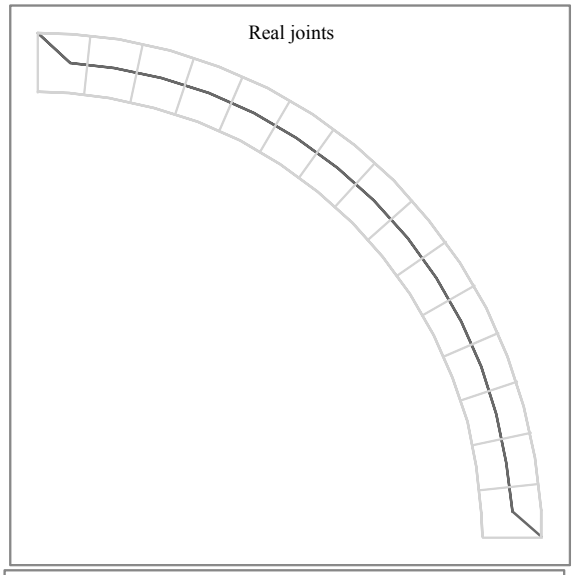

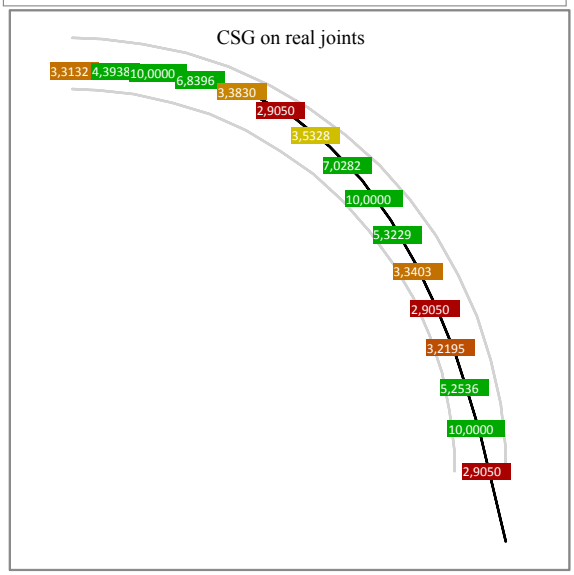

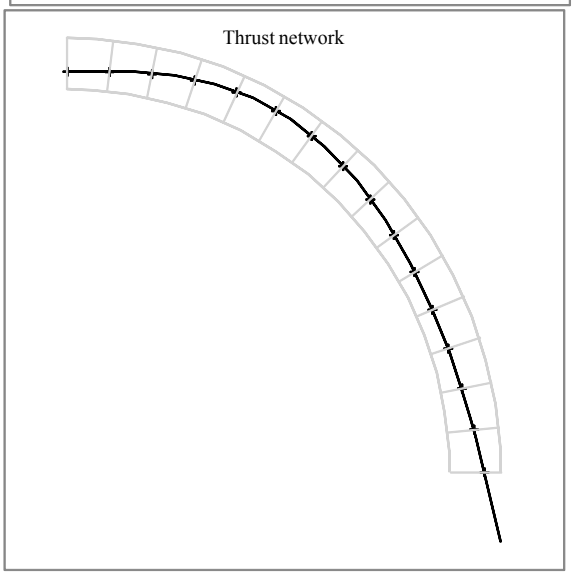

Fig 4.11 – Minimum thickness of a spherical dome without hoop forces
Comparison of Eddy 1877 and network analysis

4.3.3 Minimum and maximum thrust — Lau 2006

Lau studies in her master thesis both spherical domes and *pointed domes*, with a method that she called the *modified thrust line method*. She provides *abaques* of the minimum thrust with respect to the angle of embrace φ_1 and angle of the lune in plan $\delta\theta$.

Lau's modified thrust line method considers the hoop force. She states that "hoop forces are critical in the stability of spherical dome geometries with thickness-to-radius ratios less than 0.05". However she also points out that "the presence or absence of hoop forces has little impact on the H/W ratio [minimum thrust to weight ratio] as long as the modified thrust line method finds a satisfactory thrust line" (2006 [28, p.75,188]). Furthermore, Lau gives the following linear **estimate** for the minimal thrust to weight ratio for spherical domes. This estimate gives values within 20% of the results of Lau's modified thrust line method.

$$H_{min}/W = -0.583\varphi_1 + 1.123 \tag{4.9}$$

We compare in this section the results given by Manacoh **without hoop forces** with the one computed by Lau **with hoop forces**. Let H_{min} and H_{max} be respectively the minimum and maximum thrust of the considered lune, and W its weight.

The results found with Manacoh are given on figure 4.12 and 4.13. For the minimum thrust, the result with thrust network analysis is within 5% of Lau's estimate. The maximum thrust calculated without hoop forces (figure 4.13) is just a theoretical consideration, since hoop forces would necessarily appear in that case.

Geometry:
lune of a spherical dome 15 voussoirs
mean radius $r_m = 10$
thickness $t = r_m/10$
$\varphi \in [0°; 90°]$
$\theta \in [-7.5°; 7.5°] \Leftrightarrow \delta\theta = 15°$
$\rho = 1000$
`MeridianBoundaryNodesOnExtrados = True`

Optimization:
$f = H$
$c_2 = \mathrm{CSG}_{\mathcal{J}} = \min \mathrm{CSG}_j > 1$

Results:
$H_{min}/W = 0.19561$
Lau 2006 : $H_{min}/W = -0.583\varphi_1 + 1.123 = 0.2072$

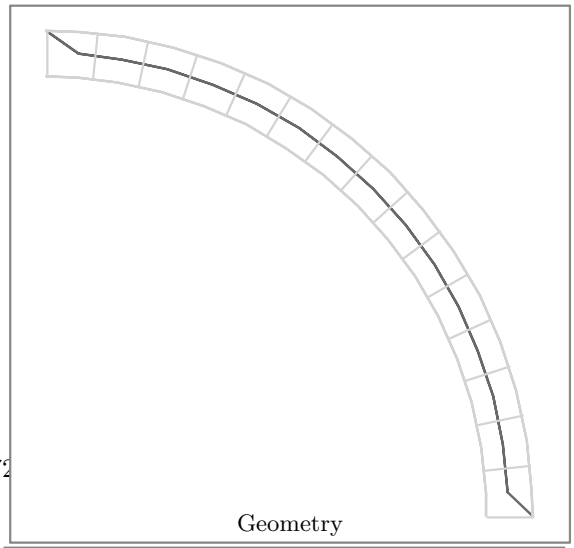

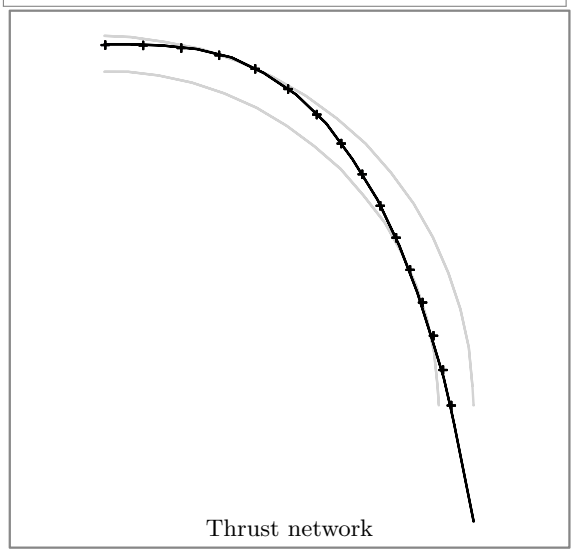

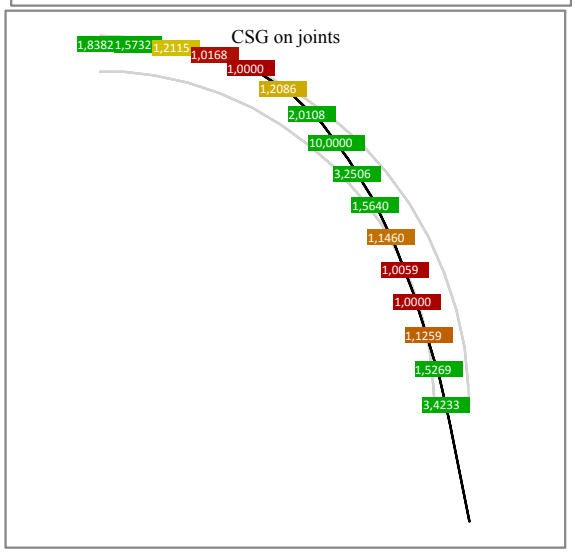

Fig 4.12 – Minimum thrust of a spherical dome without hoop thrust
Comparison of Lau 2006 and network analysis

Geometry:
lune of a spherical dome 15 voussoirs
mean radius $r_m = 10$
thickness $t = r_m/10$
$\varphi \in [0°; 90°]$
$\theta \in [-7.5°; 7.5°] \Leftrightarrow \delta\theta = 15°$
$\rho = 1000$
`MeridianBoundaryNodesOnExtrados = True`

Optimization:
$f = -H$
$c2 = \mathrm{CSG}_{\mathcal{J}} = \min \mathrm{CSG}_j > 1$

Results:
$H_{max}/W = 0.27951$

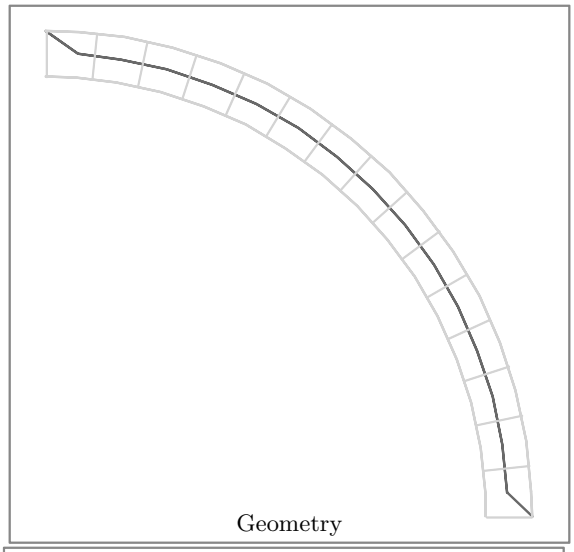

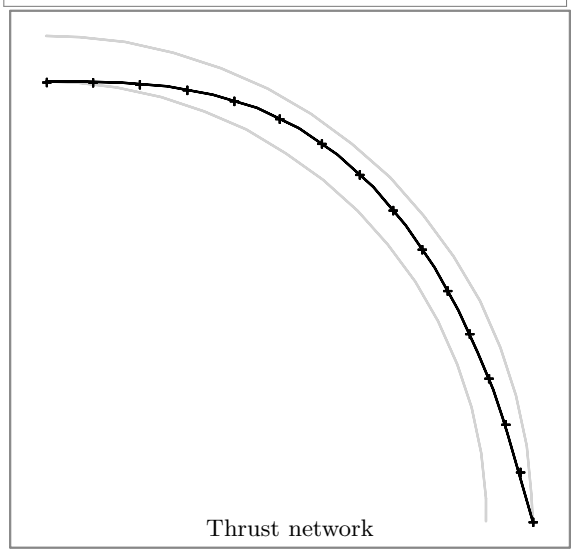

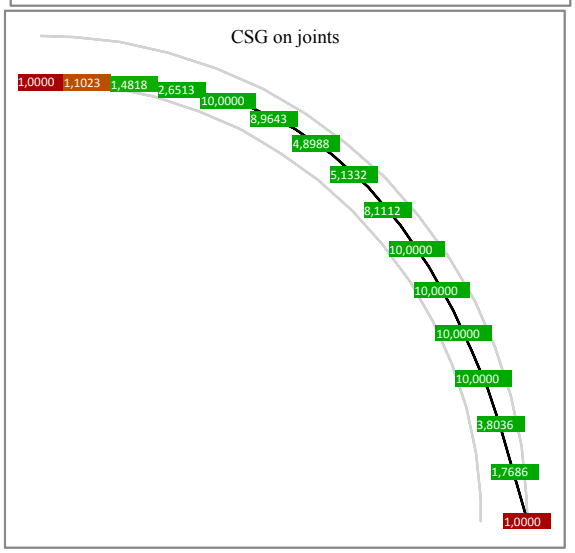

Fig 4.13 – Maximum thrust of a spherical dome without hoop forces

4.4 Domes with hoop forces - towards membrane analysis

4.4.1 Introduction

This section will address the analysis of dome lunes, for which hoop forces are considered. The hoop forces are compressive in the upper part of hemispherical dome, and in tension in the lower part. Compressive only hoop forces are taken into account by Wittmann (1879), Föppl (1881) (see Huerta 2008 [26]). We will explore this question using a later author on that subject, Wolfe (1921). We chose this author mainly because his theory was implemented by students at the MIT, and thus numerical results are available for comparison with the thrust network analysis.

4.4.2 Wolfe 1921

"Graphical analysis — a text book on graphic statics"

Wolfe gives in his book *Graphical analysis — a text book on graphic statics* an *approximate* method to investigate the stability of domes (1921 [43, p249-253]).

> *The method given above is approximate, corresponding somewhat to the method of investigating an arch by drawing a polygon which will follow the centre line as nearly as possible. However the results obtained from this method will be instructive, and when modified by good judgment, should be satisfactory for designing.*
>
> *Wolfe 1921 [43, p.253]*

Wolfe constructs his line of thrust from a starting point on the middle of the joint at the crown, and choose progressively the hoop forces necessary to constrain the line of thrust to *follow the centre line as nearly as possible.* He considers the case of a dome that can support negative hoop forces (reinforced concrete dome), and the case of *ordinary masonry dome.* For the latter, when the hoop force ceases (lest they would become negative), the line of thrust leaves the *centre line.* For that reason the depth of the blocks near the base must be larger in order to find a stable solution (on figure 4.14, compare the four voussoirs of the base on the left with tension allowed, and on the right without tension allowed).

The volume of a voussoir (called *division* by Wolfe) is approximated by the product of three lengths that are graphically constructed: u v w (see figure 4.14). However, the figure 4.14 taken from Wolfe's book shows that he does not neglect the influence of φ on the centre of gravity position: $\varphi_G \neq 0.5(\varphi_0 + \varphi_1)$. The centre of gravity of the voussoir closest to the crown is clearly distinct from the point corresponding to $0.5(\varphi_0 + \varphi_1)$.

The geometry of this example can be loaded among the pre-set examples of Manacoh. The exact parameters used by Wolfe are not known, we use an estimate of the ratio t/r, measured on his drawing. We use the exact centre of gravity location. In order to find a solution similar to Wolfe's reinforced concrete dome (hoop forces positive and negative), the optimization set-up is:

— Cost function [16]: $f = \sum_{k=1}^{n_i+n_b} (z_k - z_{G,k})^2$. Both interior and boundary nodes.
— No constraints.

16. With this cost function choice, the thrust network lies on the mid-surface. The line of thrust however, does not lie exactly on the mid-surface with this choice.

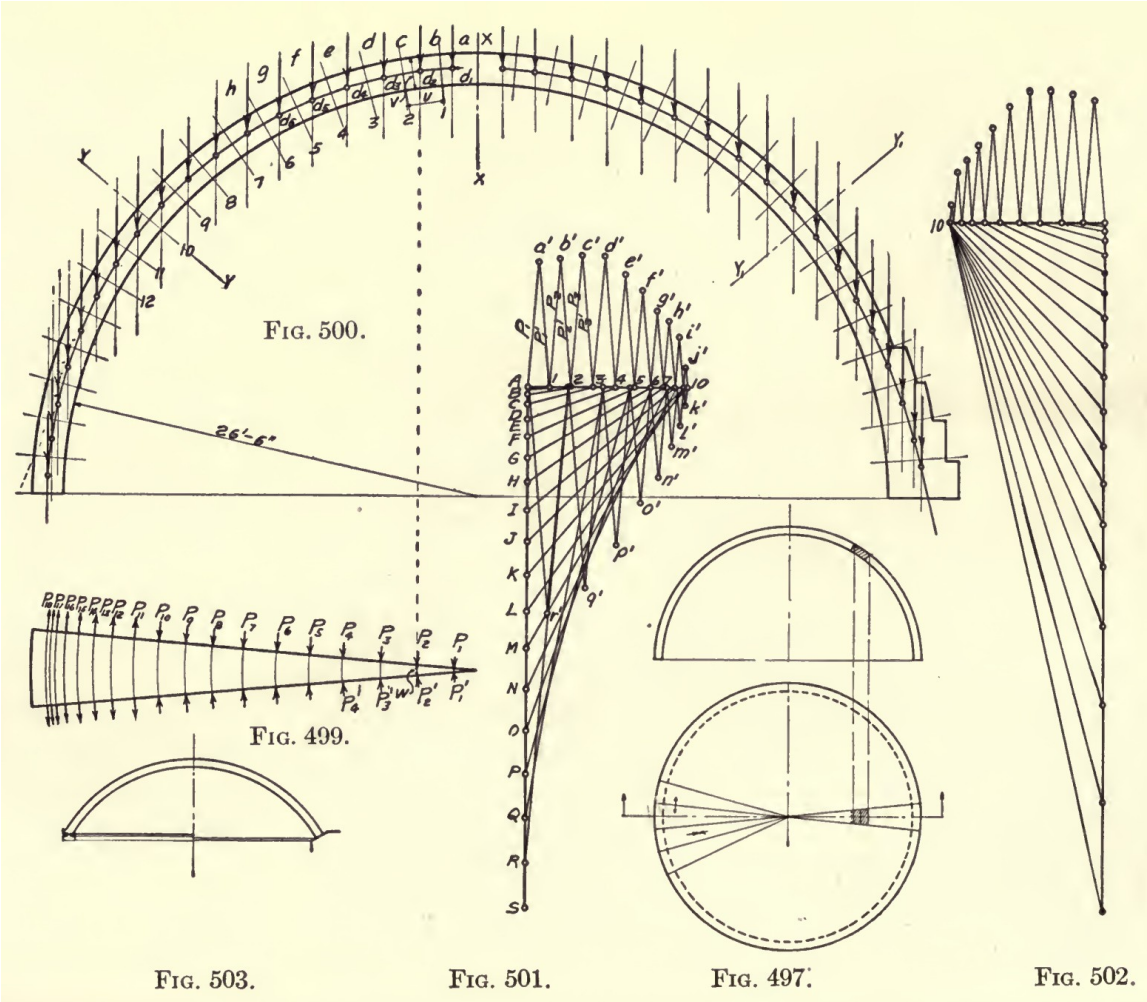

Fig 4.14 – From Wolfe 1921 [43]

The results related to a dome without tensile capacity are obtained using the previous solution as a starting point. Then the negative hoop forces are set to zero, and finally, the optimization set-up is:

— Cost function: $f = (z_i - z_{G,i})^2$, with i the index of a node in the compressive hoop forces area.

— No constraints.

— Hoop forces are fixed, the only variable is the lower boundary node vertical position.

Manacoh seems to give under these conditions similar hoop forces as Wolfe's method, though no quantitative comparison could be made (see figures 4.15, 4.16 and 4.17. It is interesting to note the following points on this example with Wolfe's method:

— On Wolfe's drawing, the hoop forces are an increasing function towards the crown, except for the last four voussoir near the crown. This fact is clearly visible on Fig. 501 and Fig. 502 of the figure 4.14. This behaviour is unique, with respect to the other examples that we will present later (Lau, Reese and membrane analysis). This behaviour could be replicated only for the last voussoir with thrust network analysis (see figure 4.16).

— If the centre of gravity are approximated, the decrease of hoop force does not appear at all near the crown (see figure 4.16)

Geometry:
lune of a spherical dome 18 voussoirs
mean radius $r_m = 10$
thickness $t = r_m/14$
$\varphi \in [0°; 90°]$
$\theta \in [-5°; 5°] \Leftrightarrow \delta\theta = 10°$
$\rho = 2000$

Optimization:
With hoop forces: $f = \sum_{k=1}^{n_i+n_b} (z_k - z_{G,k})^2$
Without hoop forces: see details in the text.

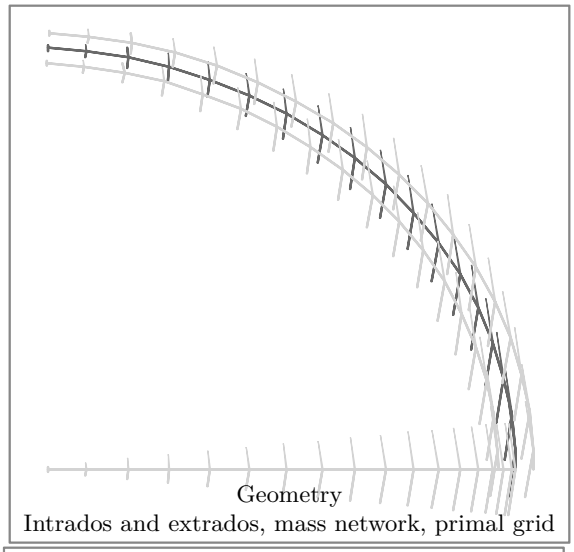

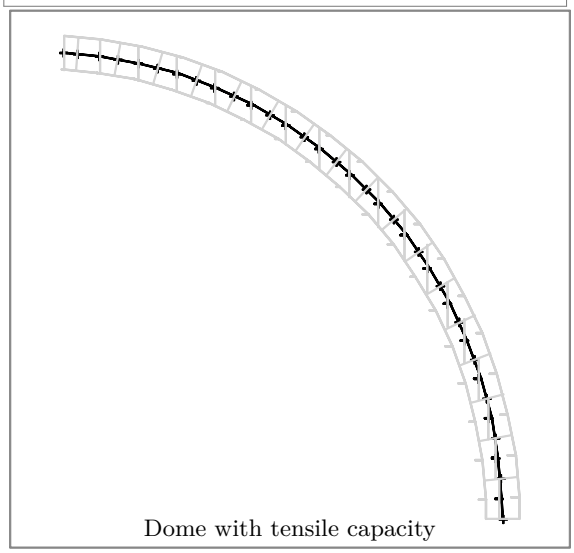

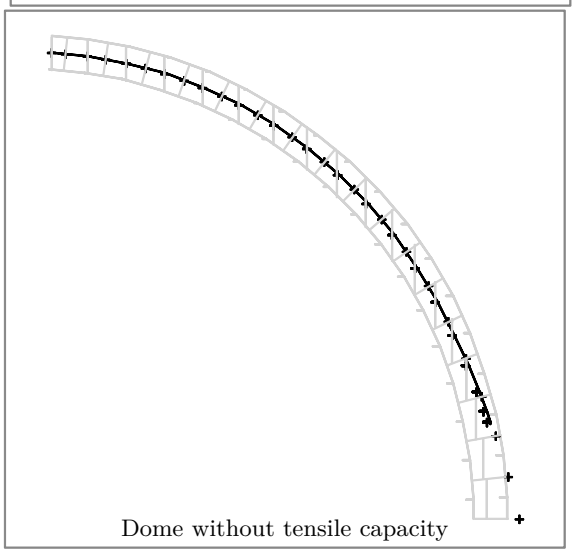

Fig 4.15 – Study of a lune with and without hoop forces, with Wolfe's method
Comparison with network analysis

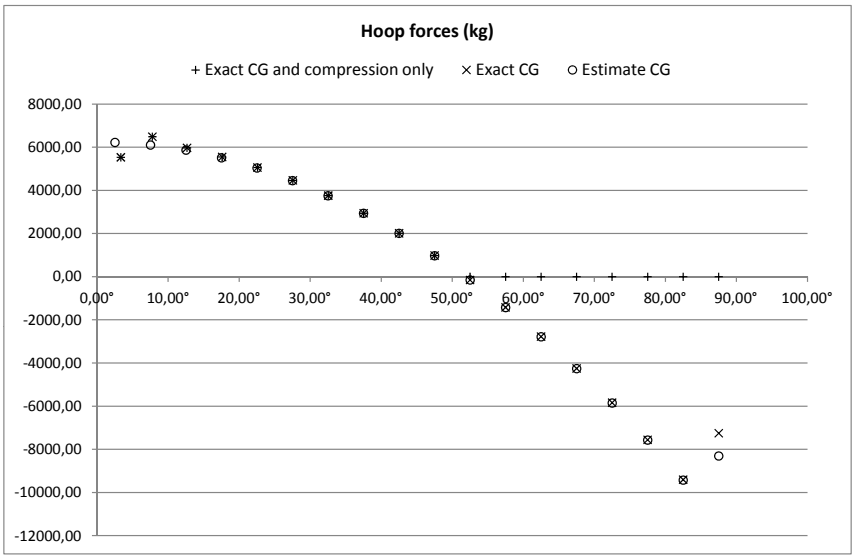

Fig 4.16 – Study of a lune with and without hoop forces
Hoop forces

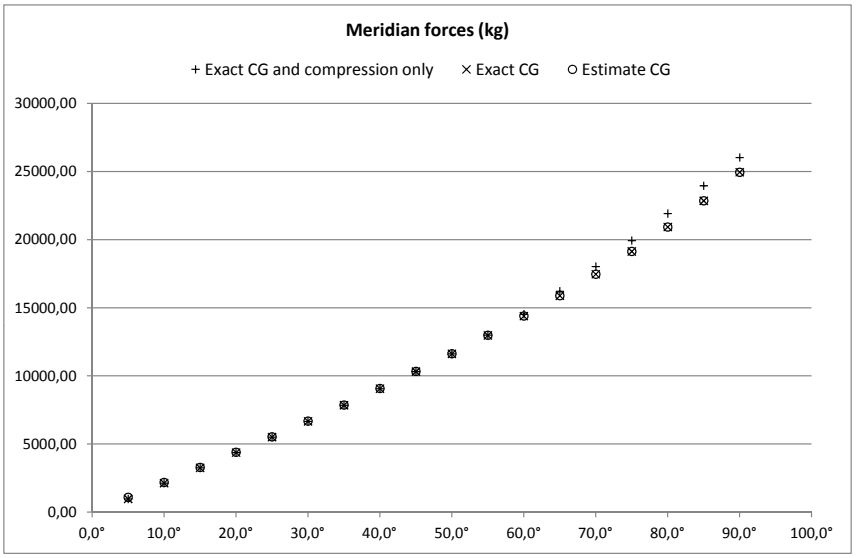

Fig 4.17 – Study of a lune with and without hoop forces
Meridian forces

Interactive implementation of Wolfe's method

Lau implemented Wolfe's method in the case of domes with tensile capacity on a web-based applet in 2006. This applet can still be accessed on her website: `http://web.mit.edu/masonry/wwlau/wolfe.html` (Lau 2006 [28]). This applet is a graphical implementation of Wolfe's method. There is a slight difference with the method of Wolfe here, since the centres of gravity used correspond to $r_G = 0.5 \cdot (r_i + r_e)$ **and** $\varphi_G = 0.5 \cdot (\varphi_0 + \varphi_1)$.

The lune of a dome corresponding to the default values of Lau's applet can be loaded among the pre-set examples of Manacoh. In this example the centre of gravity are computed with $r_G = 0.5 \cdot (r_i + r_e)$ **and** $\varphi_G = 0.5 \cdot (\varphi_0 + \varphi_1)$. In order to compute the same solution as Lau's web applet, the optimization set-up is:

— Cost function [17]: $\sum_{k=1}^{n_i+n_b} (z_k - z_{G,k})^2$. Both interior and boundary nodes
— No constraints

Manacoh gives under these conditions the same hoop forces as Lau's implementation of Wolfe's method (see figure 4.18). What is interesting in this comparison with Lau's applet is that:

— hoop forces are an increasing function towards the crown
— the way centre of gravity are estimated is important. The use of the centre of gravity exact position would not deliver the same results as Lau's applet near the crown. Elsewhere the results would be almost equal. This can be related to the fact that the approximate centres of gravity are a good estimate of the centres of gravity exact position, except near the crown.
— we constrain in this case the thrust network on the middle surface, but we should constrain instead the centres of pressure on the middle section (see section **??**). In this example, the difference between the two methods converge towards zero as the number of blocks considers increase. When the thrust network is sufficiently close to the middle surface, the distinction between line of thrust and line of pressure is not relevant.

This interactive and accessible to all applet has been used after its creation in various publications. We will see Reese's use of this applet below.

17. With this cost function choice, the thrust network lies on the mid-surface. The line of thrust however, does not lie exactly on the mid-surface with this choice.

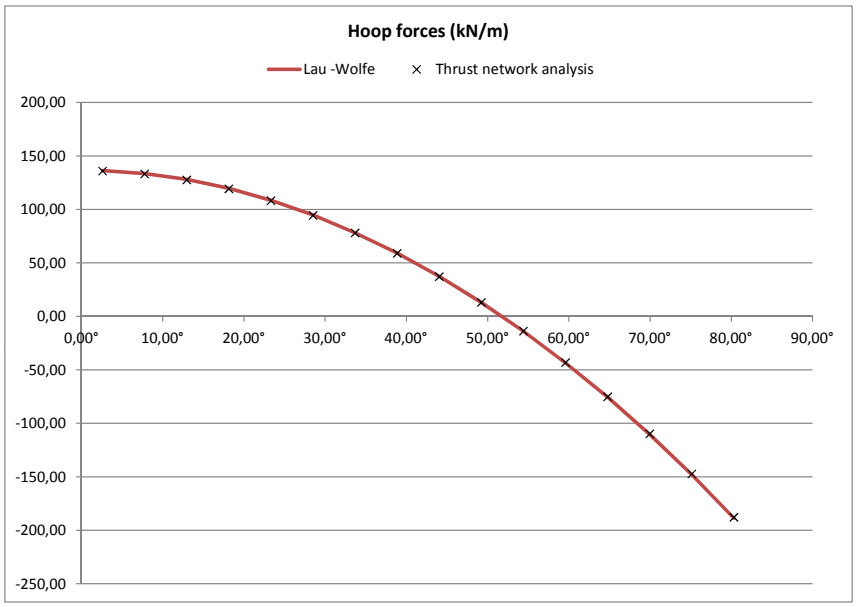

Fig 4.18 – Comparison of Lau's applet and network analysis

4.4.3 Membrane theory - Reese 2008

Comparison of Wolfe's method and membrane theory

Reese studies a typical dome of Guastavino, using successively Wolfe's method and membrane theory (2008 [36, p.42]). The considered dome has tensile capacity. She shows that both give the same results on the considered case. Let σ_φ be the meridian stress, F_φ the related force on the considered joint, σ_θ be the hoop stress and F_θ the related force on the considered joint. In membrane analysis:

$$\sigma_\varphi = R\rho t \frac{1}{1+\cos\varphi} \qquad F_\varphi = \sigma_\varphi R\delta\theta \sin\varphi \tag{4.10}$$

$$\sigma_\theta = -R\rho t(\frac{1}{1+\cos\varphi} - \cos\varphi) \qquad F_\theta = \sigma_\theta R\delta\varphi \tag{4.11}$$

The geometry of Reese's dome can be loaded among the pre-set examples of Manacoh. In this example the centre of gravity are computed with $r_G = 0.5 \cdot (r_i + r_e)$ **and** $\varphi_G = 0.5 \cdot (\varphi_0 + \varphi_1)$, since Reese seems to use the same estimate as Lau for the centres of gravity (see previous section on Lau's applet). The geometry, optimization choices, and results are given on figure 4.20. Manacoh gives the same results as Wolfe's method and membrane theory (see figure 4.19). What is interesting in this example is that:

— hoop forces are an increasing function towards the crown

— the way centre of gravity are estimated is important. The use of the centre of gravity exact position would not deliver the same results as membrane theory.

Lagrange polynomials

In order to reduce the degrees of freedom number, we suggested to use polynomials (see sections 2.2.5, 2.4.4 and **??** in previous chapters). The dome studied by Reese is a good candidate to test the efficiency of Lagrange polynomials, because the hoop forces repartition is regular (see figure 4.19). The previous results were computed using 11 parameters (10 branch-dof and 1 boundary node-dof). We replaced these 11 parameters by only 4 parameters (3 branch-dof and 1 boundary node-dof), the values of the other degrees of freedom being calculated using Lagrange polynomials. After optimization, the same hoop forces are found (difference inferior to 0.2% except the one corresponding lowest hoop force, which is only inferior to 0.8%). The computing time is markedly lower (2.9 seconds against 13,4 seconds without Lagrange polynomials during our test).

Influence of centre of gravity precision

We studied the dome studied by Reese with the following modification in order to try to understand the necessity to take $\varphi_G = 0.5 \cdot (\varphi_0 + \varphi_1)$ to get the same results as membrane theory:

— We consider a very thin slice of a dome $\theta_1 - \theta_0 = 0.1°$

— Let r_G, φ_G, θ_G be the exact spherical coordinates of centre of gravity. We project radially this centre of gravity on the mid-surface: $r_G = 0.5(r_i + r_e)$

18. The numerical values for Wolfe's method were taken in Reese thesis, and the ones for membrane theory were recomputed. The slight difference between 50°and 60°are probably due to the round up of result number indicated in Reese's table, and not to a defect of the solution computed by Reese.

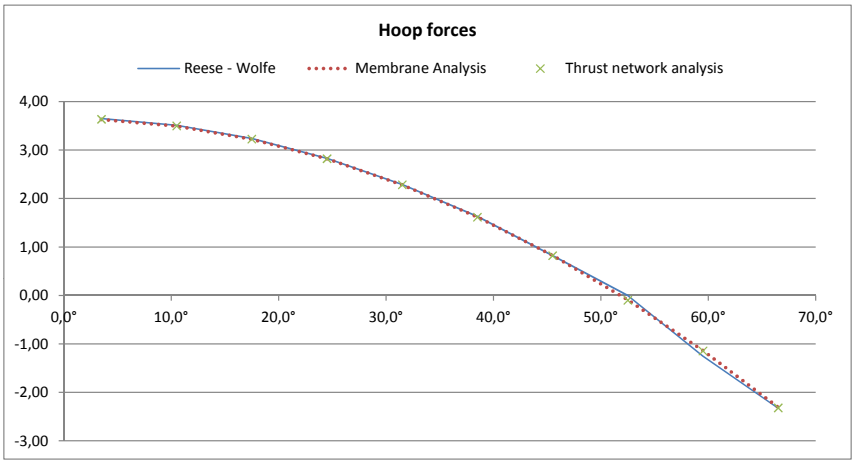

Fig 4.19 – Comparison [18] of Wolfe's method and membrane theory by Reese 2008 [36] in addition, result found with a network analysis

Under these conditions, we made the following observations:

— if $\varphi_G = 0.5(\varphi_0 + \varphi_1)$ the solution found is very close to the one given by membrane analysis.

— if no change is made to φ_G, the solution is different to the one given by membrane analysis. There is a sudden drop of hoop forces at the voussoir closest to the crown. We could not determine the reason of this drop.

Geometry:
lune of a spherical dome 10 voussoirs
mean radius $r_m = 40$
thickness $t = r_m/120$
$\varphi \in [0°; 70°]$
$\theta \in [-7.5°; 7.5°] \Leftrightarrow \delta\theta = 15°$
$\rho = 112$
`SimplifyCenterGravityFormulas = True`

Optimization:
f=$\sum_{k=1}^{n_i+n_b} (z_k - z_{G,k})^2$. Both interior and boundary nodes (since boundary nodes define the curvature of next voussoir) !
No constraints

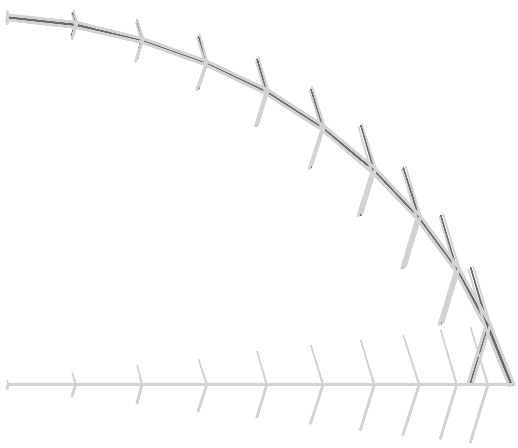

Geometry
Intrados and extrados, mass network, primal grid

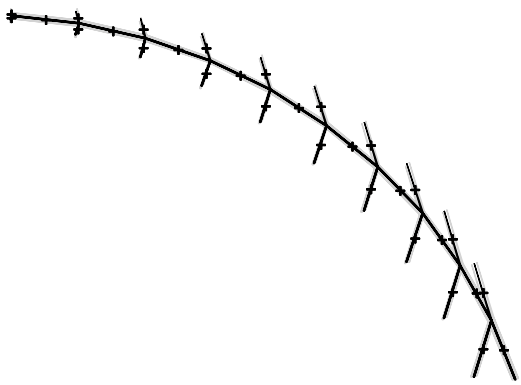

Thrust network

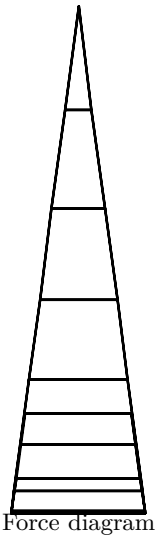

Force diagram

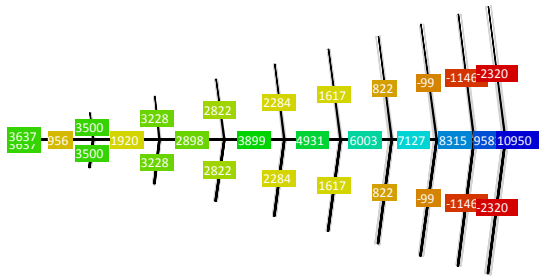

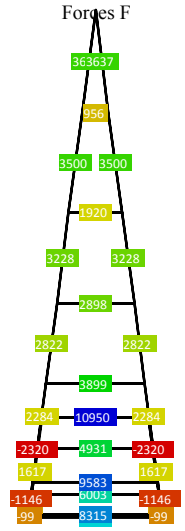

Fig 4.20 – Catalan dome studied by Reese 2008 [36]
Comparison of Reese's method and network analysis

4.4.4 Minimum thickness of domes

The minimum thickness of a spherical dome was investigated by Heyman (1967 [23]), Lau (2006 [28]) and Zessin (2012 [44]). Heyman considers a dome with compressive hoop forces only [19], and finds that the theoretical minimum thickness is zero if the angle of embrace φ_1 is lower than 51.8°, and increase until $t_{\min}/r_m = 0.0420$ for the full hemisphere ($\varphi_1 = 90°$) (1967 [23, p.235]). Lau investigated those results also considering compressive only hoop forces with her method called *modified thrust line method* in 2006. Zessin computed new results: she disregarded hoop force completely in her research [20].

When an incomplete hemispherical dome was considered (angles of embrace φ_1 lower than 90°), Lau found a close minimum thickness to Heyman, Zessin a completely different trend (since she did not consider hoop forces). However, in the case of hemispherical dome, both Lau and Zessin found a very close result to the minimum thickness given by Heyman: $t_{\min}/r_m = 0.041$ for Lau (with compressive hoop forces) and $t_{\min}/r_m = 0.043$ for Zessin (without hoop forces). An instructive chart about these trends can be found in Zessin 2012 [44, p.53].

We will take a closer look on the accuracy of our definition of the geometrical coefficient of safety later. Let us accept for now that our definition (see section **??**) and Heyman's definition of the geometrical coefficient of safety both give the same result. We found a minimal thickness close to the estimate of Zessin of $t/R/\mathrm{CSG} = 0.0428$ without using hoop forces (see figure 4.21). The following parameters have been tested:

— lunes of 15 blocks or 60 blocks gives the same result $t/R/\mathrm{CSG} = 0.0428$

— lunes of $\delta\theta = 1°$, 0.1° and 0.01° gives the same result $t/R/\mathrm{CSG} = 0.0428$

We were not able to compute a better minimum thickness for the complete hemispherical dome with the addition of the compressive hoop force to the optimization problem. Possible explanations for this difficulty are:

— the minimum thickness of a full hemispherical dome does not depend much on the consideration or not of hoop forces ($t/R/\mathrm{CSG} = 0.0420$ in one case, potentially $t/R/\mathrm{CSG} = 0.0428$ in the other)

— the consideration of hoop forces seems to *blur* the optimization problem: the force in one hoop branch can be transferred to the next hoop branch, particularly near the crown, without the result changing much. This behaviour might make it difficult for the solver to find an optimum solution.

However, it is not difficult to find for domes with an angle of embrace φ_1 lower than 51.8° a stable solution with compression only hoop forces for any small thickness (see section 4.4.3 above for the discussion of results related to membrane theory).

19. The fact that Heyman used hoop forces in order to determine the minimum thickness is pointed out by Zessin (2012 [44, p.52-53]). We follow her interpretation in this document. However, other authors seems to have different interpretations of Heyman's 1967 article: see Lau 2006 [28, p.54-55] and Paradiso et al. [32, p.1574].

20. The reason why Zessin does not take into account hoop forces is the following: "she [Lau] also states that the values of thrust obtained with the modified thrust line method are similar or identical to those obtained using the assumption of zero hoop force transfer. Based on this conclusion, the author's [Zessin] own MATLAB program MinDomeThrust (Appendix A) is developed to explore stability and permissible thrust values of a dome subject to its own self-weight. It is assumed that the horizontal thrust is constant throughout and that the transfer of hoop forces is not permitted." 2012 [44, p.46]

Geometry:
lune of a spherical dome 15 voussoirs
mean radius $r_m = 10$
thickness $t = 0.042r_m$ or $0.100r_m$
$\varphi \in [0°; 90°]$
$\theta \in [-0.5°; 0.5°] \Leftrightarrow \delta\theta = 1°$
$\rho = 1000$
no hoop branches

Optimization:
$f = -\mathrm{CSG}_{\mathcal{J}} = -\min \mathrm{CSG}_j$

Results:
$t/R = 0.042 \rightarrow \overline{\mathrm{CSG}_{\mathcal{J}}} = 0.9811 \rightarrow t/R/\overline{\mathrm{CSG}_{\mathcal{J}}} = 0.0428$

$t/R = 0.10 \rightarrow \overline{\mathrm{CSG}_{\mathcal{J}}} = 2.3288 \rightarrow t/R/\overline{\mathrm{CSG}_{\mathcal{J}}} = 0.0429$

Heyman 1967, with hoop forces:
$t_{\min}/R = 0.0420$

Zessin 2012, without hoop forces:
$t_{\min}/R = 0.043$

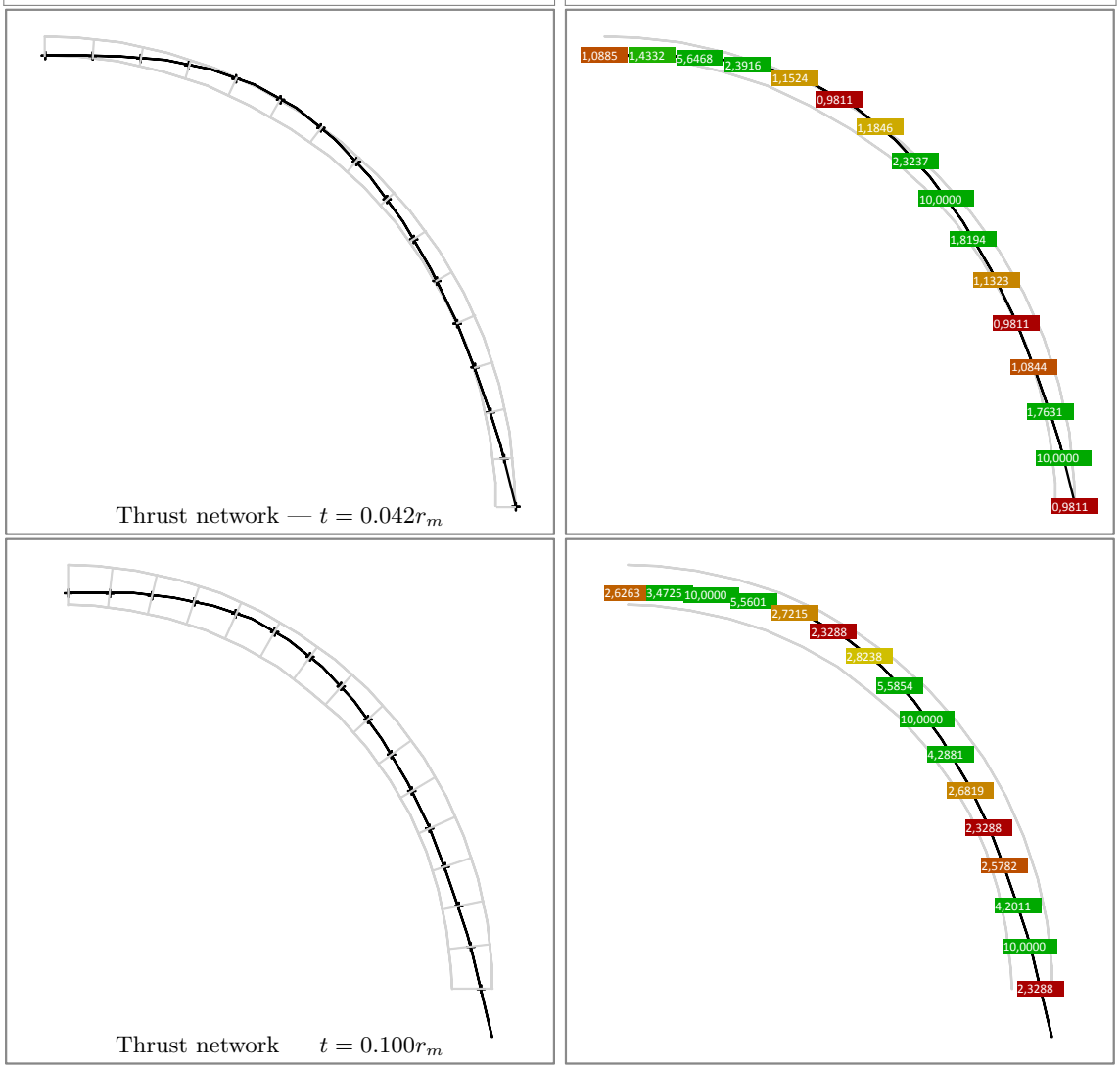

Fig 4.21 – Minimum thickness of a hemispherical dome without hoop forces
Comparison of Heyman 1967 [22], Zessin 2012 [44] and network analysis

4.5 Oval domes

4.5.1 Oval domes in construction history

The term oval domes gathers into one concept a rather large number of geometries. Huerta studied the history of these oval forms. Examples can be found in the Antiquity in Egypt, in the Middle Ages in Romanesque and then Gothic churches in Europe, then in the Renaissance and so on. These oval domes are in fact different geometries, that were build using various oval drawing techniques. Huerta writes in his study that *the ellipse has very rarely been used in buildings* (2007 [25, p.211]).

Some oval domes cannot be adequately approximated by ellipse. Nevertheless, the ellipse is a very convenient figure for parametric studies. We will study only ellipsoidal domes in the following. It would possible to continue this study with the current version of Manacoh for oval domes of non-elliptical form, provided that the geometry is computed in another program and then imported in Manacoh.

4.5.2 Affine transformations — Rankine 1858

Affine transformations

Rankine uses affine transformations to simplify the complex study of ellipsoidal domes into the study of spherical domes. Affine transformations are also called parallel projections. It is a geometrical transformation defined by two vectors $(\alpha_x; \alpha_y; \alpha_z)$ and $(u_x; u_y; u_z)$ such as:

$$(x; y; z) \rightarrow (\alpha_x x + u_x; \alpha_y y + u_y; \alpha_z z + u_z) \tag{4.12}$$

Since the translation $(u_x; u_y; u_z)$ does not deform the studied structure, it will be neglected in the following. Let us first state some properties of affine transformations. In an affine transformation, the following quantities are transformed:

— positions, known directly in function of $(\alpha_x; \alpha_y; \alpha_z)$ and the original positions $(x; y; z)$ in cartesian coordinates
— lengths
— areas of surfaces [21]
— volumes of blocks. The volumes are transformed by a factor $\alpha_x \alpha_y \alpha_z$, and consequently so are their related weights.

In an affine transformation, the following quantities are preserved:

— the relative positions of the transformed elements, and in particular the relative position of the line of thrust with respect to the intrados and the extrados
— the transformed centres of gravity of an object are the centres of gravity of the transformed object. The object can be a segment, a surface, or a volume here.

An example of affine transformation of a spherical dome is given on figure 4.22. An affine transformation transform a spherical dome of uniform thickness, into an elliptical dome of variable thickness.

21. This transformation cannot be calculated with an expression as simple as the one for the volumes. For planar surfaces, it involves both the orientation of the surface and the affine vector.

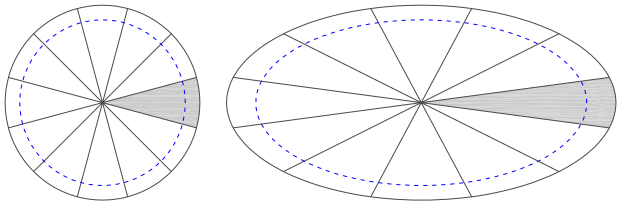

Fig 4.22 – Affine transformation of a dome — view in plan

Rankine's Theorem of Blockwork Structures

The preservation of the relative positions through an affine transformation gives a particularly interesting theorem: Rankine's theorem of blockwork structures (1858 [35]). It is stated by Huerta as follows (2010 [27, p.278-279]):

> *If a structure composed of Blocks have stability of position when acted on by forces represented by a given system of lines, then will a structure whose figure is a parallel projection of the original structure have stability of position when acted on by forces represented by the corresponding parallel projection of the original system of lines; also, the centers of pressure and the lines representing the resultant pressures at the joints of the new structure will be the corresponding projections of the centers of pressure and the lines representing the resultant pressures at the joints of the original structure.*
>
> *[...] Therefore, if a masonry structure in a state of safe equilibrium, represented by a line of thrust inside the masonry, a parallel (affine) projection of the structure will also be in a safe state of equilibrium and the new line of thrust will be the transformation of the original, the relative distances from the border at each joint remaining the same.*

We will now apply this theorem to study ellipsoidal domes and study its potentialities and limits. It can be noted that this theorem is not restricted to the domes, and will apply to any "blockwork structures": arches, helicoidal stairs, etc.

Affine transformation of uniform thickness spherical dome

Rankine's theorem is helpful to study elliptical domes. Let us consider a spherical dome of constant thickness t. The affine transformation of this dome delivers an elliptical dome with the following properties:

— the intrados and the extrados are ellipsoids.
— the thickness t of the elliptical dome is variable. It is a function of φ and θ.
— the local radius R of the elliptical dome is variable. It is a function of φ and θ.
— the quantity t/R is constant. It does not depend on φ and θ.

The thrust network analysis is only a method to write the equilibrium equations. We know before the calculations that we must found the same results as those given by Rankine's theorem. Let us consider the dome of thickness $t/R = 0.1$ that we studied while investigating the minimum thickness of domes (section 4.4.4). We apply an affine transformation of a factor 2 along axis xx, and of factor 1 along axes yy and zz. We find with Manacoh coherent results (see figure 4.23):

— The weight of the blocks is doubled

- The geometrical coefficient of safety is not modified by the transformation. For the degrees of freedom corresponding to this coefficient of safety, we get:
  - the thrust is multiplied by 4, as expected because the weight is doubled and the lever arm along xx (principal axis of the lune) is doubled, thus the multiplication of the thrust by 4.
  - the friction coefficient are not preserved — see Huerta 2010 [27, p.279]

Manacoh delivers the same results that Rankine's theorem would have given. In this situation, applying Rankine's theorem would have been much more efficient. However we will see in the next example, Rankine's theorem is not adapted to study elliptical domes with constant thickness.

Geometry:
lune of a spherical dome (before affine transformation)
15 voussoirs
mean radius $r_m = 10$
thickness $t = r_m/10$
$\varphi \in [0°; 90°]$
$\theta \in [-0.5°; 0.5°] \Leftrightarrow \delta\theta = 1°$
$\rho = 1000$
`MeridianBoundaryNodesOnExtrados = True`
affine transformation along xx of factor 2

Optimization:
$f = -\mathrm{CSG}_{\mathcal{J}} = -\min \mathrm{CSG}_j$

Results: before affine transformation
$\overline{\mathrm{CSG}_{\mathcal{J}}} = 2.3288$
$H = 418$
$W = 1746.8$

Results: after affine transformation
$\overline{\mathrm{CSG}_{\mathcal{J}}} = 2.3288$
$H = 1672 = 4 \cdot 418$
$W = 3493.6 = 2 \cdot 1746.8$

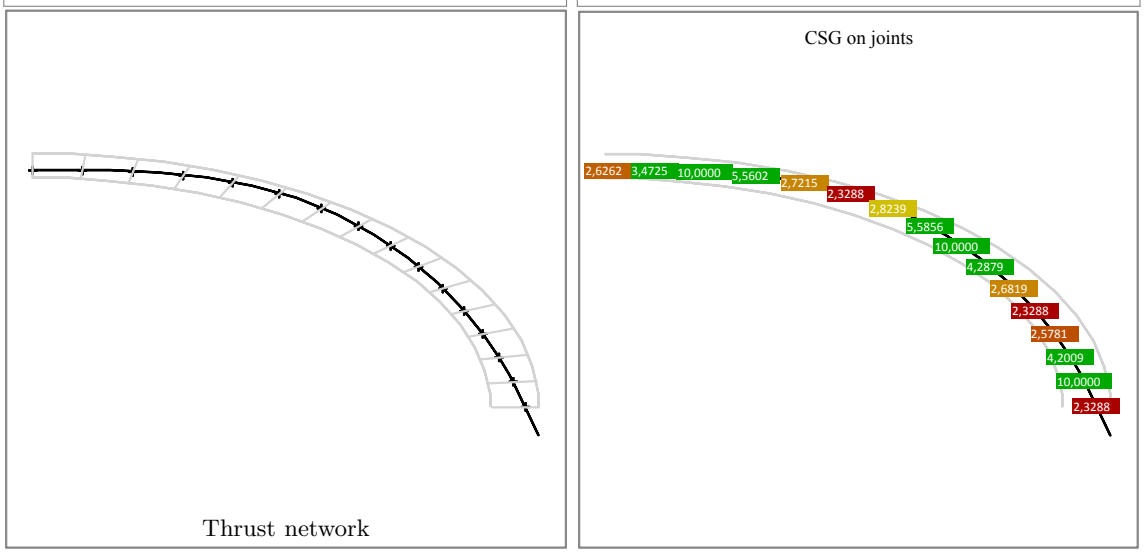

Fig 4.23 – Elliptical lune obtained from affine transformation of spherical lune
Comparison with original spherical lune (see figure 4.21)

4.5.3 Elliptical dome with constant thickness

Definition of the geometry

Rankine's theorem is useful, since it delivers the results of elliptical domes, with calculus on spherical domes. Yet, the affine transformation needed to apply this theorem transforms also the uniform thickness of the spherical dome into the variable thickness of the elliptical dome. Thus the study of an elliptical dome with constant thickness seems out of reach of Rankine's theorem.

There is several ways to define the voussoirs of elliptical domes with constant thickness. We chose to use the obvious parametrization of ellipsoids (with r, φ and θ and $(r_x cos\theta sin\varphi; r_y sin\theta sin\varphi; r_z cos\varphi))$. It is important to note here that the variable of this parametrization φ and θ do not correspond to the spherical coordinates any more.

The parametrization of the ellipsoids (intrados and extrados) with φ and θ is also used to define the joints. Joints along meridians are defined with $\theta =$ constant, and joints along parallels are defined with $\varphi =$ constant. See details in appendix on elliptical voussoirs page **??**.

To conclude this section on geometry, it is true that elliptical domes of constant thickness are a theoretical case study, since most elliptical dome do not have a constant thickness near the base.

Comparison with Rankine's theorem

We study in this section an elliptical dome similar to the one studied before, but with constant thickness. We consider two cases:

— Case 1 : lune of constant thickness, completely included in the "affine lune" studied above. See results on figure 4.24.

— Case 2 : lune of constant thickness, that includes entirely the "affine lune" studied above. See results on figure 4.25.

In both cases, the geometrical coefficient of safety is inferior to the one of "affine lune" that was studied with Rankine's theorem. This could be expected in case 1, since we have less masonry, but this result is less trivial in case 2. In fact, the "affine lune" has an optimum form near the crown, with less thickness near the crown than near the base. On the contrary, the additional thickness of case 2 near the crown brings more weight, and thus more thrust, than the stabilization effect obtained thanks to the enlarged space for the line of thrust.

Geometry: Case 1
lune of a elliptical dome of constant thickness
15 voussoirs
mean radius $r_z = 10, r_x = r_y = 20$
thickness $t = r_z/10$
$\varphi \in [0°; 90°]$
$\theta \in [-0.5°; 0.5°] \Leftrightarrow \delta\theta = 1°$
$\rho = 1000$
`MeridianBoundaryNodesOnExtrados = True`

Optimization:
$f = -\mathrm{CSG}_{\mathcal{J}} = -\min \mathrm{CSG}_j$

Results:
$\overline{\mathrm{CSG}_{\mathcal{J}}} = 0.9928$
$H = 2621.8$
$W = 4655.9$

The geometrical coefficient of this lune (0.9928) is lower than the coefficient of safety of the affine lune of variable thickness studied before (2.3288 — see figure 4.23).

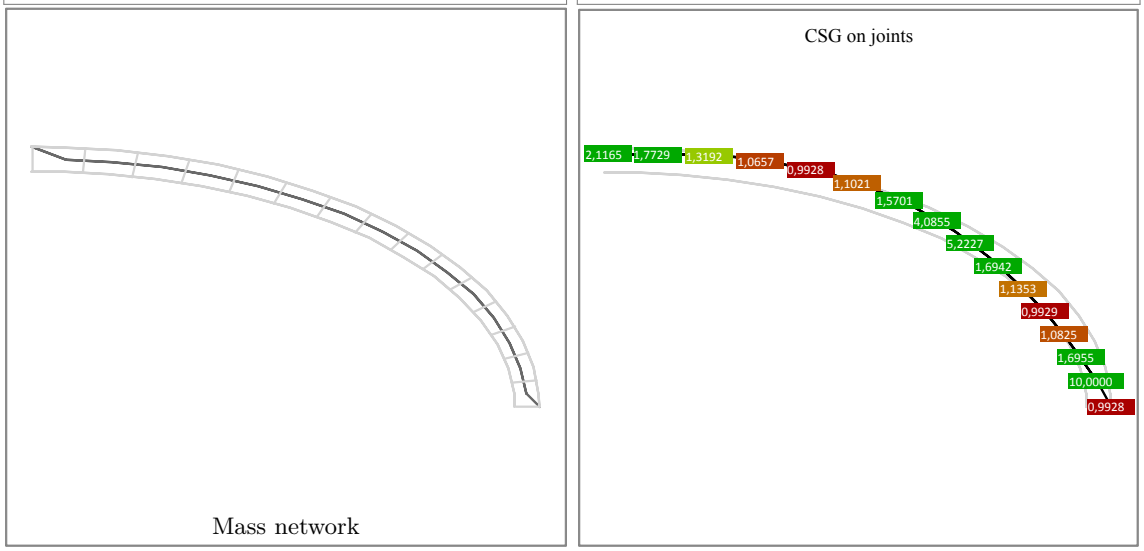

Fig 4.24 – Elliptical lune with t constant, smaller than affine elliptical lune of figure 4.23

Geometry: Case 2
lune of a elliptical dome of constant thickness
15 voussoirs
mean radius $r_z = 10, r_x = r_y = 20$
thickness $t = r_z/5 = 0.2r_z$
$\varphi \in [0°; 90°]$
$\theta \in [-0.5°; 0.5°] \Leftrightarrow \delta\theta = 1°$
$\rho = 1000$
`MeridianBoundaryNodesOnExtrados = True`

Optimization:
$f = -\mathrm{CSG}_{\mathcal{J}} = -\min \mathrm{CSG}_j$

Results:
$\overline{\mathrm{CSG}_{\mathcal{J}}} = 1.9922$
$H = 5225.4$
$W = 9328.0$

The geometrical coefficient of this lune (1.9922) is lower than the coefficient of safety of the affine lune of variable thickness studied before (2.3288 — see figure 4.23).

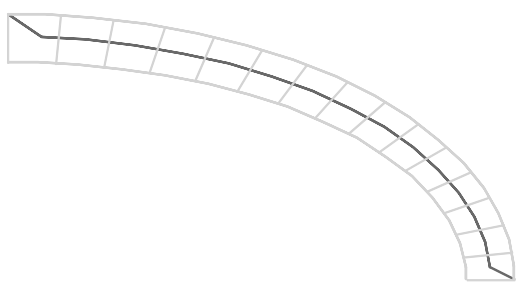

Mass network

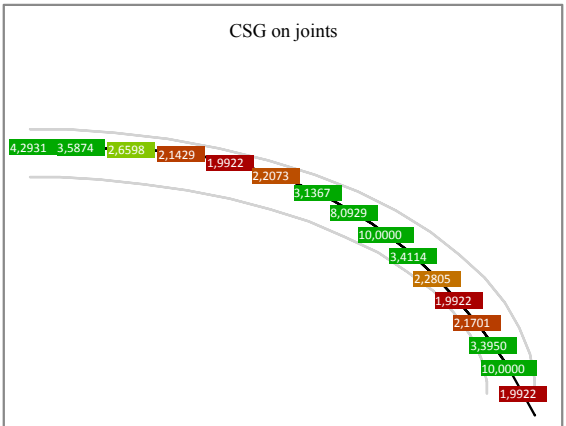

Fig 4.25 – Elliptical lune with t constant, larger than affine elliptical lune of figure 4.23

Oval domes and principal stresses

The use of meridians and parallels in order to slice a studied dome in voussoirs is particularly well adapted for domes with axial symmetry (such as spherical domes). In that case, the direction of the branches in the mass network corresponds to the principal stresses expected in membrane theory. That is why it is possible to compare accurately the thrust network analysis to membrane theory (*p. ex.* section 4.4.3).

However, oval domes are not domes with axial symmetry. If the same kind of slicing technique is kept (with meridians and parallels), the correspondence between branches and principal stresses is lost. It is not possible to find a membrane-like solution (see figure 4.26).

Geometry:
6 lunes of a elliptical dome 6x10 voussoirs
mean radius $r_x = 1.6 \cdot 40; r_y = 40; r_z = 40$
thickness $t = r_m/120$
$\varphi \in [0°; 70°]$
$\theta \in [0°; 45°] \Leftrightarrow \delta\theta = 6 \cdot 15°$
$\rho = 112$
`SimplifyCenterGravityFormulas = True`

Optimization:
f=$\sum_{k=1}^{n_i+n_b} (z_k - z_{G,k})^2$
No constraints

Results:
$f = 4.3 \cdot 10^0$
The thrust network cannot be superimposed to the mass network in the case of the elliptical dome. The equivalent spherical dome (with $r_x = r_y = r_z = 40$) would have given $f \approx 10^{-7}$

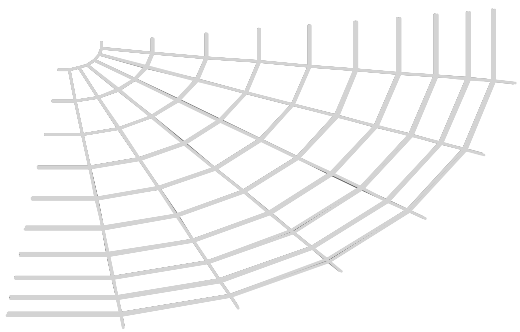

Mass network

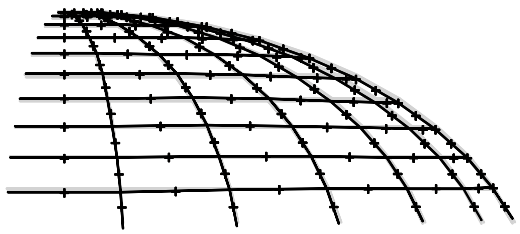

Thrust network

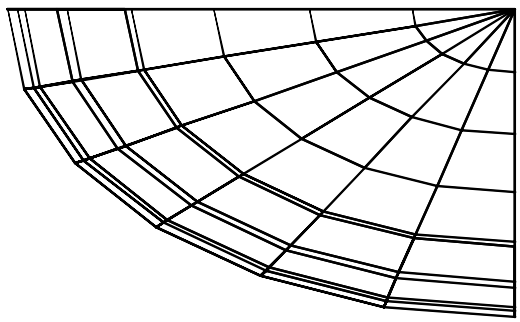

Dual grid

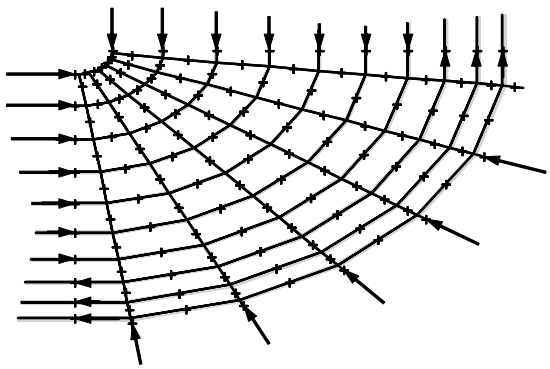

Support forces

Fig 4.26 – Oval dome and membrane-like solutions

4.6 Cylindrical arch - classical results

4.6.1 Minimum thickness of an arch

Heyman defines the geometrical coefficient of safety as the ratio between the thickness of the studied arch and the thickness of the thinnest stable arch (1995 [23, p.21]). In order to determine the exact value of this coefficient, the minimal thickness of the studied arch must be known. On the contrary, the definition that we gave of the geometrical coefficient of safety (defined locally on the joint, and extended globally – see section **??**) does not need the determination of the minimal thickness of the studied arch. But our geometrical coefficient of safety it is not the theoretic geometrical coefficient of safety defined by Heyman.

The numerical difference between this two coefficients is quite low, and is usually neglected by practitioners. We checked, as an exercise, that the coefficient of safety $\overline{\mathrm{CSG}_{\mathcal{J}}}$ that we use in this manual has the two following properties on specific cases:

— $\overline{\mathrm{CSG}_{\mathcal{J}}}$ allows to give a good estimate of the real minimal thickness $t_{\min}$ by taking $t/\overline{\mathrm{CSG}_{\mathcal{J}}}$ for arches.

— $\overline{\mathrm{CSG}_{\mathcal{J}}}$ converges towards 1 when the thickness t of the studied arch converges towards the minimal thickness $t_{\min}$.

— if $\mathrm{CSG}_j = \overline{\mathrm{CSG}_{\mathcal{J}}}$ in k joints, then these k joints correspond to the expected mechanism of failure hinges.

The results obtained with Manacoh for a cylindrical arch are given on figures 4.27 and 4.28. The graph 4.29 shows that the relative error between our coefficient of safety and Heyman's is lower than 0.18% on the considered example. Our analysis with Manacoh delivers the same minimum thickness ($t_{\min}/R = 0.1075$ as the one computed by Ochsendorf (2002 [29, p.91-95]).

Geometry:
cylindrical arc
15 voussoirs
mean radius $r_m = 10$
thickness $t = 0.15 r_m$
$\varphi \in [0°; 90°]$
$y \in [0; 1] \Leftrightarrow \delta y = 1$
$\rho = 1000$
`MeridianBoundaryNodesOnExtrados = True`

Optimization:
$f = -\mathrm{CSG}_{\mathcal{J}} = -\min \mathrm{CSG}_j$

Results:
$\overline{\mathrm{CSG}_{\mathcal{J}}} = 1.3952$ thus $t/R/\overline{\mathrm{CSG}_{\mathcal{J}}} = 0.10751$

(Moseley 1830 and Ochsendorf 2002 [29, p.92]: $t_{\min}/R = 0{,}1075$)

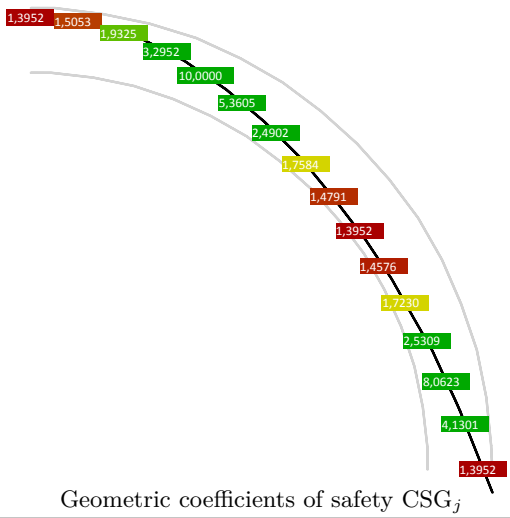

Geometric coefficients of safety CSG_j

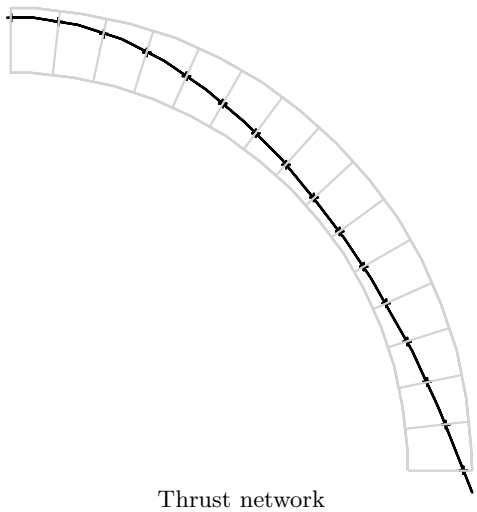
Thrust network

Fig 4.27 – Semi-cylindrical arch with t/R=0.15
Derivation of the minimum thickness $t/R/\overline{\mathrm{CSG}_{\mathcal{J}}}$

Geometry:
cylindrical arc
15 voussoirs
mean radius $r_m = 10$
thickness $t = 0.1075 r_m$
$\varphi \in [0°; 90°]$
$y \in [0; 1] \Leftrightarrow \delta y = 1$
$\rho = 1000$
`MeridianBoundaryNodesOnExtrados = True`

Optimization:
$f = -\mathrm{CSG}_{\mathcal{J}} = -\min \mathrm{CSG}_j$

Results:
$\overline{\mathrm{CSG}_{\mathcal{J}}} = 1.0004$ very close to 1
Note that the force is not parallel to the intrados in the vicinity of the potential hinge of the intrados ($\Leftrightarrow$ tangential force on joint not zero here). See Ochsendorf 2002 [29, p.92] and Heyman 2009 [24] on that subject.

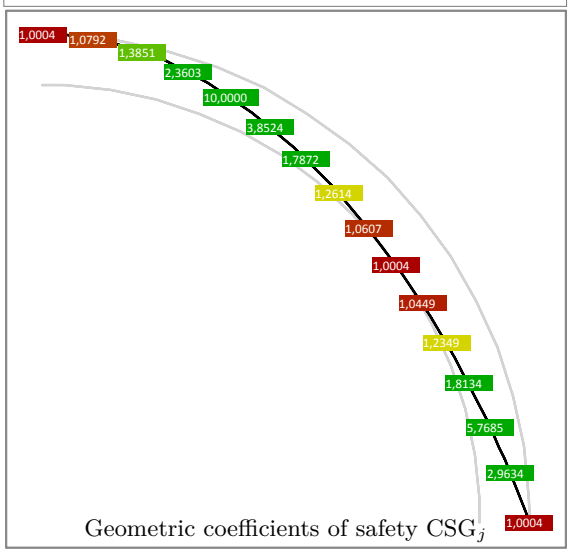

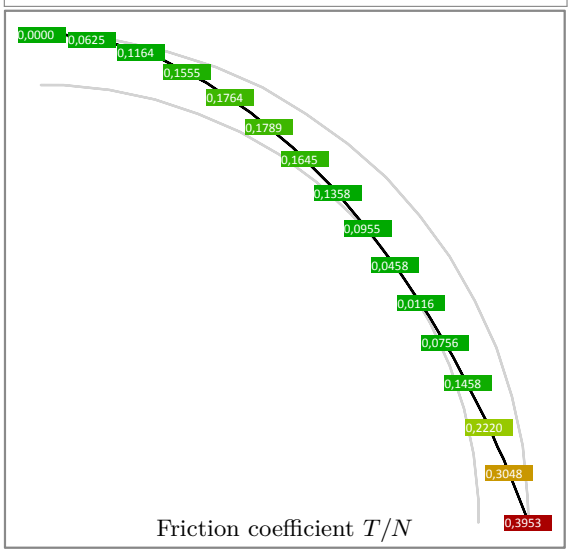

Fig 4.28 – Minimal thickness of a semi-cylindrical arch: $t/R = 0.1075$

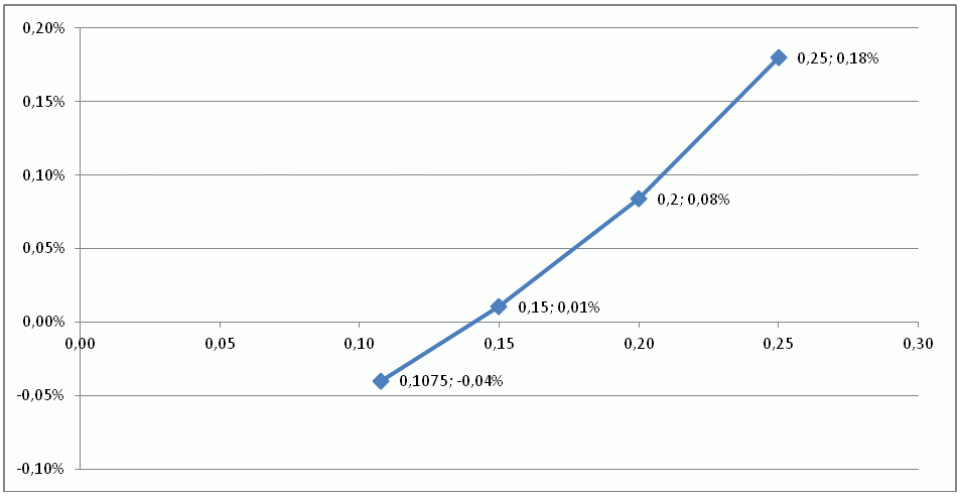

Fig 4.29 – Relative error of $t/R/\overline{\mathrm{CSG}_{\mathcal{J}}}$ w.r.t $t_{\min}/R$=0.1075 in function of t/R cylindrical arch of 15 voussoirs (see figures 4.27 and 4.28)

4.6.2 Minimum and maximum thrust of an arch - Oikonomopoulou 2009

There is two different methods to check if the thrust network that has been found is representative of a stable equilibrium. We can use the geometrical coefficient of safety on the joints $\overline{\mathrm{CSG}_{\mathcal{J}}}$ (see its definition in section **??**). If $\overline{\mathrm{CSG}_{\mathcal{J}}} > 1$ then the centres of pressure lie inside the masonry. This is the traditional approach of static graphics. We can also use the geometrical coefficient of safety on the nodes $\overline{\mathrm{CSG}_{\mathcal{N}}}$ (see its definition in section **??**). If $\overline{\mathrm{CSG}_{\mathcal{N}}} > 1$ then the thrust network lies inside the masonry (method used by O'Dwyer 1999 [30], Block 2009 [2], Oikonomopoulou 2009 [31]). This is in essence the difference between the line of thrust and the line of pressure (see section **?? ??**).

The method with $\overline{\mathrm{CSG}_{\mathcal{N}}}$ is the easiest to implement with the thrust network method, because it only uses the thrust network itself. However this method is a little bit conservative (we will see it on an example), and does not correspond to a physical law: there is no limitation to give at the point of intersection of the forces of the network. On the contrary, with the method with $\overline{\mathrm{CSG}_{\mathcal{J}}}$, imposing that the centres of pressure lie in the joint directly stems from the hypothesis of no tension. This method requires additional computation to find the centres of pressure, and requires that the joints geometry are known and stored while computing geometry.

In a nutshell, it is possible for the thrust network nodes to be outside the masonry, while the centres of pressure still remain inside the masonry.

Let H_{min} and H_{max} be the minimal and maximal thrust of the arch, and $W_{tot} = 2W$ the total weight of the arch (twice the weight of the half arch drawn below, in order to be able to compare directly our results with the one given in Oikonomopoulou 2009 [31]). We were able to found with Manacoh the same results as those of Oikonomopoulou, using the coefficient of security expressed at the nodes. However we could also compute classical minimum and maximum thrust using the coefficient of security expressed at the joints. The results are given on figures 4.30 and 4.31.

Geometry:
cylindrical arc
15 voussoirs
mean radius $r_m = 10$
thickness $t = 0.25 r_m$
$\varphi \in [0°; 90°]$
$y \in [0; 1] \Leftrightarrow \delta y = 1$
$\rho = 1000$
`MeridianBoundaryNodesOnExtrados = True`

Optimization:
$f = -H$ and $c_2 = \mathrm{CSG}_{\mathcal{J}}$ or $\mathrm{CSG}_{\mathcal{N}} > 1$

Results:
Maximum thrust, determined with the geometrical coefficient of safety expressed on the nodes (figure on the left), or on the joints (figure on the right)
We get here the same result the two cases: $H_{max}/W_{tot} = 0.27718$

Oikonomopoulou 2009 [31, p.97]:
$H_{max}/W_{tot} = 0.2772$

The use of CSG_j or CSG_n gives the same result because the hinges are located on the boundary joints segments (use of option `MeridianBoundaryNodesOnExtrados = True`).

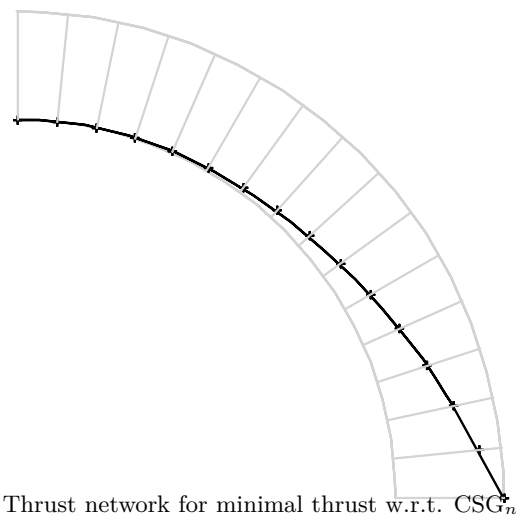

Thrust network for minimal thrust w.r.t. CSG_n

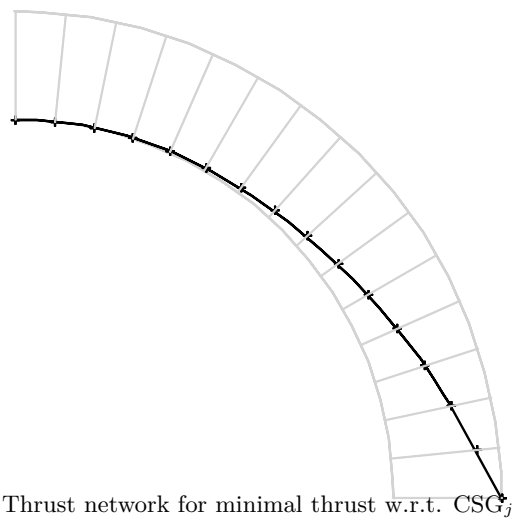

Thrust network for minimal thrust w.r.t. CSG_j

Fig 4.30 – Cylindrical arch – Maximum thrust
Comparison of Oikonomopoulou 2009 [31] and network analysis

Geometry:
cylindrical arc
15 voussoirs
mean radius $r_m = 10$
thickness $t = 0.25 r_m$
$\varphi \in [0°; 90°]$
$y \in [0; 1] \Leftrightarrow \delta y = 1$
$\rho = 1000$
`MeridianBoundaryNodesOnExtrados = True`

Optimization:
$f = H$ and $c_2 = \mathrm{CSG}_{\mathcal{J}}$ or $\mathrm{CSG}_{\mathcal{N}} > 1$

Results:
Minimum thrust, determined with the geometrical coefficient of safety expressed on the nodes (figure on the left), or on the joints (figure on the right).

With $\mathrm{CSG}_{\mathcal{N}} \geq 1$: $H_{min}/W_{tot} = 0.14042$
With $\mathrm{CSG}_{\mathcal{J}} \geq 1$: $H_{min}/W_{tot} = 0.13470$

Oikonomopoulou 2009 [31, p.97]:
$H_{min}/W_{tot} = 0.1412$

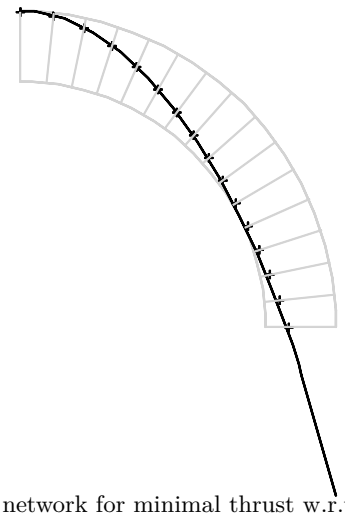

Thrust network for minimal thrust w.r.t. CSG_n

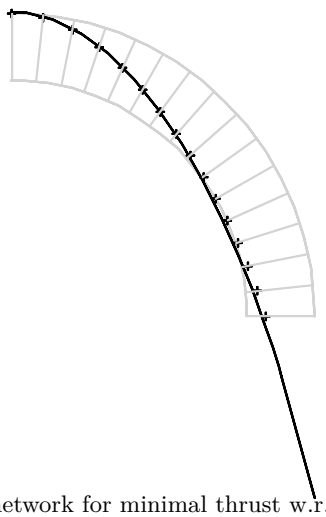

Thrust network for minimal thrust w.r.t. CSG_j

Fig 4.31 – Cylindrical arch – Minimum thrust
Comparison of Oikonomopoulou 2009 [31] and network analysis

4.6.3 Minimum thrust of an arch with consideration of friction - Smars 2000

For very thick arches, the collapse mechanism might not be the formation of hinges, but the formation of sliding joints. This kind of mechanism is taken into account by Petit (1835 [33]) in order to determine the minimum thrust of an arch. He created numeric tables to calculate in a few minutes the minimum thrust. These tables have been re-published in various nineteenth century construction manual: Claudel (1857 [7], 1864 [8, p.1098-1106] etc.), Demanet (1861 [13, p.515...])...

We study here an example by Smars of the determination of minimum thrust of an arch with consideration of friction (2000 [39, p.47]). The results are given on figure 4.32. This example can be loaded among the pre-set examples of Manacoh.

4.6.4 Arches with fill

The geometries of arches with fill cannot be generated yet with our program. The weights and centres of gravity of the blocks should be modify to take into account the additional load. For that reason, the examples given by Durand-Claye in his memoire of 1867 could not be investigated. However, if the geometries were entered manually, the network analysis would fully apply to these situations as well.

Geometry:cylindrical arc
16 voussoirs
mean radius $r_m = 10$
thickness $t = 2r_m(1.5 - 1)/(1.5 + 1)$
$\varphi \in [-90°; 90°]$
$y \in [0; 1] \Leftrightarrow \delta y = 1$
$\rho = 1000$
`MeridianBoundaryNodesOnExtrados = True`

Optimization:
$f = H$ and $c_1 = \text{angle} - 20 > 0$ and $c_2 = \text{CSG}_{\mathcal{J}} > 1$

Results:
The upper part of the arch acts like a wedge with respect to the lower part. The line of thrust found is close to Smars'. There is a little difference on the location of the sliding.

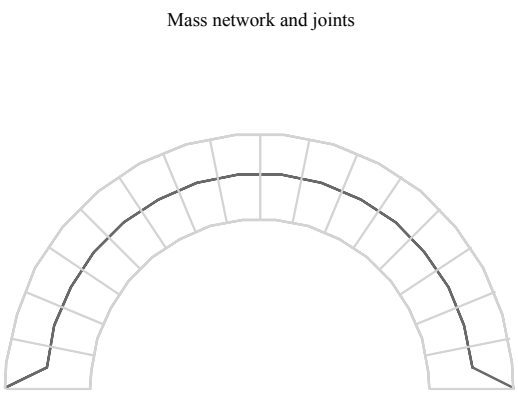

Mass network

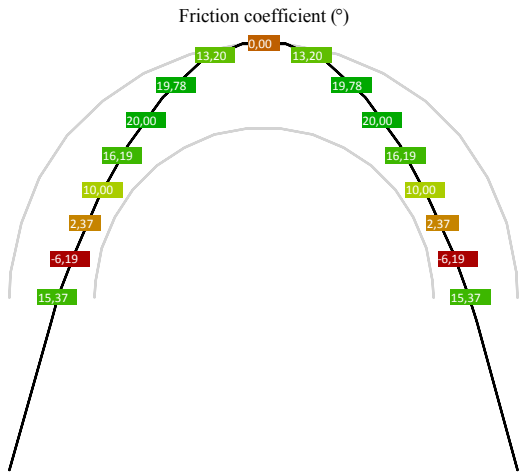

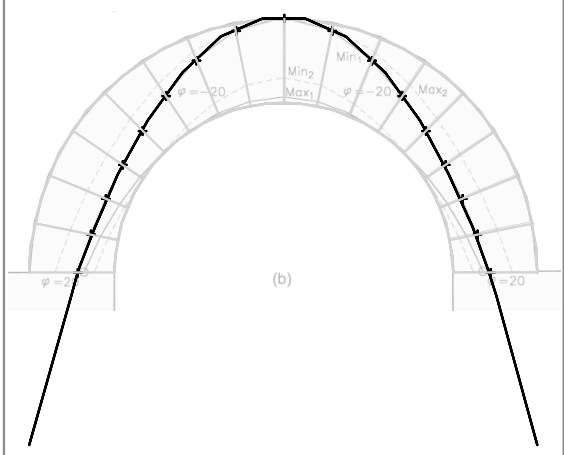

Thrust network superimposed on Smars's drawing

Fig 4.32 – Cylindrical arch – Minimum thrust for a friction angle of 20°
Comparison of Smars 2000 [39] and network analysis

4.7 Helicoidal stairs

García Ares exposed in 2007 a equilibrium solution for thin helicoidal stairs (2007 [20]). He considers the stair as a succession of helicoidal strips. Each strip is studied as a flat arch, and García Ares calculated analytically the minimal thrust of these arches. Of course, a lateral thrust develops against the wall supports in order to ensure equilibrium, since the arch is curved. This equilibrium solution exerts thrust on the landings (downward in the lower landing, upward in the upper landing), and on the wall support. Using García Ares's notations, the horizontal thrust on the lower landing is:

$$R_H = \frac{1}{8}\rho\gamma^2 r^2 \Delta r \tag{4.13}$$

with r the radius of the helicoidal strip, Δr its width, γ its angle in plan, and ρ the specific weight.

García Ares considered in his article the following example: a spiral stair with $r_0 = 1.5\text{m}$, $r_1 = 2.5\text{m}$, $\gamma = \pi$, $\rho = 3333.3\text{kg/m}^3$, $h = 4\text{m}$, and a vertical thickness of $t_z = 0.15\text{m}$ (figure 4.33). For the longest strip, the thrust is thus $R_H(r = 2.5\text{m}) = 25.7\text{kg/mm}$. The total thrust according to García Ares's solution is:

$$\int R_H = \int_{r_0=1.5\text{m}}^{r_1=2.5\text{m}} \frac{1}{8}\rho\gamma^2 r^2 \,\mathrm{d}r = 16792\text{kg} \tag{4.14}$$

If the strips are considered independently, a network analysis will give the same result. Indeed we found the same result as García Ares when considering a single 1mm strip (see figure 4.34). This example can be loaded among the pre-set examples of Manacoh.

However, if the strips are considered at the same time, they are connected to one another. There will be vertical load transfers between the strips, which are not considered by García Ares's solution. The figure 4.35 gives different minimum thrusts, according to the definition given to the minimum thrust (sum of the thrust of the strips, maximum of the thrust of the strips, sum of the square value of the strips etc.). The minimum total thrust computed are lower than the one calculated with García Ares's solution, but the results are somewhat close (4% difference). The thrust repartition is on the contrary very different. In García Ares's solution, the thrust of the strips grows with r^2. Here, if the total thrust is considered as a cost function, the minimum is attained when the thrust in all strips is

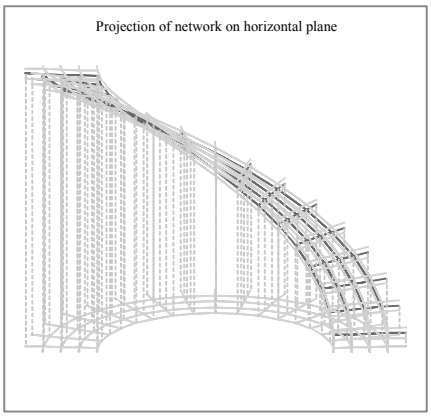

Fig 4.33 – Helicoidal stair model, for comparison with García Ares 2007 [20]

Geometry:
helicoidal vault
1x17 voussoirs
thickness $t_z = 0.15$m
$r_0 = 2.499$m and $r_1 = 2.500$m
$\theta \in [0°; 180°]$
$z \in [0; 4]m \Leftrightarrow \delta z = 4$m
$\rho = 3333.3$kg/m^3
`MeridianBoundaryNodesOnExtrados = True`

Optimization:
$f = H$ and $c_2 = \mathrm{CSG}_{\mathcal{J}} > 1$

Results:
Manacoh: H=25.7kg/mm

In García Ares's solution: H=25.7kg/mm

Manacoh will issue warning when computing the geometry, since the 2D joints are located outside the real joints (the strip considered is to thin).

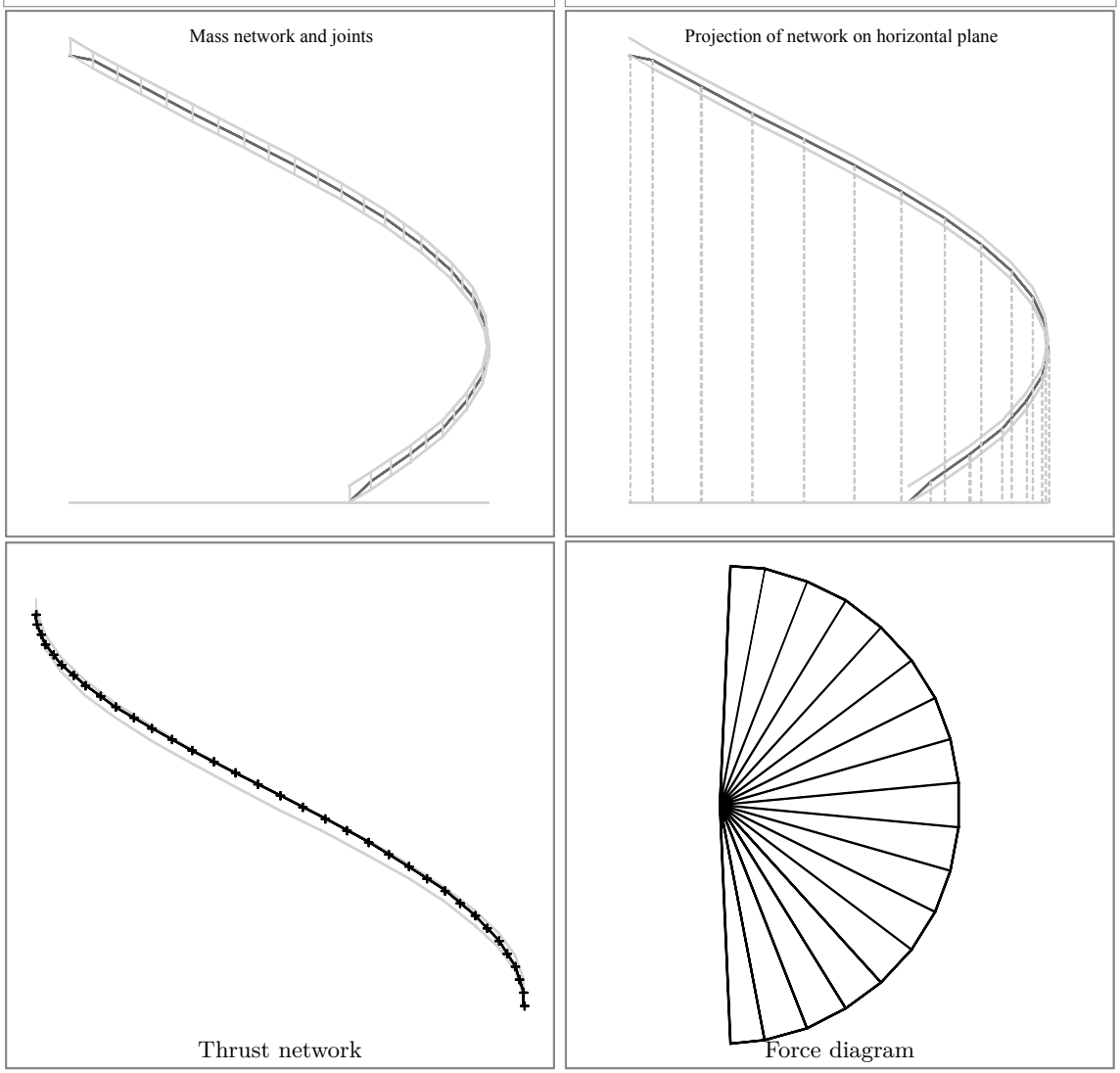

Fig 4.34 – Minimal thrust of a strip of a helicoidal stair
Comparison of García Ares 2007 [20] and network analysis

zero except the one closest to the axe of the stair. If the sum of the squared values of the thrusts is considered as a cost function, the minimum is attained when the thrust in all strips are almost equal (the difference between the highest thrust and the lowest thrust of the strips is inferior to 5% of their values). The difference between the results of each cost function can also be seen by considering each step separately. The natural arch that forms within each step, between the staircase stringer [22] and the wall support is more important for $f = \sum H$ than for $f = \sum H^2$. This difference is visible figure 4.36. Thus the choice of the cost function is very important and conditions the results. This example can be loaded among the pre-set examples of Manacoh.

We could find numerical results close to those of García Ares's article, and we showed that the consideration of the interaction between strips is a solution to lower the minimum thrust computed. The solution considered is a lower bound solution, that proves the stability of the helicoidal stair considered in this example. However, it is just one solution among the multiple ones that could be studied using a different slicing technique. García Ares's exposes in a more recent article other equilibrium solutions, that are not studied here (2011 [21]).

22. The staircase stringer is here the strip closest to the vertical axis of the staircase.

Geometry:
helicoidal vault
4x17 voussoirs
thickness $t_z = 0.15$m
$\theta \in [0°; 180°]$
$z \in [0; 4]m \Leftrightarrow \delta z = 4$m
$\rho = 3333.3$kg/m^3
`MeridianBoundaryNodesOnExtrados = True`

Optimization:
Different choices were considered:
$f = \sum H$ and $c_2 = \mathrm{CSG}_{\mathcal{J}} > 1$
$f = \sum H^2$ and $c_2 = \mathrm{CSG}_{\mathcal{J}} > 1$

Results:
Let H_i be the thrust of the ith strip. The strip 1 is the closest to the stair axis.
The minimum thrust computed depend on the choice of the cost function.

For $f = \sum H$:
only one thrust is not null, and $\sum H = H_1 = 16134$kg

For $f = \sum H^2$:
$H_1 = 4264$kg, $H_2 = 4216$kg, $H_3 = 4150$kg, $H_4 = 4074$kg, $\sum H = 16705$kg

In García Ares's solution $\sum H = 16792$kg

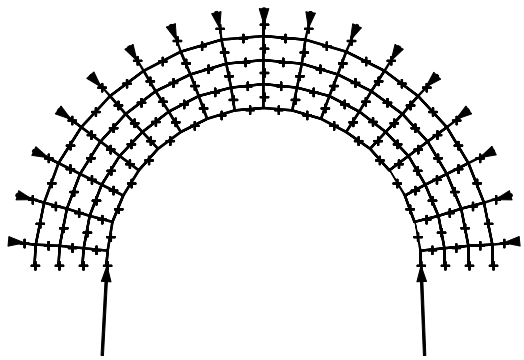

form diagram and support forces for $f = \sum H$

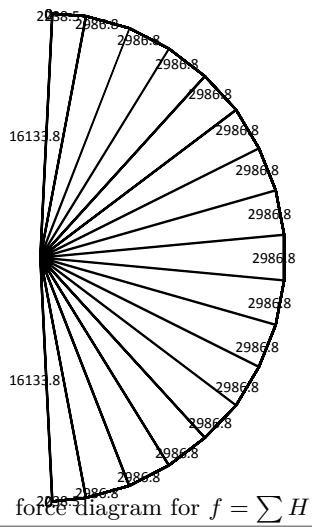

force diagram for $f = \sum H$

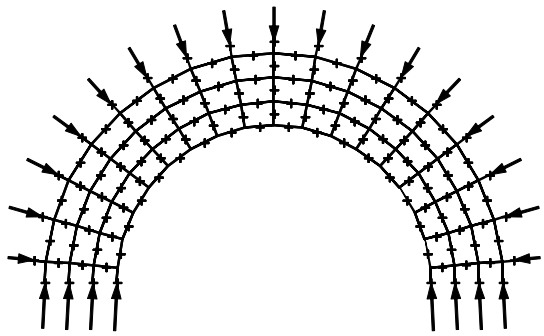

form diagram and support forces for $f = \sum H^2$

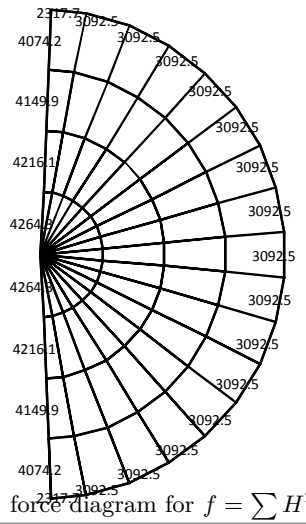

force diagram for $f = \sum H^2$

Fig 4.35 – Minimal thrust of a helicoidal stair
Comparison of García Ares 2007 [20] and network analysis

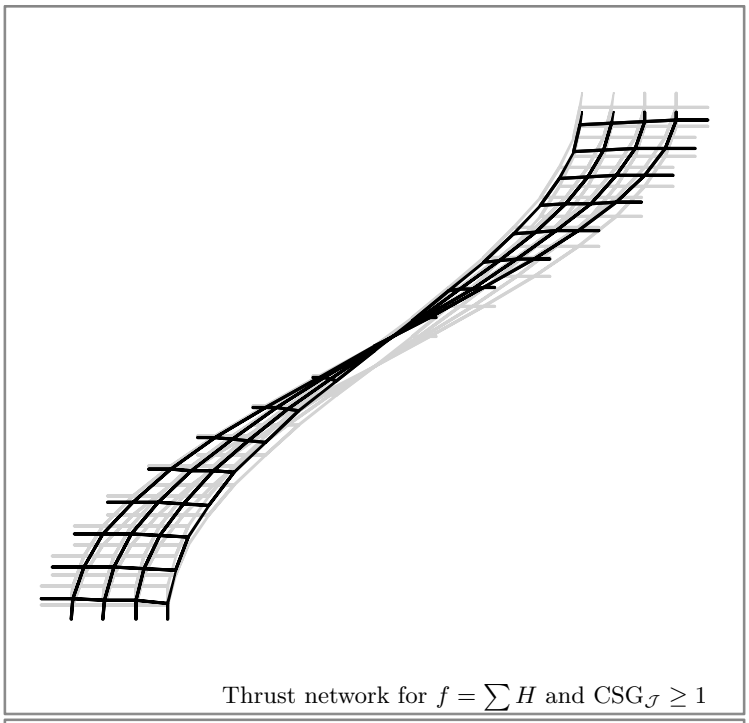

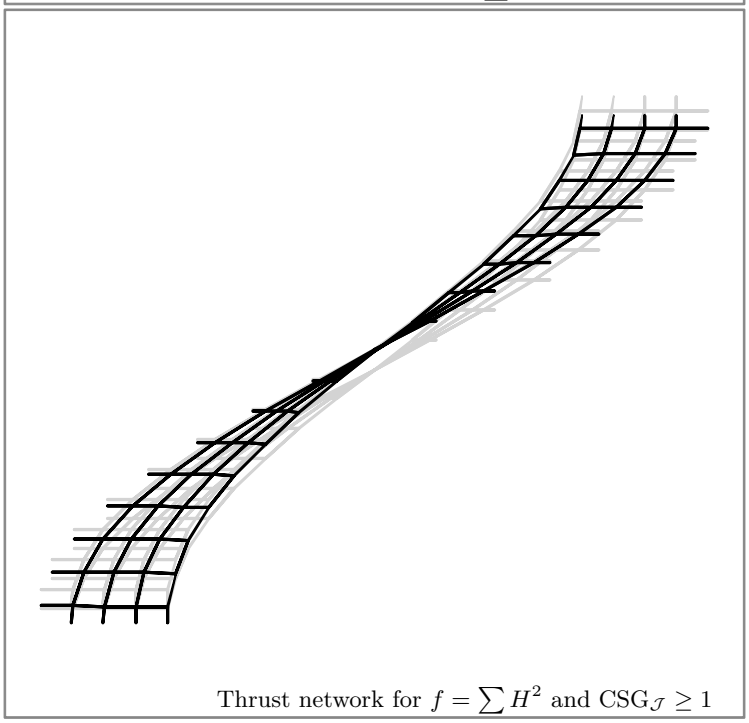

Fig 4.36 – Thrust networks of helicoidal stair
Additional figures to figure 4.35

4.8 Pavilion vaults

Recent studies have shed new light on the structural behaviour of pavilion vaults (or cloister vaults) (Tomasoni 2008 [40], D'Ayala et Tomasoni 2011 [10]). It has been shown that the horizontal thrust along the support is deeply dependant on the slicing technique used to study the vault. D'Ayala and Tomasoni introduce a new method within the framework of limit analysis with limited friction, and show that the natural arches that develop inside each groin have a real impact on the structural behaviour (2011 [10, p.21]).

Although the reproduction of such results is not theoretically impossible with the thrust network analysis, it would require the use of much more degrees of freedom than currently used, in order to represent the natural arches. The implementation of Manacoh is not advanced enough to do so.

However, the consideration of this kind of example is interesting regarding the construction of geometry. Indeed, with the slicing technique indicated on figure 4.37, some branches between blocks intersect the plane of the related joint **outside** the joint. This is due to the skewed form of some blocks located at the base of the groins. For such joints, no 2D-equivalent joints can be constructed. This is a theoretical question that should be addressed. For now, we go around this problem by expending a ficticious 2D-joint, so that the result is not relevant regarding the various coefficient of safety we consider (see the scaling joint factor page 19).

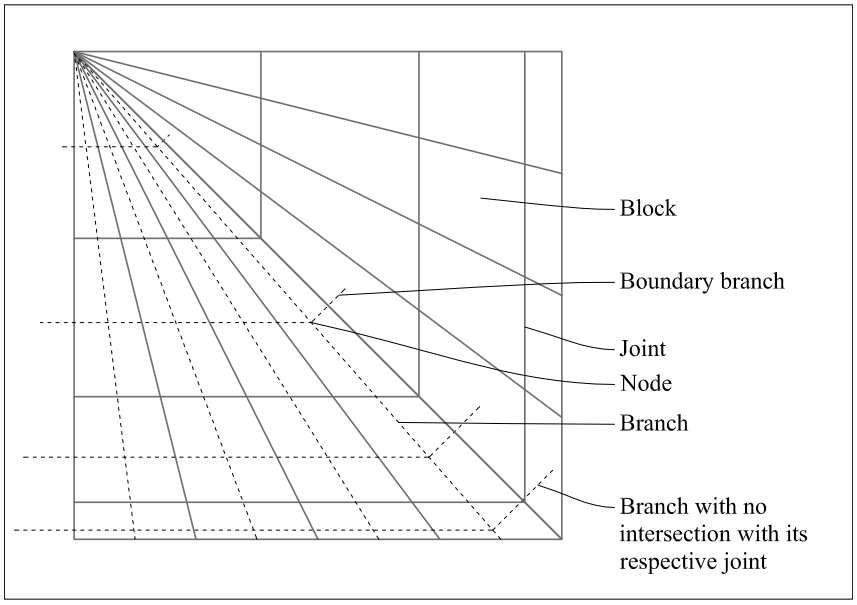

Fig 4.37 – Pavilion vault — joints and mass network

4.9 Conclusion

This chapter illustrates the large possibilities of the thrust analysis method regarding the emulation of various historic methods for evaluating the stability of masonry structures. Our implementation of this method allows to compare a large panel of solutions. The main conclusions that can be drawn from the consideration of these examples are:

- for arches
  - the geometrical coefficient of safety that we use is not the theoretical coefficient of safety defined by Heyman, but it has been shown on an example that our implementation of that it gives very good estimates of the latter
  - the minimum thickness of a semi-cylindrical arch can be computed: $t/R = 0.1075$
  - the difference between line of thrust and line of pressure was illustrated on examples
- for domes
  - a minimum thickness of a hemispherical dome without hoop forces can be computed: $t/R = 0.428$ This result is close to the minimum thickness of a hemispherical dome with hoop forces computed by Heyman: $t/R = 0.420$
  - the current implementation of Manacoh does not allow form finding, and thus cannot strictly emulates the method of Bossut (1774-1776). However the consideration of his hypotheses (no friction) with the thrust network method is instructive
  - Manacoh finds the same results as those given by Rankine's theorem of blockwork structures on an example. Furthermore, it can compute results for elliptical dome of constant thickness that are out of reach of Rankine's theorem.
  - Manacoh allows to find partially the final results that would be given with Durand-Claye's method

Chapter 5

Conclusion

O'Dwyer article in 1999 and then Block's PhD thesis in 2009 are two fundamental steps towards a better understanding of historic masonry structures. Our implementation of their methods intends to show that thrust network analysis can also be a useful tool for a better understanding of the history of analysis of masonry structures.

— Manacoh implementation of thrust network analysis proved effective to compute equilibrium solutions that were published by various authors using different methods and criteria to evaluate the stability of masonry structures.
— Manacoh can thus be used to compare the result that would be given by the methods of different authors (analytical, graphical, analytical-graphical) on new examples, using only one tool.
— The thrust network is a 3D extension of the line of pressure, a concept that has been (with reason) put aside in scientific literature for the study of historic masonry structure. Thus thrust network analysis requires additional calculus in order to define the centres of pressure on the joints, for which there is a consensus on their physical meaning.
— Various coefficient of safety can be defined, and then exploited through optimization processes in order to find the related collapse mechanisms.
— Keeping the number of degrees of freedom to a minimum is fundamental because of computation cost of optimization process. We suggest in this document the use of Lagrange polynomials in order to lower the computed degrees of freedom, while preserving the physical meaning of the parameters that are use for the optimization process.

The worked examples developed in this document focused on published examples that use the axi-symmetry of the studied structure in order to simplify the calculations. Thus this document is more about proving the efficiency of the method, than bringing new solutions. However, now that the efficiency of this implementation is proven, the next step of the research would be to exploit the possibilities of the method for non-symmetric 3D structures.

Mise à jour : see extensions and new examples (flat archs, flat vaults, influence of stereotomy) in Fantin [17]

Bibliography

[1] E. Benvenuto : *An introduction to the history of structural mechanics - Part II : Vaulted structures and elastic systems*, vol. 2. Springer-Verlag, New York, 1991.

[2] P. Block : *Thrust Network Analysis : exploring three-dimensional equilibrium.* Thèse de doctorat, Massachusetts Institute of Technology, Dept. of Architecture, 2009. URL `http://dspace.mit.edu/handle/1721.1/49539`.

[3] P. Block et L. Lachauer : Three-dimensional funicular analysis of masonry vaults. *Mechanics Research Communications*, 56:53–60, mars 2014.

[4] C. Bossut : Recherches sur l'équilibre des voûtes. *In Histoire de l'Académie Royale des sciences.* Imprimerie royale, Paris, 1774. URL `http://gallica.bnf.fr/ark:/12148/bpt6k3573n`.

[5] C. Bossut : Nouvelles recherches sur l'équilibre des voûtes en dôme. *In Histoire de l'Académie Royale des sciences.* Imprimerie royale, Paris, 1776. URL `http://gallica.bnf.fr/ark:/12148/cb32786820s/date`.

[6] P. Bouguer : *Sur les lignes courbes qui sont propres à former les voûtes en dôme.* Histoire de l'Académie Royale des sciences. Imprimerie royale, Paris, 1734. URL `http://gallica.bnf.fr/ark:/12148/cb32786820s/date`.

[7] J. Claudel : *Formules, tables et renseignements pratiques ; aide-mémoire des ingénieurs, des architectes, etc.* Victor Dalmont, Paris, 4e édn, 1857. URL `http://www.google.fr/books?id=111AAAAAIAAJ`.

[8] J. Claudel : *Formules, tables et renseignements usuels ; aide-mémoire des ingénieurs, des architectes, etc.* Victor Dalmont, Paris, 6e édn, 1864. URL `http://www.google.fr/books?id=VF5AAAAAcAAJ`.

[9] M. Como : *Statics of historic masonry constructions.* Springer, Berlin; New York, 2013.

[10] D. F. D'Ayala et E. Tomasoni : Three-Dimensional Analysis of Masonry Vaults Using Limit State Analysis with Finite Friction. *International Journal of Architectural Heritage*, 5(2):140–171, fév. 2011. URL `http://opus.bath.ac.uk/23076/`.

[11] F. De Goes, P. Alliez, H. Owhadi et M. Desbrun : On the Equilibrium of Simplicial Masonry Structures. *ACM Transactions on Graphics*, 32(4), 2013. URL `http://hal.inria.fr/hal-00826280/`.

[12] J.-M. Delbecq : *Analyse de la stabilité des ponts en maçonnerie par la théorie du calcul à la rupture.* Thèse de doctorat, Ecole nationale des ponts et chaussées, Paris, 1983.

[13] A. Demanet : *Cours de construction*, vol. 1. E. Lacroix, Paris, 2e édn, 1861. URL `http://www.google.fr/books?id=Ss09AAAAcAAJ`.

[14] A. Durand-Claye : Note sur la vérification de la stabilité des voûtes en maçonnerie et sur l'emploi des courbes de pression. *Annales des ponts et chaussées*, p. 63–96, 1867.

[15] A. Durand-Claye : Vérification de la stabilité des voûtes et des arcs - Application aux voûtes sphériques. *Annales des ponts et chaussées*, 1880. URL `http://gallica.bnf.fr/ark:/12148/cb34348188q/date`.

[16] H. T. Eddy : *New constructions in graphical statics.* D. Van Nostrand, New York, 1877. URL http://archive.org/details/newconstruction00eddygoog.

[17] M. Fantin : *Étude des rapports entre stéréotomie et résistance des voûtes clavées.* Thèse de doctorat, Université Paris-Est, Paris, 2017. URL https://tel.archives-ouvertes.fr/tel-01834617.

[18] F. Foce et D. Aita : The Masonry Arch Between "Limit" and "Elastic" Analysis. A critical re-examination of Durand-Claye method. *In Proceedings Of The First International Congress On Construction History*, vol. 2, p. 895–908, Madrid, 2003.

[19] F. Fraternali : A thrust network approach to the equilibrium problem of unreinforced masonry vaults via polyhedral stress functions. *Mechanics Research Communications*, 37(2):198–204, mars 2010.

[20] J. A. García Ares : Un enfoque para el análisis límite de las escaleras de fábrica helicoidales. *In Actas del quinto congreso nacional de historia de la construcción*, p. 335–343, Burgos, juin 2007. URL http://oa.upm.es/3958/.

[21] J. A. García Ares : Una nueva solución de equilibrio para el análisis límite de helicoides de fábrica con óculo central como los construidos por Guastavino. *In VII Congreso Nacional de Historia de la Construcción*, p. 469–477, oct. 2011. URL http://oa.upm.es/9812/.

[22] J. Heyman : On shell solutions for masonry domes. *International Journal of Solids and Structures*, 3(2):227–241, mars 1967.

[23] J. Heyman : *The Stone Skeleton: Structural Engineering of Masonry Architecture.* Cambridge University Press, 1995.

[24] J. Heyman : La Coupe des Pierres. *In Proceedings of the Third International Congress on Construction History*, p. 807–812, Cottbus, 2009. URL http://www.bma.arch.unige.it/ENGL/engl_proceedings_construction_history.html.html.

[25] S. Huerta Fernández : Oval Domes: History, Geometry and Mechanics. *Nexus Network Journal*, 9(2):211–248, 2007.

[26] S. Huerta Fernández : The Analysis of Masonry Architecture: A Historical Approach. *Architectural Science Review*, 51(4):297–328, déc. 2008. URL http://oa.upm.es/1273/.

[27] S. Huerta Fernández : Designing by Geometry. Rankine's Theorems of Transformation of Structures.. *In Geometría y proporción en las estructuras. Ensayos en honor de Ricardo Aroca*, p. 263–285. Lampreave, sept. 2010. URL http://oa.upm.es/4368/.

[28] W. W. Lau : *Equilibrium analysis of masonry domes.* Master thesis, Massachusetts Institute of Technology, 2006. URL http://dspace.mit.edu/handle/1721.1/34984.

[29] J. A. Ochsendorf : *Collapse of Masonry Structures.* Thèse de doctorat, King's College, Cambridge, 2002.

[30] D. O'Dwyer : Funicular analysis of masonry vaults. *Computers & structures*, 73(1-5):187–197, 1999.

[31] A. Oikonomopoulou : *Approches numériques pour l'étude du comportement des structures maçonnées anciennes : un outil basé sur le calcul à la rupture et la visualisation graphique.* Thèse de doctorat, Université Paris-Est ENSA Paris La Villette, Paris, déc. 2009. URL http://tel.archives-ouvertes.fr/tel-00493588/fr/.

[32] M. Paradiso, M. Rapallini et G. Tempesta : Masonry domes. Comparison between some solutions under no-tension hypothesis. *In Proceedings Of The First International Congress On Construction History*, Madrid, jan. 2003. URL http://www.sedhc.es/biblioteca/actas/CIHC1_148_Paradiso%20M.pdf.

[33] Petit : Mémoire sur le calcul des voûtes circulaires. *In Mémorial de l'officier du génie*, num. 12, p. 73–150. de Fain, Paris, 1835. URL http://www.google.fr/books?id=zX8OAAAAYAAJ.

[34] P. Radelet-de-Grave : La théorie des voûtes de Pierre Bouguer : Jeu mathématique et enjeu pratique. *Eprouver la science..., op. cit. in*, (6):397–421, 1999. URL http://www.fyma.ucl.ac.be/files/UCL-IPT-99-13.pdf.

[35] W. J. M. Rankine : *A manual of applied mechanics.* Griffin, London, 1858.

[36] M. L. Reese : *Structural analysis and assessment of Guastavino vaulting.* Master thesis, Massachusetts Institute of Technology, Dept. of Architecture, 2008. URL `http://dspace.mit.edu/handle/1721.1/44748`.

[37] M. Rippmann, L. Lachauer et P. Block : Interactive Vault Design. *International Journal of Space Structures*, 27(4):219–230, déc. 2012. URL `http://block.arch.ethz.ch/brg/publications/260`.

[38] J. Résal : *Ponts en maçonnerie - Tome 1 - Stabilité des voûtes*, vol. 1 de *Encyclopédie des travaux publics - Ponts en maçonnerie.* Baudry, Paris, 1887. URL `http://gallica.bnf.fr/ark:/12148/bpt6k91083k`.

[39] P. Smars : *Études sur la stabilité des arcs et voûtes - confrontation des méthodes de l'analyse limite aux voûtes gothiques en Brabant.* Thèse de doctorat, Université Catholique de Louvain, Leuven, 2000. URL `http://smars.yuntech.edu.tw/phd/phd_f.html`.

[40] E. Tomasoni : *Le volte in muratura negli edifici storici : tecniche costruttive e comportamento strutturale.* PhD thesis, Università degli Studi di Trento, 2008. URL `http://www.unitn.it/files/download/9646/phd_thesis_elide_tomasoni_-_ciclo_xx.pdf`.

[41] T. Van Swinderen et J. Coenders : Tool to design masonry double-curved shells. *In Symposium of the International Association for Shell and Spatial Structures*, Valencia, 2009. URL `http://dspace.cc.upv.es/handle/10251/7002`.

[42] E. Vouga, M. Höbinger, J. Wallner et H. Pottmann : Design of self-supporting surfaces. *ACM Transactions on Graphics (TOG)*, 31(4):87, 2012.

[43] W. S. Wolfe : *Graphical analysis - a text book on graphic statics.* McGraw-Hill book company, New York, 1st édn, 1921. URL `http://archive.org/details/graphicalanalysi00wolfrich`.

[44] J. F. Zessin : *Collapse analysis of unreinforced masonry domes and curving walls.* Thèse de doctorat, Massachusetts Institute of Technology, Dept. of Architecture, 2012. URL `http://dspace.mit.edu/handle/1721.1/70879`.

Index

abaque, 63
affine transformation, 18, 78
arch
    cylindrical, 87

Benvenuto, 42
Bossut, 42
Bouguer, 42
boundary condition, 26
Bramante, 55
branch, 22
    boundary, 16

centre
    of gravity, 18
coefficient of safety
    Delbecq, 52
    Durand-Claye, 52
Como, 44
constraint, 33
cost function, 33

degree of freedom, *see* DOF
Delbecq, 19
diagram
    force, 10
    form, 10
DOF, 10, 26
    manual control, 35
dome
    elliptical, 78
    frictionless joints, 42
    metal, 59
    oval, 78
    pointed, 63
    with hoop forces, 66
    without hoop forces, 51
dual grid, 10
Durand-Claye, 19, 51

Eddy, 59

extrados, 19

force network method, 6

graphical user interface, *see* GUI
Guastavino, 73

Heyman, 76, 87

intrados, 19

joint, 19, 101

Lau, 63, 71, 76

Mascheroni, 43
mass network, *see* network
modified thrust line method, 63

network
    mass, 10
    thrust, 10
node, 22
    boundary, 16
    meridian boundary, 19
nomogram, *see* abaque

oculus, 19, 55
Oikonomopoulou, 91
optimization, 33

parallel projection, *see* affine transformation
point load, 18
polynomials, Lagrange, 29, 34, 73
primal grid, 10

Rankine, 78
Reese, 73

Salimbeni, 43
Smars, 94
stair
    helicoidal, 96

theorem
    Rankine, 79
thrust
    minimal, 44
thrust network, *see* network
thrust network analysis, 6

vault
    cloister, 101
    pavilion, 101

weight
    estimate, 22
Wolfe, 66

Zessin, 76

Chapter 6

License


```
'Licence Expat
'
'Copyright (c) 2014-2018 Mathias Fantin
'
'Permission is hereby granted, free of charge, to any person obtaining a copy
'of this software and associated documentation files (the "Software"), to deal
'in the Software without restriction, including without limitation the rights
'to use, copy, modify, merge, publish, distribute, sublicense, and/or sell
'copies of the Software, and to permit persons to whom the Software is
'furnished to do so, subject to the following conditions:
'
'The above copyright notice and this permission notice shall be included in
'all copies or substantial portions of the Software.
'
'THE SOFTWARE IS PROVIDED "AS IS", WITHOUT WARRANTY OF ANY KIND, EXPRESS OR
'IMPLIED, INCLUDING BUT NOT LIMITED TO THE WARRANTIES OF MERCHANTABILITY,
'FITNESS FOR A PARTICULAR PURPOSE AND NONINFRINGEMENT. IN NO EVENT SHALL THE
'AUTHORS OR COPYRIGHT HOLDERS BE LIABLE FOR ANY CLAIM, DAMAGES OR OTHER
'LIABILITY, WHETHER IN AN ACTION OF CONTRACT, TORT OR OTHERWISE, ARISING FROM,
'OUT OF OR IN CONNECTION WITH THE SOFTWARE OR THE USE OR OTHER DEALINGS IN
'THE SOFTWARE.
```